Structural and Functional Studies of Activation and Inhibition of ELIC, a Prokaryotic Member of the Pentameric Ligand-Gated Ion Channel Family

Dissertation

zur

Erlangung der naturwissenschaftlichen Doktorwürde
(Dr. sc. nat.)

vorgelegt der

Mathematisch-naturwissenschaftlichen Fakultät

der

Universität Zürich

von

Iwan Zimmermann

von

Schwanden GL

Promotionskomitee

Prof. Dr. Raimund Dutzler (Leitung und Vorsitz)
Prof. Dr. Ben Schuler
PD Dr. Ian Forster

Zürich 2013

Acknowledgement

I am grateful for the support and help of many people who have directly or indirectly contributed to this thesis.

First, I would like to thank my thesis supervisor Prof. Raimund Dutzler, not only for giving me the opportunity to work on this interesting and exciting project, but also for the support he has provided in all stages of my work.

I am thankful to Prof. Ben Schuler and PD Dr. Ian Forster for being on my thesis committee and Ian Forster additionally for his help and patience in solving several technical problems I encountered in electrophysiology.

I wish to thank my collaborators, Dr. Peter Kolb for performing the *in silico* agonist screening, Prof. Lucia Sivilotti and Alessandro Marabelli for the performed experiments and the fruitful discussions and Prof. Dirk Trauner and his group for the custom synthesis of several compounds.

I would like to thank the staff of the Institute of Biochemistry, the workshop and the IT support for keeping everything running and Beat Blattmann and Céline Stutz-Ducommun of the NCCR crystallization facility.

Many thanks to all present and former members of the Dutzler group for many suggestions, chats and a nice atmosphere in the lab and outside as well. I especially thank Carlo Bertozzi, Eric Geertsma and Yvonne Neldner for their support in and outside the lab.

I would also like to thank all my friends in Zürich for making the last years most enjoyable.

My parents have always supported and motivated me during the long time of my education. Thank you very much!

Finally, unfortunately not yet in Italian, I thank Elisa for her never-ending support, patience and love in the last years.

Content

Abstract

The family of pentameric ligand-gated ion channels participates in the fast signal transmission at chemical synapses in the central nervous system and at neuromuscular junctions. All members of the family are pentamers, formed by either identical or homologous subunits. Each subunit consists of an N-terminal extracellular ligand-binding domain and a transmembrane domain of four α-helices. The protein scaffold allows specific binding of small molecules, called neurotransmitters. Their binding to the receptor stabilizes a conformation with an aqueous pore in the center of the pentamer. This ion permeation path is selective for either cations, as in acetylcholine or serotonin receptors, or for anions, as in glycine and GABA receptors. The membrane potential is depolarized by cation selective channels and hyperpolarized by anion selective channels. Several diseases are known to be related to the dysfunction of pLGICs, as Alzheimer's disease, epilepsy or schizophrenia. The family of pLGIC has been studied since the middle of the last century and their function and pharmacology is thus well understood. These studies led to the discovery of a variety of drugs, which target pLGICs, not only to treat the mentioned diseases, as some of them are widely used as tranquilizers, anesthetics or for smoking cessation.

In contrast to the wealth of biochemical data that was collected over decades, structural information clarifying the underlying molecular mechanisms of the function of pLGICs is only available since ten years. The first insights at high resolution came from the structures of the acetylcholine binding proteins, small soluble proteins homologous to the extracellular domain of the acetylcholine receptor. At the same time, cryo-electron microscopy studies have provided a structural model of the full length acetylcholine receptor at comparably low resolution. These structures have clarified the overall topology of this receptor family and the mechanism of agonist and antagonist binding. The first high resolution structures of full-length receptors were obtained from the prokaryotic homologues ELIC and GLIC, which were determined by X-ray crystallography in two different functional states. GLIC is unusual in the family of pLGICs since it is activated by protons, whereas ELIC is a ligand-gated ion channel. However, since the physiological function of ELIC and thus the nature of activating ligands were unknown, its use as model system for mechanistic studies was limited.

In my PhD studies, I have identified a set of small molecules, which are capable of activating ELIC. These molecules are linear primary amines and include the neurotransmitter GABA. The initial biophysical characterization of ELIC by electrophysiology revealed a complex functional behavior that resembles eukaryotic receptors. The ligand recognition site in ELIC is similar to glycine and GABA receptors but its cation selectivity is a hallmark of acetylcholine and serotonin receptors. In the course of the electrophysiological experiments, a strong inhibitory effect of divalent cations on agonist induced currents was observed. A thorough mechanistic investigation of this effect by X-ray crystallography and electrophysiology has allowed the identification of five equivalent binding sites in the pentamer, responsible for the

observed allosteric inhibition of ELIC by divalent cations. Our study demonstrates that divalent cations act by reducing the efficacy of channel opening by a mechanism that is also found in eukaryotic receptors.

In combination with the previously determined crystal structure, the work of my PhD thesis has thus provided first insights into the activation and inhibition of ELIC and has established a model system to study the detailed molecular mechanisms underlying the function of pentameric ligand-gated ion channels.

Zusammenfassung

Die Familie der pentameren ligandengesteuerten Ionenkanäle (pLGIC) ermöglicht die schnelle Signalübertragung an chemischen Synapsen im zentralen Nervensystem und an neuromuskulären Übergängen. Alle Mitglieder dieser Familie besitzen eine pentamere Struktur, die sich aus fünf identischen oder homologen Untereinheiten zusammensetzt. Jede Untereinheit besteht aus einer N-terminalen extrazellulären Ligandenbindungsdomäne und einer Transmembrandomäne, die aus vier α-Helices aufgebaut ist. Das Proteingerüst ermöglicht die Bindung spezifischer kleiner Moleküle, sogenannte Neurotransmitter. Die Bindung dieser Neurotransmitter stabilisiert den Rezeptor in einer Konformation mit einer wässrigen Pore im Zentrum des Pentamers. Dieser Durchgang für Ionen ist entweder selektiv für Kationen, wie im Acetylcholin- oder Serotoninrezeptor, oder für Anionen, wie im GABA oder Glycinrezeptor. Das Membranpotenzial wird durch kationenselektive Kanäle depolarisiert, durch anionenselektive Kanäle jedoch hyperpolarisiert. Dies führt dann zu einem erregenden, respektive zu einem inhibierenden Signal am Neuron. Diverse Krankheiten werden mit einer Fehlfunktion dieser Rezeptoren in Verbindung gebracht, wie Alzheimer, Epilepsie oder Schizophrenie. Die Funktion und die Pharmakologie der pLGIC sind sehr gut verstanden, da diese Familie schon seit der Mitte des letzten Jahrhunderts erforscht wird. Verschiedenste Medikamente, die mit pLGIC interagieren, wurden entdeckt und deren Einsatz erstreckt sich über die Behandlung der genannten Krankheiten hinaus und sie werden als Beruhigungsmittel, in der Anästhesie und der Therapie von Rauchern eigesetzt.

Im Gegensatz zu der Fülle von biochemischen Daten, die über Jahrzehnte zusammengetragen wurden, sind Informationen über die Struktur dieser Rezeptoren, die einen Schluss über die grundlegenden molekularen Mechanismen zulassen, erst seit ungefähr zehn Jahren erhältlich. Die ersten Strukturen waren von Acetylcholin-bindenden Proteinen, kleinen löslichen Proteinen die der extrazellulären Domäne des Acetylcholinrezeptors entsprechen. Zur gleichen Zeit folgte die erste Struktur eines ganzen Acetylcholinrezeptors, welche durch Kryo-Elektronenmikroskopie bei vergleichsweise niedriger Auslösung erreicht wurde. Diese ersten Strukturen erklärten sowohl die Architektur dieser Rezeptoren als auch die Mechanismen der Agonist- und Antagonistbindung. Die ersten hochaufgelösten Strukturen von kompletten Rezeptoren wurden mit den prokaryotischen Homologen ELIC und GLIC erreicht, die mit Hilfe der Röntgenkristallographie in zwei verschiedenen funktionellen Zuständen ermittelt wurden. GLIC ist ungewöhnlich in dieser Familie, da es sich um einen protonengesteuerten Ionenkanal handelt, wohingegen ELIC ein ligandengesteuerter Ionenkanal ist. Jedoch war dessen physiologische Funktion als auch die Art der aktivierenden Liganden unbekannt. Deshalb war der Nutzen als Modellsystem für mechanistische Studien trotz der bekannten Struktur begrenzt.

In meiner Doktorarbeit habe ich einen Satz von Molekülen identifiziert welche ELIC aktivieren können. Es handelt sich ausschliesslich um lineare primäre Amine, darunter

auch der Neurotransmitter GABA. Die erste biophysikalische Charakterisierung von ELIC durch Elektrophysiologie zeigte eine komplexe Funktion mit einer starken Ähnlichkeit zu den eukaryotischen Rezeptoren. Obwohl die Ligandenbindungstasche in ELIC den GABA- und Glycinrezeptoren ähnelt, ist die Selektivität von ELIC für Kationen jedoch eine Eigenschaft der Acetylcholin- und Serotoninrezeptoren. Im Verlaufe der elekrophysiologischen Experimente wurde ein starker inhibierender Effekt von divalenten Kationen auf die auf ELIC zurückzuführenden Ströme beobachtet. Eine gründliche Untersuchung dieses Effekts mit Röntgenkristallographie und Elektrophysiologie erlaubte die Identifizierung von fünf äquivalenten Bindungsstellen im Pentamer, welche für die allosterische Inhibition von ELIC durch divalente Kationen verantwortlich sind. Unsere Studie zeigt, dass die divalenten Kationen eine Verringerung der Effektivität der Kanalöffnung verursachen und dass der zugrunde liegende Wirkungsmechanismus auch in eukaryotischen Rezeptoren vorkommt.

Zusammen mit der vorgängig bestimmten Kristallstruktur hat meine Doktorarbeit erste Einsichten in die Aktivierung und Inhibition von ELIC verschafft und ein Modellsystem etabliert um die molekularen Mechanismen zu studieren, die der Funktion der pentameren ligandengesteuerten Ionenkanäle zugrunde liegen.

Introduction

Ligand gated ion channels

Certain families of ligand gated ion channels (LGIC) act as ionotropic receptors for neurotransmitters. These integral membrane proteins form ion-selective pores across the plasma membrane that can be controlled by ligands. At chemical synapses in the nervous system, neurotransmitters are released into the synaptic cleft, where they bind to a specific site of a LGIC. Ligand binding triggers a conformational change, which opens an ion conduction pore. This pore allows selected ions to flow passively along their electrochemical gradient. The process of neurotransmitter binding and gating is very fast. It occurs in the millisecond time scale, which is required for fast signaling at chemical synapses in the central nervous system and at neuromuscular junctions.

There are three different families of LGIC forming neurotransmitter receptors. The first family is formed by the ionotropic glutamate receptors (NMDA and AMPA receptors), the second contains nucleotide gated ion channels (P2X receptors) and the third consists of the pentameric ligand gated ion channels (pLGICs or cys-loop receptors).

The family of pLGICs is quite diverse and further divided in exitory and inhibitory receptors. The exitory pLGICs are Acetylcholine receptors (AChR), Serotonin receptors ($5HT_3R$) and the recently discovered Zinc-activated channels (ZAC). They are cation selective and their activation leads to the depolarization of the cell, thereby triggering further downstream signaling.

Inhibitory pLGICs are gamma-amino-butyric acid receptors ($GABA_AR$ and $GABA_CR$) and glycine receptors (GlyR). Besides these large receptor subfamilies, certain glutamate and serotonin activated inhibitory pLGICs are found in invertebrates. In contrast to the exitory receptors, inhibitory receptors are anion selective and their activation leads to a hyperpolarization of the cell preventing further downstream signaling. pLGICs are the only currently known family of ion channels that contains both cation and anion selective members. Their importance is also underlined by the fact that glycine and GABA are the main inhibitory neurotransmitters in the central nervous system.

The diversity of the family is further increased by multiple genes, which code for different subunits. In the assembled receptor, the subunits are arranged as either homo- or heteropentamers. In that way, up to four different subunits can be combined in a single pentameric receptor (*1*).

Due to their abundance in the nervous system and their large diversity, pLGICs are important therapeutic targets for the treatment of different diseases. Therapeutic applications reach from the treatment of schizophrenia, Alzheimer's and Parkinson's disease to smoking cessation and anesthesia. Very potent toxins that target pLGICs were also identified and find their use as insecticides and antiparasidic drugs.

Prokaryotic homologues

Ion homeostasis and electrical signaling through ion channels is important to all phylae of life. It is therefore not surprising that related genes, e.g. those coding for shaker-type potassium channels and voltage gated sodium channels, were found in genomes of multi- and unicellular eukaryotes as well as in genomes of prokaryotes (*2*). In contrast, genes coding for pLGICs were initially only found in the phylum of animals. It was therefore believed that only organisms with a nervous system possess genes coding for pLGICs. This contradicted a phylogenetic analysis among the pLGICs, which stated that the common ancestor of all pLGICs appeared 2.5 billion years ago (*3*), long before the appearance of the first eukaryotes. Through the advances in genome sequencing, more genomes of prokaryotic organisms became available and finally, in 2005, Tasneem et al published the identification of prokaryotic pLGICs (*4*). Even though the sequence conservation is below 20%, the key residues of the family are well conserved. In 2006, Bocquet et al showed the first heterologous expression of GLIC, the pLGIC of the cyanobacterium *Gloebacter violaceus*. The protein was successfully expressed in *E.coli*, HEK293 cells and *Xenopus laevis* oocytes. The work has identified GLIC as pH-activated, cation selective ion channel and it confirmed the pentameric structure of the protein by electron microscopy and unspecific crosslinking (*5*).

Structural information of pLGICs

The first view of a component of a pLGIC at high resolution was obtained in 2001, when Brejc et al determined the structure of the acetylcholine binding protein of the mollusk *Lymnaea stagnalis* by X-ray crystallography. This protein is homologous to the ligand binding domain of the nAChR and it is most probably involved in the regulation of nonsynaptic cholinergic signal transmission (*6*). The structure at 2.7Å provided insight in the pentameric organization of the extracellular ligand binding domain, the location and architecture of the ligand binding sites and the binding modes of ligands. The structure also revealed the effect of neurotoxins like α-bungarotoxin and α-connotoxin on a molecular level (*7*).

Following on a long term effort to determine the structure of a full-length channel by electron microscopy, in 2003, Miyazawa et al determined the 4Å EM structure of a nAChR in tubular crystals formed from membranes of the electric organ of *Torpedo marmorata*. In 2005, they used crystallographic refinement methods to improve the model. Despite the comparably low resolution, they were able to interpret the electron density map and build a model containing most of the protein backbone and the side chains of bulky aromatic residues. This pioneering work has provided the first structural information on a full length pLGIC and it lead to the first hypothesis of the gating mechanism (*8*, *9*).

In 2004, the identification of prokaryotic homologues also nourished the hope to determine a high resolution structure of a bacterial family member by X-ray crystallography. As it was shown in several cases, prokaryotic homologues have

characteristics that make them very superior targets for crystallization when compared to eukaryotic proteins. Prokaryotic proteins are usually more compact, they do not contain post translational modifications, such as glycosylations and, in case of ion channels, their regulation is often tighter than that of their eukaryotic counterparts. These features are exploited in the structure determination of membrane proteins. In 2008 and 2009, the structures of two homologues were determined by X-ray crystallography. The structure of ELIC, the homologue of *Erwinia chrysanthemi* (*10*), was followed the previously described pH activated GLIC (*11*, *12*). ELIC and GLIC provided the first insights into the architecture of full receptors at high resolution, as they were determined 3.3Å and 3.1Å respectively. Both structures had a large impact on the understanding of the architecture of these ion channels and they also suggested an initial mechanism of gating which is relevant for the entire family. In 2011, the first crystal structure of a eukaryotic pLGIC, GluCl of *Caenorhabditis elegans*, was solved at 3.3Å. GluCl was the first structure of an anion selective member of the family and provided detailed insight into agonist binding, anion selectivity and the allosteric modulation by ivermectin (*13*).

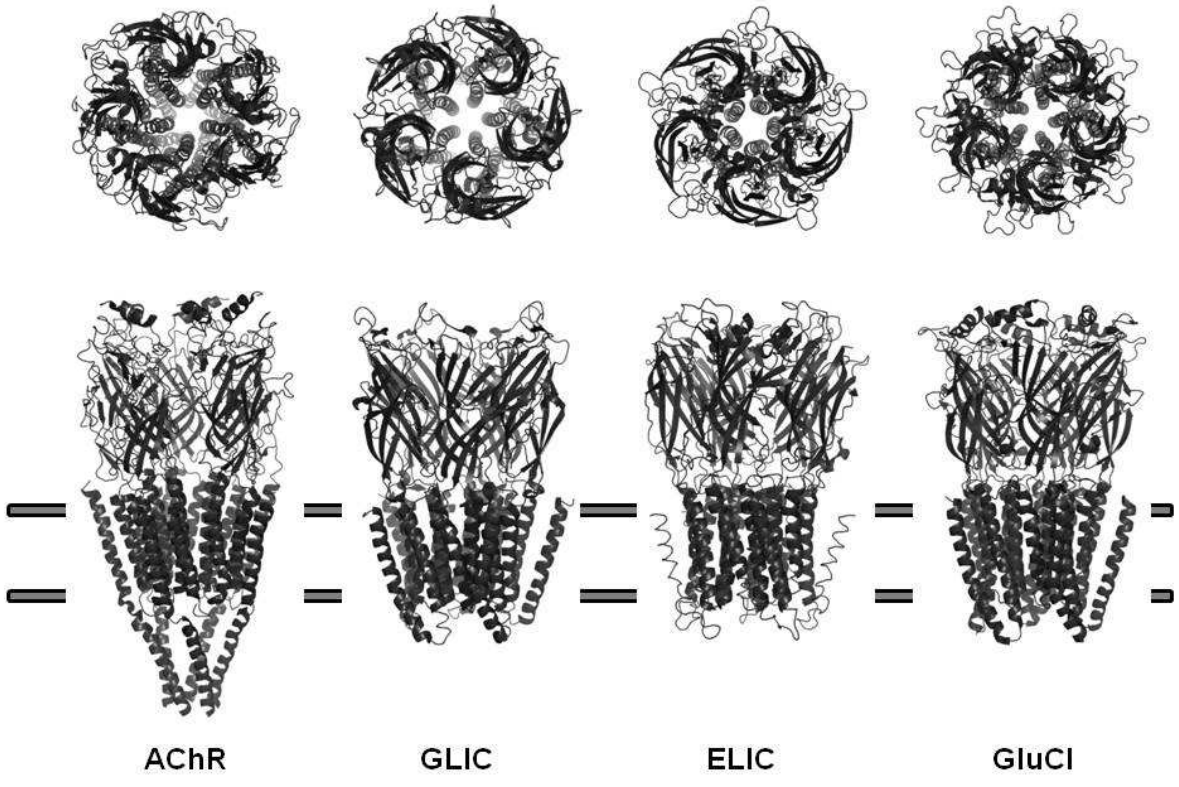

Figure 1 Top and side view of the available structures of pLGICs. The membrane is indicated as grey bars. A comparison of the cartoon representations of the secondary structure elements reveals the strong structural conservation within the family. Each of the five protomers is formed by an extracellular domain which consists of two β-sheets and a transmembrane domain of four α-helices. The residues of the second transmembrane helix line the pore which spans the membrane along the symmetry axis of the pentamer.

Despite the low similarity on the sequence level, all existing structures underline the conservation within the family (Figure 1). As all members of the family, they are pentamers. Each subunit consists of a mainly beta stranded extracellular ligand binding domain and a transmembrane domain formed by four transmembrane helices. The extracellular domains surround a wide and water-filled vestibule giving access to the pore, which is formed by the second transmembrane helices of all five subunits.

The extracellular domain

The pentameric assembly of the extracellular domains is a cylindrical structure with a height of 60Å and a diameter of 80Å. The protein domains enclose a large 20Å wide aqueous vestibule in the center of the pentamer (Figure 2). Viewed along the five-fold axis, it resembles a windmill with petal-like protomers. Each of the protomers consists of ten β-strands forming a β-sandwich with an immunoglobulin-like fold. In the pentamer, the only contacts of the subunits are dimer interfaces. Every protomer has two interaction sites; one on the principal and another on the complementary side. This interaction interface is very large with a buried surface of about 2500Å^2. The agonist binding site is a part of this subunit interface as the ligand binding pocket is formed by the β-strands and loops from both the principal and the complementary subunits (7). In contrast to the large interface between the protomers of the extracellular domain, the interface between the extracellular and the transmembrane domain is comparably small. The contacts are mediated by three loops of the extracellular domain and the M2-M3 loop of the transmembrane domain. These loops are strongly conserved within the family and they are responsible to transmit the conformational changes of the extracellular domain upon agonist binding to the pore.

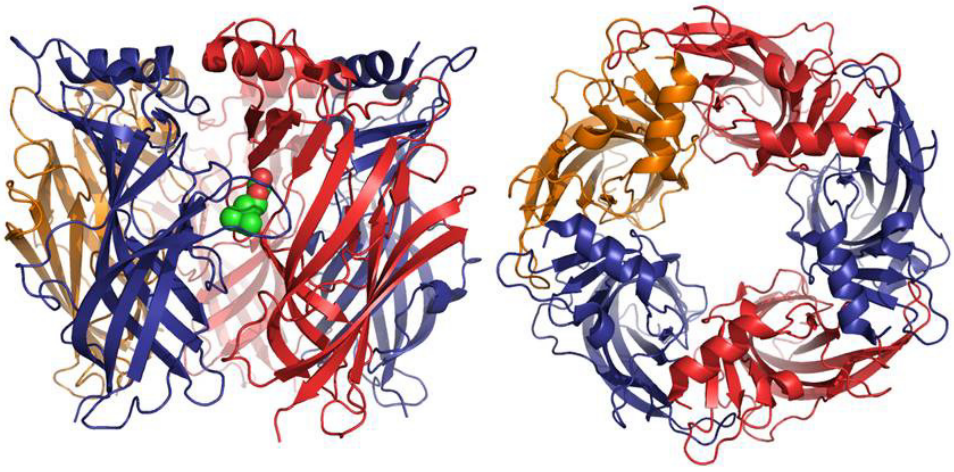

Figure 2 The structure of the acetylcholine binding protein of *T.californica* representing the extracellular domain of the AChR with the typical pentameric assembly of the pLGIC family. (left) The side view shows the ligand binding site, indicated by the bound carbachol. It is located in the large interface between the principal (blue) and the complementary (red) subunit. (right) The top view along the fivefold axis depicts the windmill-like structure of the pentamer formed by five subunits. It encloses a large vestibule in the center of the pentamer, which gives access to the pore in the full receptor.

The pore

Early studies with chimeric AChRs revealed a link between the conductance and the second transmembrane helix, the M2 segment of the receptor (*14*). Later on, it was shown that mutations in the M2 of AChRs altered the ion conduction properties and the affinity of a voltage dependent pore blocker. Therefore the M2 helix was attributed to be involved in the formation of the pore. In the 90's, the substituted cystein accessibility method (SCAM) was used in AChRs, GABARs and $5HT_3R$ to identify water accessible residues in the transmembrane domain (*15*–*17*). Interestingly, these studies found that every third or fourth amino acid in M2 was prone to modification and it was thus concluded that M2 had to be the pore lining helix and that the pore itself is formed by the side chains of all five M2 helices, one of each subunit of the pentamer. This was later confirmed by structural biology.

As known from sequence alignments, the chemical properties of the pore lining residues are conserved throughout the family of pLGICs. The extracellular halve of the pore is formed by three rings of hydrophobic amino acids (labeled as positions 9', 13' and 16' in the nomenclature derived for the nAChR), followed by two rings of polar residues (2' and 6'). The cytosolic ring (-1') varies in dependence of the selectivity of the channel. It is formed by glutamates in cation-selective and alanines in anion selective receptors.

The location of the gate was subject of controversial discussions. Miazawa et al reported in their EM structure from the resting state of the AChR a constriction at the hydrophobic 9' position of the pore. The diameter of the pore in this region is 3Å. Even though the pore is not fully obstructed computational simulations suggest that this diameter in a hydrophobic environment would form a barrier for sodium ions and can therefore act as a gate for the ion channel (*18*).

Similar results were obtained from experiments using photoaffinity labeling of the AChR with the radiolabeled noncompetitive antagonist 3-(trifluoromethyl)-3-(m-[^{125}I]iodophenyl)diazirin (TID), which was applied to the extracellular lumen of the channel. In the absence of agonist, TID specifically labeled the hydrophobic amino acids at the 9' and 13' position. In the presence of agonist, TID was able to penetrate deeper into the pore and label the polar residues at the 2' and 6' position. These results are consistent with a gate formed by the hydrophobic rings at the extracellular halve of the pore (*19*).

After the success of SCAM in identifying the pore lining residues, Wilson and Karlin applied this method to achieve a state-specific labeling of the AChR (*20*). By measuring electrophysiologically the time-dependence of the reaction of the introduced cysteines with MTS reagents applied from the extra- and intracellular side, they calculated the rate constants of the modification. They found that the residues at the -1' and 2' position at the intracellular part of the pore can be labeled much faster if the channel is in the open conformation than in the closed or desensitized state. Therefore they concluded that the residues at the -1' and 2' position form the activation gate. Additionally, they observed that the reaction rates of the introduced cysteines at position 6' and 9' dropped significantly if the receptor was in the desensitized state. In this way they could show that the pore lining is altered in these

3 different states of the receptor and they postulated a desensitization gate that reaches from the -1' position to the 9' position.

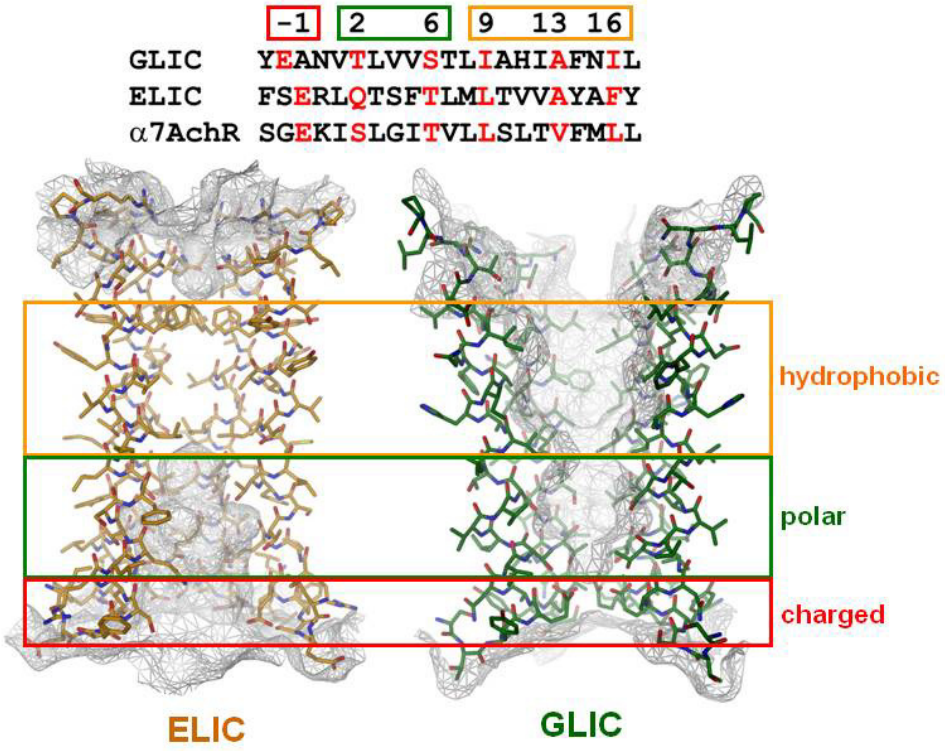

Figure 3 (top) Sequence alignment of the pore forming M2 helix of GLIC, ELIC and AChR. The pore lining residues are conserved and form six rings with distinct chemical properties. The three hydrophobic rings on the extracellular side constitute the gate, whereas the inner two polar and the intracellular charged ring build the selectivity filter. (bottom) Comparison of the pore structures of ELIC and GLIC showing two conformational states. ELIC is in a non-conductive state, in which the hydrophobic rings obstruct the pore. The GLIC pore is in the open conformation, where the hydrophobic rings separated from each other to open the gate whereas the polar and charged rings contracted to form a selectivity filter.

The structure of ELIC was the first pLGIC resolved at high resolution. It was crystallized in the absence of agonists and shows a non-conducting conformation. The pore is completely obstructed by two hydrophobic rings formed by the residues at the 9' and 16' position (Figure 3). The alanines of the third hydrophobic ring at the 13' position line a cavity of hydrophobic nature, where xenon atoms were trapped (*10*). Even though it is not entirely clear if this structure represents a resting or a desensitized state, it clearly supports the model where the amino acids of position 9' to 16' form the activation gate as the overall chemical characteristics of the pore of the AChR are also conserved in ELIC and GLIC. In contrast to ELIC, the structure of GLIC reveals a pLGIC in the active state. The hydrophobic residues of the activation gate have separated from each other, whereas the polar and charged rings have contracted to form a selectivity filter. This conformational change leads to the formation of a funnel-shaped and aqueous pore, which allows ions to pass through the membrane. The first high resolution structure of a eukaryotic homologue was determined in a conductive conformation which is almost equivalent to GLIC (*13*). The high degree of structural conservation between prokaryotic and eukaryotic receptors is very likely to extend to the mechanism of channel gating. It emphasizes

the suitability of the prokaryotic homologues as model systems, to gain a deep understanding into the molecular mechanisms underlying the function of pLGIC.

Activation of pLGICs

Since the middle of the last century, pharmacologists are inventing and refining mathematical models to describe the quantitative activity of drugs on a receptor, called drug receptor theory. These models are derived from enzyme kinetics and form the major link between the experimental observations and the events taking place on a molecular level. The first dose response experiments on a pLGIC, performed on *Torpedo* electroplax and frog endplates, showed that the obtained curves were not related to a classical hyperbolic Langmuir curve. This classical model assumes the agonist to interact with identical and independent binding sites and simply the occupancy of a receptor with an agonist leads to activation. The obtained curves in contrast, were sigmoid and accompanied by a slope bigger than one in a Hill plot. Since the receptors showed a cooperative behavior similar to the observations in hemoglobin, it was concluded that the receptors contain several allosterically linked agonist binding sites. Del Castillo and Katz also found that the classical model failed to explain their findings of partial agonism and therefore postulated a two state model where an agonist A binds to a receptor R to form an AR complex that is still not conducting. This complex can subsequently undergo a conformational change to the active state AR* (*21*).

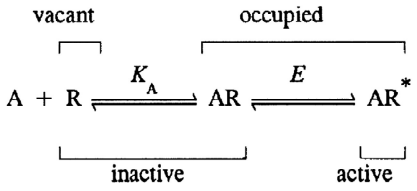

Figure 4 A schematic representation of the del Castillo-Katz model of receptor activation. The vacant receptor binds the agonist to form an agonist-bound but inactive complex. This step only depends on the affinity of the agonist to the receptor. In the second step, the receptor undergoes a conformational change which leads to the active and conductive state. This transition is dependent on the efficacy E, a measure of the ability of the agonist to convert the receptor to its active state.

The first step in this model requires the binding of the agonist to the receptor and this step is only dependent on the affinity of the agonist. The second step is the structural reorientation of the receptor and its equilibrium constant is called efficacy. The efficacy is an intrinsic property of the agonist, describing its potency to activate the channel. Using this model, del Castillo and Katz could finally explain the observation that partial agonist could not evoke the same response as full agonists even at full occupancy of the receptor, simply by stating that the efficacy of the partial agonist is smaller than the efficacy of a full agonist.

From the theory of cooperative enzymes, Monod et al proposed a model of pLGICs as allosteric proteins which could coexist in both open and closed states (*22*). This model is similar to the two state model of Del Castillo and Katz, but it includes an

open state without agonist bound to the receptor and a state with two agonists bound to the receptor.

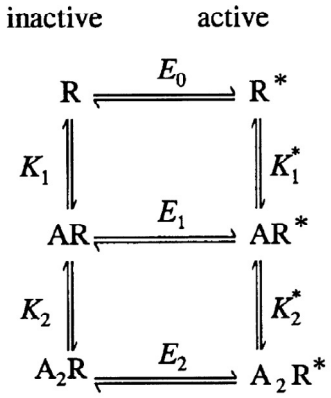

Figure 5 The schematic representation of the Monod-Wyman-Changeux (MWC) model of allosteric receptor activation. In this model, the receptor can adopt both the inactive and the active conformation in the presence or absence of agonist. The agonist can stabilize the active conformation and as a result, the efficacies increase from the unliganded to the biliganded state. It also follows that the active conformation has a much higher affinity to the agonist than the inactive conformation, which can explain the cooperative behavior in the activation of pLGICs.

This model predicts that the channel can be active in the absence of the agonist, even though this state is not highly populated as the efficacy of the unliganded receptor is very low. With higher occupancy of the receptor, also the efficacy of the conformational change is increasing.

The first use of this model was to explain the experimental findings of constitutive activity in pLGICs where the model of Del Castillo and Katz failed. For certain receptors, very short openings were observed in the absence of agonist and mutations were identified that increased the probability of these openings, thus confirming the constitutive activity (*23*, *24*). Furthermore, this model also includes distinct affinities for the agonist in the closed and the open state, as observed previously and it also explains the cooperative behavior of the receptors. With several ligand binding sites, the concerted movement of the different subunits from the resting to the active state creates cooperativity even without increasing the actual affinity of the individual binding sites (*25*).

The problem in the measurement of dose-response curves of LGICs is that the affinity of the agonist to the receptor and its efficacy are coupled as the response of open channels is measured upon application of agonist. The determined constant of a dose response experiment is the agonist concentration at the halve-maximal response, termed the EC_{50}. It gives the apparent affinity of an agonist to its receptor because it is a measurement that unites the two microscopic constants affinity and efficacy. The EC_{50} is related to the affinity and efficacy by the following equation:

$$EC_{50} = \frac{K_D}{1 + E}$$

Therefore, neither the true affinity nor the efficacy of an agonist can be determined by dose-response experiments and furthermore, if the EC_{50} is changed by a mutation in

the receptor or by a modulator, it cannot be determined if the affinity or the efficacy has changed.

Ligand recognition in the extracellular domain

The first step to the activation of a pLGIC is the binding of the ligand to the receptor. The best studied receptor in terms of ligand recognition is the AChR. The ligand binding site was expected to be part of the extracellular domain as the permanently positive charged ammonium group of ACh cannot diffuse through the membrane. The first information about the location of the binding site came for specific crossinking studies. Silman and Karlin showed that bromo-ACh activated the receptor and got covalently linked to a disulfide bond that had to be in vicinity of the ligand binding site (*26*). From the knowledge of the primary sequence, site directed mutagenesis and chemical labeling, the residues involved in ligand binding were identified. From this information it became obvious that amino acids from six loops (A-F) contributed to ligand binding, loop A-C from the principal and loop D-F from the complementary subunit (*27*). The first structures confirmed the hypothesis of a multi-loop binding site located in the interface of two adjacent subunits called the principal and the complementary side. In the structure of AChBP in complex with carbachol (*28*), the ligand binding pocket is mainly formed by a network of aromatic residues interacting with the ligand (Figure 6). There are three tyrosines (Y89, Y185, Y192) and one tryptophan (W143) from the principal side as well as one tryptophan (W53) from the complementary side. They stabilize the positive charge of the quaternary ammonium. Other hydrophobic contacts involve the disulfide bond (S187, S188) from the principal and a methionine (M114) and a leucine (L112) from the complimentary side. Also arginine 104 interacts with carbachol but the interaction is not of ionic nature.

The interactions of different agonists have been studied, also in the context of the AChBP. Nicotine is a neurotoxin and a very potent agonist of AChRs. The interactions in the binding site are comparable to carbachol as it also shows interactions with the aromatic side chains (Figure 7). Additionally, nicotine interacts through hydrogen bonds with the backbone carboxyl and amide groups of leucine 10, methionine 114 and tryptophan 143. This explains the much higher binding affinity of nicotine compared to carbachol.

As previously described, the main interaction of the cationic agonist carbachol with the protein is not mediated by salt bridges but by interactions with the π-electrons of the aromatic residues in the pocket, called cation-π interaction. The lab of Dennis Dougherty developed a method to quantify the cation-π interaction in pLGICs. They use a nonsense suppression method in *X.laevis* oocytes to introduce artificial amino acids in the receptor, in this case fluorinated aromatic amino acids. The fluorine withdraws the electrons from the aromatic ring due to its high electronegativity and with increasing the degree of fluorination, the capacity for an interaction with a cation decreases. The effect of the fluorinated amino acids is measured by determination of the EC_{50} by electrophysiology.

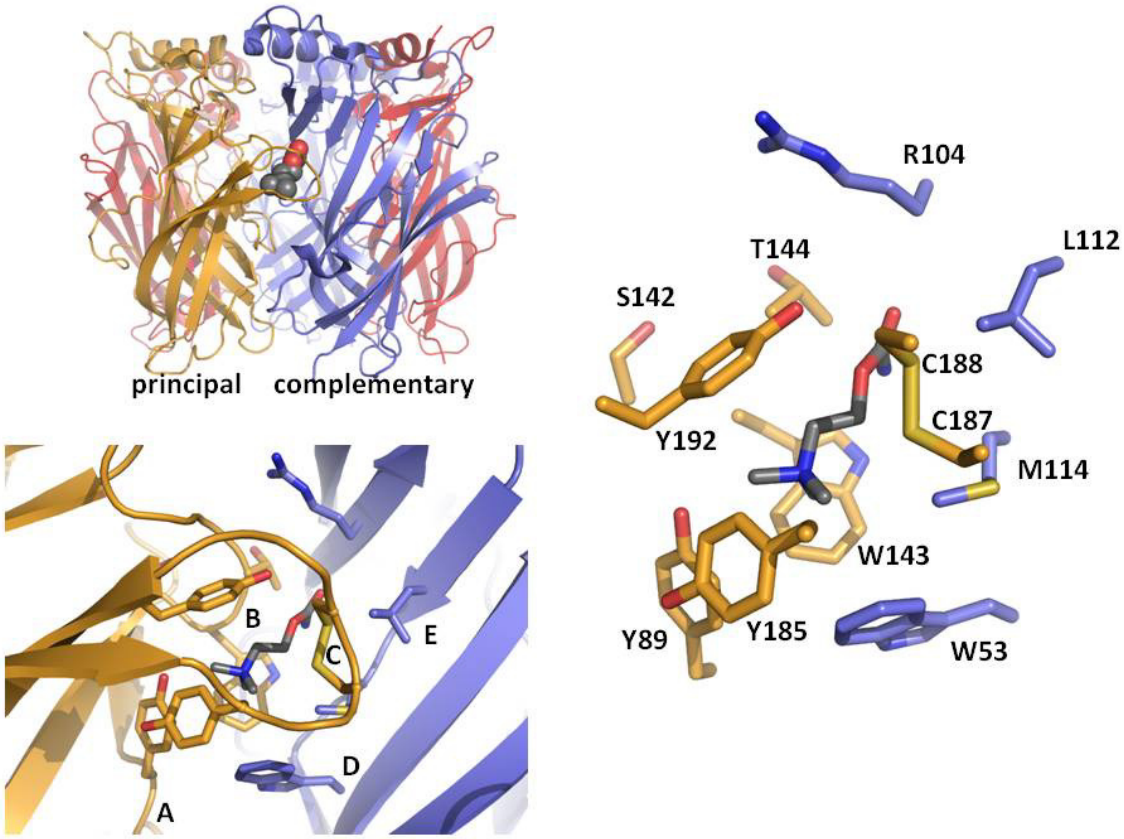

Figure 6 The secondary structure of the acetylcholine binding protein (AChBP) depicted as cartoon representation. The carbachol indicates the agonist binding pocket located in the dimer interface of the principal and complementary subunit. Carbachol is bound in the multi-loop binding site. It is interacting with residues of loop A to E. The main interactions in the ligand binding site are the cation-π interaction of the quaternary amine moiety with the aromatic ring formed by the tyrosines and tryptophans.

Experiments with an AChR containing a fluorinated tryptophan of loop B (residue 143 in AChBP numbering) with ACh and carbachol showed a linear dependence of the EC_{50} on the degree of fluorination. The fluorination of the other aromatic residues in the ligand binding pocket did not produce a similar shift in the EC_{50}, clearly demonstrating that the cation-π interaction is the main source of the interaction of tryptophan 143 with the natural agonists (*29*). Nicotine on the other hand exhibited a different behavior. In the same experiment, the EC_{50} of nicotine was independent of the fluorination of the tryptophan (*30*). These experiments proved that the physiological agonists ACh and carbachol exhibit a different binding mode than the neurotoxin nicotine, even though all of them are able to activate the receptor (Figure 7).

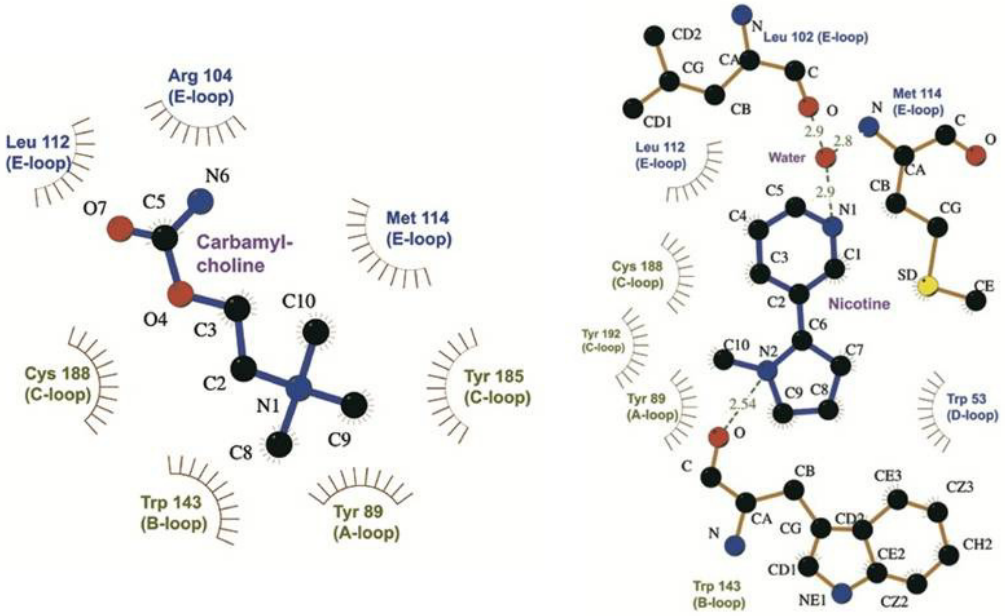

Figure 7 Detailed representation of the interactions of carbachol and nicotine in the ligand binding pocket of the AChBP. The binding mode of carbachol is mainly determined by the cation-π interaction, stabilizing the positive charge. The other amino acids interact with the agonist via van der Waal's contacts. Even the positively charged arginine 104 does not form an ionic interaction with carbachol. Nicotine is interacting differently. No cation-π interaction is required as the secondary and tertiary amino moieties are stabilized by hydrogen bonds to the protein backbone. Due to these interactions, nicotine has a much higher affinity to the AChR than carbachol.

The same method was also applied to $5HT_3$, GABA and glycine receptors whose aromatic amino acids in the ligand binding sites were fluorinated. The effects on the EC_{50}s are homologous to the AChR. Like the AChR, the $5HT_3$ receptor contains a tryptophan in the loop B, responsible for the cation-π interaction. In GABA and glycine receptors, there are two amino acids involved in a cation-π interaction with the agonist. They are tyrosines in the case of GABA receptors and phenylalanines in the case of glycine receptors. Equivalent to the ACh and $5HT_3$ receptors, one of them is located on loop B. The other position is unique to GABA and glycine receptors and located on loop C (*31*, *32*). All pLGICs thus share a similar chemistry for ligand binding and, despite this interaction was first observed in AChRs, it is even stronger in GABA and Gly receptors.

The chemistry involved in ligand recognition and binding is strongly conserved within the family of pLGICs. Despite there is no single determinant for agonist specificity, the activation of different receptors is very specific to their agonists. The agonist specificity is achieved through the interplay of all the residues which interact with the agonist, as they are distributed over all the loops within the ligand binding pocket (*33*).

Conformational changes

Movements of the ligand binding site upon ligand binding

The ligand binding domain is a dynamic structure that exists in different conformational states. pLGICs have a low affinity to their ligands in the closed, resting state and a higher affinity in the active open, state, reflecting the conformational changes in the ligand binding domain which ultimately lead to the activation of the channel. Upon prolonged exposure to the agonist, pLGICs enter a desensitized, closed state with an up to a thousand-fold higher affinity for the ligand than the active state. According to the ligand binding affinities, at least three different conformations of the ligand-binding domain are proposed to exist.

The conformational changes upon ligand binding were investigated using the AChBP from *Alpysia californica*. The protein was crystallized in the apo form and in complex with several agonists and antagonists (*34*). The most prominent difference in the structures was identified in loop C. Upon agonist binding, the loop undergoes an inward rigid body movement of 7Å. This movement, called loop C capping, closes the ligand binding pocket. In the presence of the antagonist α-conotoxin, the loop swings outward by about 4Å (Figure 8). Apart from the movements of loop C, there was also a minor outward movement of loop F observed in certain subunits.

The restriction of the ligand-induced conformational changes in the AChBP to the capping movement of loop C raised the question if the AChBPs are good model systems to understand channel activation. Although they are very homologous to the ligand binding domains of the AChR, the loops that interact with the transmembrane domain in the full receptor are different. No conformational change was detected in these loops so that the mechanism of signal transmission from the ligand binding site to the gate of the channel still remained to be elucidated. Additionally, agonist binding to pLGICs is highly cooperative, whereas the binding to the AChBP is not. Still, several observations in full length receptors are in accordance with the structural data obtained from AChBPs. Differences in the accessibility of residues in the AChR probed by deuterium exchange experiments, showed that residues of the loop C are less accessible in the presence of agonist, which is consistent with C loop capping (*35*). Additionally, Bouzat et al produced a functional chimera of the AChBP and the transmembrane domain of a $5HT_3$ receptor by adopting the loops that interact with the pore (*36*). This indicates that C loop capping might trigger a conformational change leading to activation. Even though the AChBPs cannot explain all aspects of the gating mechanism, similar movements of the loop C have been observed in the full receptors and seem to be conserved in the family.

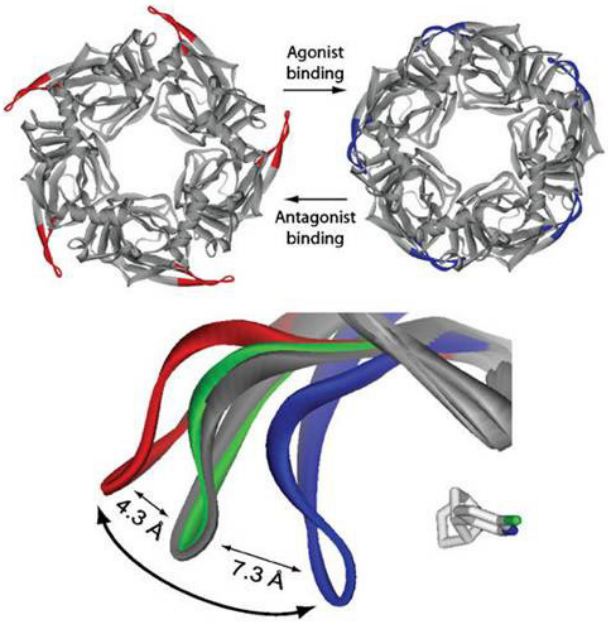

Figure 8 Mechanism of C-loop capping derived from structures of the AChBP, crystallized in the apo-, agonist- and antagonist bound state. The C-loop experiences a contraction from the apo structure (in green) to the agonist bound structure (in blue). This conformational change is believed to be the first step in the activation process of pLGICs. Antagonists on the other hand were found to push the C-loop outwards, corresponding to the observed difference between the apo structure (in green) and the antagonist bound structure (in red). Competitive inhibitors are therefore believed to inhibit receptor activation by preventing the C-loop capping.

Further insights into the conformational changes underlying channel activation were gained with the structures of the prokaryotic homologues ELIC and GLIC. GLIC is a proton gated channel and the region of the consensus ligand-binding site is filled with protonable side-chains of residues of the respective loops A-F. Ligand recognition in GLIC is therefore believed to occur by alteration of the protonation state of these amino acids although the residues involved in proton sensing still have to be elucidated. Despite the differences of the activation ligand, both pLGICs allowed first insights into potential structural changes of full length receptors upon ligand binding as GLIC was crystallized at low pH in a conductive conformation whereas the structure of ELIC was solved in the absence of agonist showing a non-conductive state.

The comparison of the two structures reveals large conformational differences in the extracellular domains. Very striking again is the loop C capping in GLIC compared to ELIC. Rearrangements are also evident for the F loop as well as the β1-β2 and the cys-loop, the main regions interacting with the transmembrane domain. The best way to describe the conformational change between GLIC and ELIC is a 12° rotation around an axis parallel to the two beta sheets of the extracellular domain (Figure 9) (*37*). It will have to be shown whether this relation is truly representative for a movement of the extracellular domain upon agonist binding.

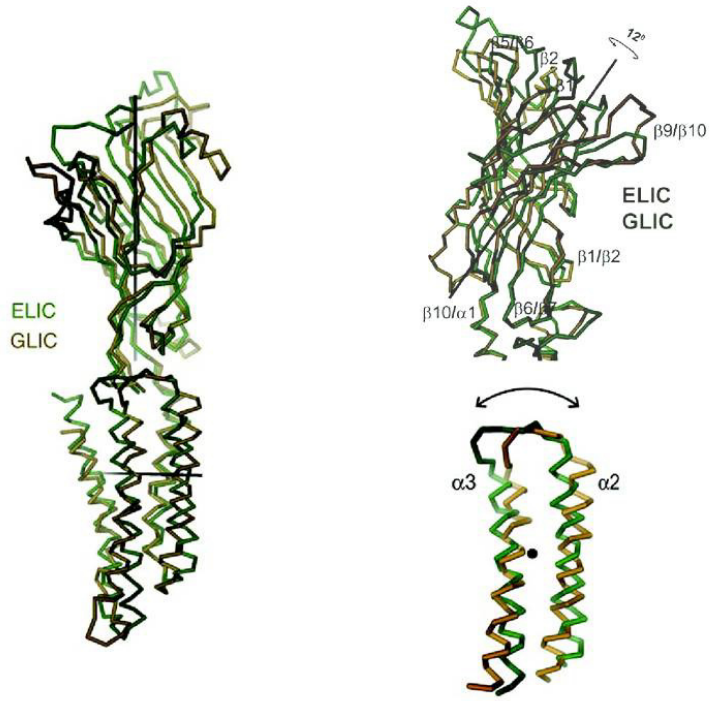

Figure 9 Conformational differences between the structures of ELIC and GLIC. Both the movements of the extracellular and the transmembrane domain can be described as rotations. The extracellular domain is rotated along an axis between the β-sheets. The movements in the transmembrane are restricted to the helices M2 and M3. They rotate along an axis parallel to the membrane. This movement was hypothesized to open the gate of the channel during the activation process.

Gating

LGICs are allosteric proteins. Binding of the ligand to its binding site in the extracellular domain triggers a conformational change in the molecule, which is transmitted over several nanometers to the pore.

The structures of both prokaryotic homologues offered insight into potential structural transitions of the pore upon gating. In contrast to the ELIC, the pore of GLIC is open, showing a funnel shaped and water accessible cavity that allows ion to flow through the membrane. The most striking difference between the two structures is found in the conformation of the transmembrane helices M2 and M3. As encountered before, the pore of ELIC is completely obstructed whereas in GLIC, the M2 and M3 helices underwent a 12° rotation relative to ELIC. This movement separates the three hydrophobic rings at the 9' to 16' positions, opening the gate of the ion channel. In contrast to the extracellular halve of the pore, the two polar and the charged rings at positions -1' to 6' moved closer, thereby forming a polar constriction that only allows desolvated ions to pass (*37*).

There are several interaction sites that potentially transmit the conformational changes in the extracellular domain upon ligand-binding to the transmembrane domain. The interface couples the independent movements of the two domains. The main interaction site in the pore region is the M2/M3 loop, which closely interacts with the cys-loop and the β1/β2 loop of the ligand binding domain. The involved regions

are highly conserved throughout the family. The comparison of the structures of ELIC and GLIC shows only minor changes in the cys-loop, whereas the β1/β2 loop adopts different conformations (Figure 10). In GLIC, the lysine at the tip of the loop interacts tightly with a proline on the M2/M3 loop, keeping the pore in the open conformation. This interaction is not evident in the structure of ELIC, where the equivalent residues are about 7Å apart. A salt-bridge that was identified in GLIC to stabilize the interaction between the β1/β2 loop and the pre M1 region, is absent in ELIC, which might be the cause of the big movement of the β1/β2 loop.

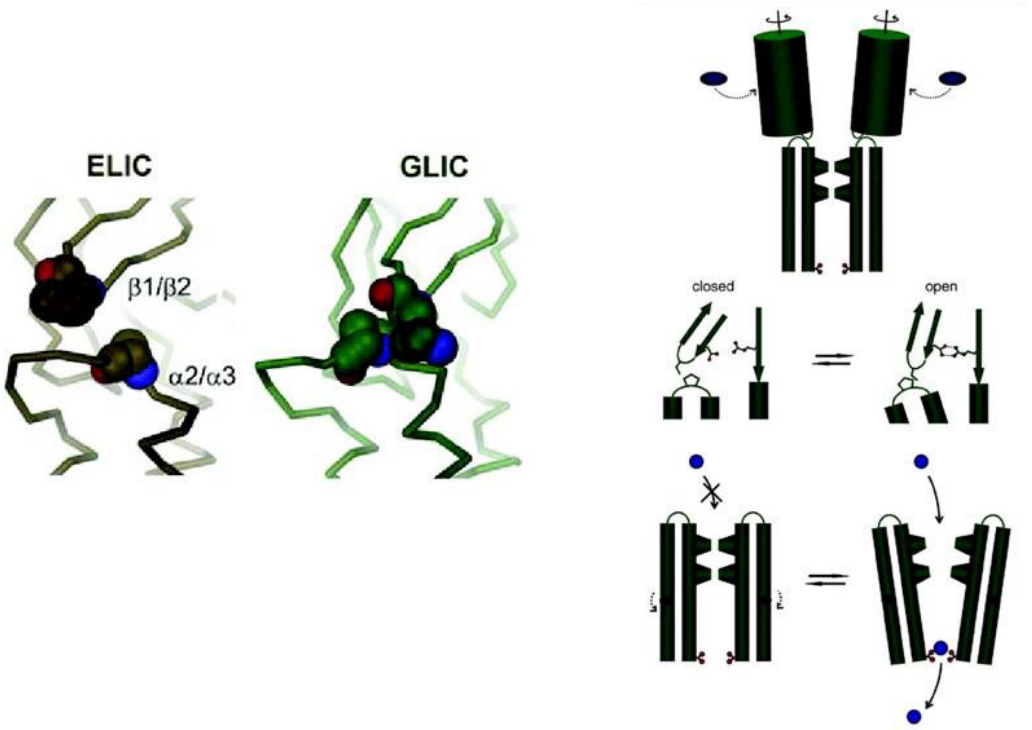

Figure 10 Differences between the ELIC and the GLIC structures in the coupling interface of the extracellular and the transmembrane domain. The interaction of the residue at the tip of the β1/β2 loop with the M2/M3 loop is believed to couple the movement of the domains. The schematic representation depicts the interactions in the principal pathway of coupling, where the signal of agonist binding is transmitted to the M2/M3 loop via the β1/β2 loop which is additionally stabilized by a hydrogen bond to the pre M1 region.

The laboratory of Steven Sine used single channel recording and thermodynamic mutant cycle analysis to investigate the interactions involved in gating of the AChR. They identified interactions of the β1/β2 loop and the cys loop with the M2M3 loop as well as the salt-bridge of the β1/β2 loop to the pre M1 as the main elements for coupling. The interactions were thus termed the principal pathway of coupling (*38–40*).

Desensitization

Desensitization is the reversible decrease or loss of a biological response upon prolonged or repetitive stimulation. Upon exposure to high concentrations of their agonist, pLGIC adapt an open conformation which exists only transiently. If the agonist is applied for a prolonged time, the channel closes by entering a desensitized

state. This is visible in electrophysiological experiments as a steady decline of macroscopic current in the presence of agonist. pLGICs desensitize also if they were purified and reconstituted, therefore desensitization has to be an intrinsic property of the receptors and it is not mediated by cytosolic components of the cells (*41*). The recovery from desensitization is a slow process that can only take place if the agonist is completely removed because desensitization can occur at very low concentrations of the agonist. The mechanism of desensitization can only be explained by a circular model where the receptors exist is at least 3 different states, the resting (R), active (R*) and desensitized state (D). In contrast to the transition from the R to the R* state, that requires high agonist concentrations, the transition from the R to the D state can already be induced by much lower concentrations. Consequently the D state must have an at least twentyfold higher affinity to the agonist (*42*). An intermediate desensitized state (I) was introduced to account for the observations that the decrease of the current due to desensitization shows a biexponential behavior and the time the receptor needs to recover from desensitization is dependant of the duration of the prior agonist exposure. For the muscle AChR the affinities of the different states were determined. The dissociation constant of the resting state is 50-100μM, of the intermediate state is 1μM and the desensitized state is 1nM.

Desensitization represents a classical property of allosteric proteins. The receptor population is distributed among different states of discrete conformations. Also in the absence of agonist, a small proportion populates the D state. The most recent quantifications report a fraction below 1% of the receptors (*43*). Due to the high affinity of the D state to the agonist, the receptors can be quantitatively desensitized by low concentrations of agonist without activating the receptor. On the other hand, the estimated rate of dissociation of the agonist from the desensitized state is much faster than the rate of recovery and it is therefore assumed that the recovery from desensitization is independent of the agonist affinity (*44*).

Even though desensitization is an intrinsic feature of almost all pLGICs, the physiological function is still ambiguous. In synapses, neurotransmitters are instantly reabsorbed or degraded and only present for several milliseconds but the desensitization rates of most pLGICs are on the second time scale and thus much slower. Desensitization could still accumulate during repetitive excitations of a synapse. The most common explanations are that desensitization is either a mechanism for the protection of the cells against excitotoxicity (*41*) or a mechanism to shape the short term plasticity of synapses.

Ion selectivity and conductance in pLGICs

Ions are hydrated in aqueous solutions and the energy difference of a naked Na^+ ion placed in a lipid bilayer compared to its hydrated state was estimated to be 164kJmol^{-1}. This high energy difference makes ions virtually insoluble in the low dielectric environment of the lipid bilayer, which therefore forms a potent barrier for ions. The water filled pores of ion channels offer a low energy path for ion through the membrane. The main determinants of selective ion permeation of an ion channel are the pore radius and the electrostatic interactions between the channel pore and the transported ion. It is obvious that a small pore radius can prevent bigger ions from passing through the pore, but also the chemical properties of the pore lining residues have to be taken into account for ion permeation. Calculations showed that a pore consisting of hydrophobic amino acids, despite being filled with water, would create an image potential of the entering ion. This image potential has the same charge as the ion and is strongest at the narrowest constriction of the pore. This leads to a strong repulsion which makes ion transport unfavorable, at least at physiological membrane potentials (*45*). The introduction of hydrophilic or charged amino acids into the pore reduces this energetic barrier and allows ion flux through the channel. The combination of the steric features and the polar and charged residues make an ion channel capable to discriminate between different ions.

The selectivity filter of an ion channel is usually located at the narrowest position in the pore. It consists of polar or charged groups that coordinate the ion during their passage it through the pore. One of the best understood ion channel is the potassium channel KcsA, since its structure revealed basis of its selectivity. The selectivity filter is formed by backbone carbonyl groups of all four chains of the tetramer. The main chain atoms are oriented in a way that the oxygen atoms of the carbonyl groups can exactly replace the water of the hydration shell of potassium. The interactions of the carbonyls with potassium compensate for the energetic costs of the removal of their hydration shell. In contrast, the desolvation energy of a sodium ion is much larger and it is too small to be coordinated with similar efficiency. Anions are simply electrostatically repelled by the selectivity filter. The potassium channel selectivity filter is an elongated structure with a diameter of about 3Å which contains multiple ion binding sites. It can accommodate two potassium ions in an almost fully dehydrated state at the same time which is important for the mechanism of permeation (*46*).

Compared to potassium channels, pLGICs are not as selective. The cation selective receptors do not discriminate between monovalent cations and additionally, they conduct divalent and even bigger organic cations. Also anion selective receptors do not discriminate between different halide anions and they conduct big anions such as nitrate, thiocyanate and formate. Due to this poor selectivity, pLGIC are termed charge selective.

The open pore of pLGICs is a funnel shaped structure with a constriction that is located at the intracellular, hydrophilic mouth of the channel. The diameter of the selectivity filter was estimated to be about 5-9Å, depending on the experimental technique and the receptor (*15*, *16*, *47*). The high resolution structures of the pLGICs

GLIC and GluCl show conducting conformations of the pore. Their structures revealed a constriction of 5-6Å in both cation- and anion-selective channels (*13*, *48*). Due to their larger pore radius and the fact that they are only charge selective, the selectivity filter of pLGIC is thought to conduct ions that are only partially dehydrated.

The main determinants of charge selectivity in pLGICs consist of the pore lining amino acids at the intracellular mouth of the channel. Site directed mutagenesis studies in the AChR revealed that the removal of this negative charge altered the permeability ratio of magnesium ions relative to potassium and decreased the conductance of potassium (*49*). Based on sequence conservation of the M2 helix of AChRs and GlyR, mutations were introduced to alter the charge selectivity of the receptors. Interestingly, only three mutations were necessary to reverse the selectivity of AChRs. The valine at position 13' was replaced with a threonine, the negatively charged residue at -1' was removed by truncation to alanine and a proline was inserted at the -2' position (*50*). Equivalent mutations could also change $5HT_3$Rs from cation to anion selective (*51*).

Similar mutations converting the charge selectivity of GlyRs allowed to identify the selectivity filter at the constricted region of the pore. The GlyR lost most of its anion selectivity when either the alanine at the -1' position was mutated to glutamate or the proline of the -2' position was deleted. If the two mutations were combined, the GlyR was cation selective (*52*). The equivalent mutations in GABAR also resulted in cation selective channels (*53*).

The structures of GLIC and GluCl confirm these earlier findings and reveal the structural basis for ion selectivity in pLGICs. Electrostatic calculations show that the entire pore of GLIC is negatively charged with the strongest charge at the intracellular mouth of the channel. GluCl carries a weak negative charge at the extracellular side of the pore, whereas the selectivity filer is strongly positively charged (Figure 11). The intracellular constrictions in both structures were shown to bind ions, caesium and rubidium in GLIC and iodide in GluCl, thus revealing a specific interaction of the ions with the selectivity filter. These structures thus suggest that the main determinants of ion selectivity in pLGICs comes from the electrostatic potential of the pore which attracts ions of opposite charge and repels ions carrying the same charge as the pore (*11*, *13*). It is remarkable that cation selective pLGICs require negatively charged amino acid side chains in the pore region, whereas anion selective channels do not contain charged groups lining the transmembrane part of the pore. This feature may be due to the fact that anion selective channels exploit the positive dipole moment at the N-terminus of the M2-helix to create the positive charge required for their selectivity. Cation selective channels, in contrast, would have to insert a negative charge at the end of the helix, the -1' position, to introduce the negative charge required for cation selectivity.

Two positions at the extra- and intracellular mouth of the pore were identified to be essential for the permeability of divalent cations. If the negative ring at the position -1' in the AChR is mutated, the channel is still permeable to monovalent but no longer to divalent cations (*50*). A GlyR, carrying the three mutations converting its selectivity

from anion- to cation selective, was found to be weakly permeable to divalent cations. The receptor harbors a positively charged ring of arginines at the 19' position at the extracellular entrance of the pore. The removal of this ring increased the permeability of divalent cations, even more if a ring of negative charges was introduced (*52*). These results underline the importance of negative charges at the intracellular and extracellular mouth of the pore for cation selectivity and the permeation of divalent cations.

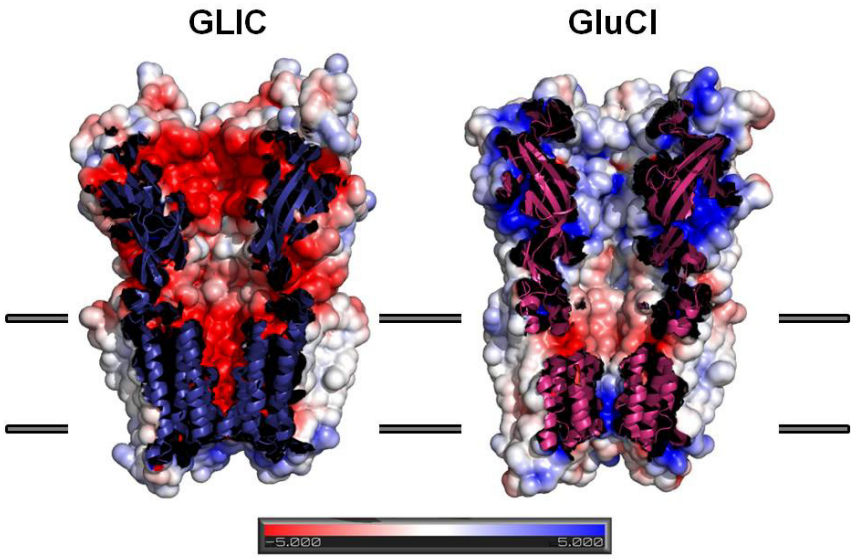

Figure 11 The calculated surface potential of the cation selective GLIC and the anion selective GluCl are shown (negative potential red and positive potential blue). The figure highlights the role of the electrostatic potential on the underlying mechanism of the charge selectivity of pLGICs. They create an attractive environment for the conducted ions and an insurmountable barrier for their counterions.

Determinants of conductance

The chemistry of the pore lining residues does not only alter the ion selectivity but also the conduction properties pLGICs. Several positions along the ion permeation pathway alter the conductance of the channel. The removal of the negative ring at the -1' position at the intracellular mouth of the AChR reduced the single channel conductance from 80 to 20 pS (*49*). Polar substitutions at the 2' position increased the conductance, whereas the introduction of non-polar amino acids decreased the conductance inversely proportional to their size (*54*).

Charged rings at the extracellular entrance of the pore also affected the conductance in AChRs, GlyRs and GABARs. The mutant inverting the charge selectivity of the GlyR contains a ring of arginines at the 19' position, which is unusual for native cation selective pLGICs. The substitution by alanine increased the conductance from 7pS to 14pS. The effect is even stronger if a negative charged glutamate is introduced at this position, increasing the conductivity to 22pS (*50*).

Next to the pore itself, also the intracellular domain located between M3 and M4 can influence the ion conduction. Three arginines matching the pattern of an α-helix were

identified on the intracellular domain a $5HT_3R$ subtype and the mutation of all of them in a homopentameric receptor increased the conductance from <1pS to 20pS (*55*).

Finally, also the wide extracellular vestibule contributes to the conductance of the channel. Using the structure of the AChBP, Hansen et al identified a conserved site in the vestibule of the extracellular domain of pLGICs. All cation selective receptors carry an aspartate at this position, whereas it is a lysine in anion selective receptors. By charge reversal mutations of this position in the AChR, they showed that the single channel conductance decreased fivefold (*56*). This charged ring in the vestibule of pLGICs is thought to initially stabilize the conducted ions and thereby increasing their local concentration. A similar feature is also observed in the comparison of the electrostatic potential of the extracellular vestibule of GLIC and GluCl (Figure 11). GLIC is cation selective and its vestibule is negatively charged whereas it is positively charged in the anion selective GluCl.

The positions influencing the permeation of ions across pLGICs are thus not concentrated in a single location of the protein. Similar to the determinants of ion selectivity, the charged surface of the entire ion permeation pathway, including the pore and the extracellular vestibule, determines the conductance of the receptors.

Modulation of pLGICs

Thanks to their important function in the central nervous system, pLGICs are targets of a variety of drugs as well as natural and artificial toxins. All of these compounds work by modulating the function of the target receptor, either by enhancing or inhibiting the response to the agonist which is called positive or negative modulation. Modulators are divided in three groups depending of their site and mechanism of action. The first group is formed by pore blockers, the second by orthosteric ligands which bind to the agonist binding site whereas the third group contains allosteric modulators which act at a site remote from the agonist binding site.

Pore Block

The simplest case of inhibition is pore block, where the ion flux is obstructed by the binding of the blocker and thereby the total response to agonist is reduced. Pore block is a general mechanism of inhibition of ion channels and it is pharmaceutically exploited, e.g. in the block of voltage gated sodium channels by the local anesthetic lidocaine (*57*). Big cations like tetraalkylammonium ions, quinacrine or lidocaine were also identified as inhibitors of the AChR and GLIC (*58*–*61*). A recent functional and structural investigation of GLIC showed that these molecules indeed bind to a site in the open pore. As shown by X-ray crystallography, the charged moiety of lidocaine is located close to the polar residue at the 6’ position whereas its bulky aromatic part is localized close to the 9’ and 13’ positions. The study thus confirmed that open pore blockers act by physically obstructing the pore as there are too big to permeate though the channel and thereby prevent other ions to enter the pore and pass through the channel (*62*).

Competitive Inhibition

Competitive inhibitors are orthosteric ligands that bind to the agonist binding site but, in contrast to an agonist, they fail to trigger the conformational changes that open the channel and instead even stabilize the resting conformation of the receptor. The agonist can compete with the antagonist for the binding site and thereby remove the inhibitor from the binding site. The inhibition by a competitive antagonist is therefore surmountable as all receptors can still be activated if the agonist concentration is high enough. In the presence of a competitive inhibitor, a dose response curve of a receptor shifts to higher agonist concentrations. This shift will not saturate because a higher concentration of inhibitor can always be surmounted by an even higher concentration of agonist. Competitive inhibitors are known for all members of the pLGIC family. There are small molecules, such as plant alkaloids which act as potent competitive antagonists. The most famous antagonists are DHβE and d-tubocurarine, both acting on AChRs, strychnine acting on GlyRs, bicuculline on GABARs and morphine and methadone on the $5HT_3$Rs. Besides these small inhibitors, a variety of animals, such as snails or snakes, evolved specific peptide toxins, like Bungarotoxin or α-conotoxin, acting as competitive antagonists of AChRs.

The affinity of a competitive inhibitor can be analyzed using the displacement of the agonist dose response curves by a Schild plot which was derived from the Gaddum equation (*63*, *64*):

$$\log(DR - 1) = \log[B] - pA_2$$

Where DR is the dose ratio, meaning the ratio of equiactive agonist concentrations in the absence and presence of inhibitor (e.g.$\frac{EC50'}{EC50}$), [B] is the concentration of the inhibitor and pA_2 corresponds to the logarithm of the dissociation constant K_B of the inhibitor. A plot of [B] against (DR-1) in a double logarithmic graph gives a linear relationship with a slope of unity and the intercept pA_2 which is the logarithm of the inhibitor concentration that is required to double the equiactive concentration of the agonist. This value corresponds to the dissociation constant of the inhibitor.

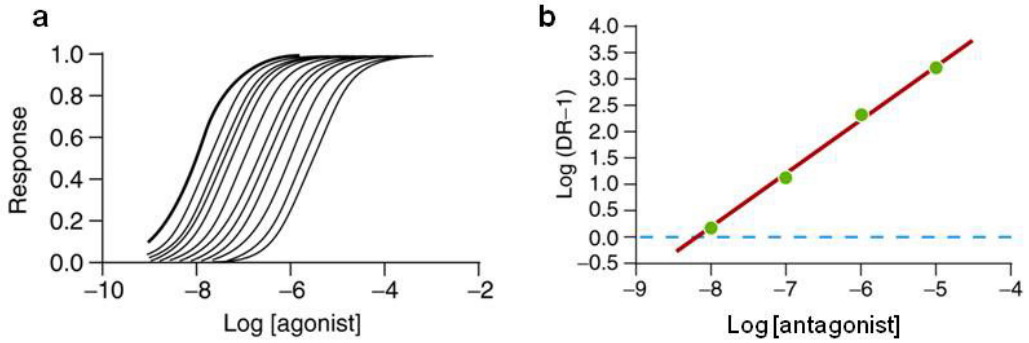

Figure 12 (a) Dose response curves of a receptor activated by its agonist at different concentrations of a competitive inhibitor. Due to the presence of the inhibitor, the curves shift to higher agonist concentrations. The data is transformed to the dose ratio at the corresponding antagonist concentrations and plotted in a Schild plot (b). The dissociation constant of the inhibitor can be deduced from the x-axis intercept.

Partial agonists

Another class of orthosteric modulators is formed by partial agonists. Partial agonists are often chemically related to the full agonist of a receptor. They bind to the same site as the agonist but only produce a small maximum response even at concentrations where the receptor is fully occupied. For 50 years partial agonism was explained by a difference in the efficacy of gating. The equilibrium of the gating step for a full agonist lies at the open state, whereas for a partial agonist it is shifted towards the closed state (*21*). The most thorough study on partial agonism was performed on the AchR and the GlyR (*65*). Based on the analysis of single channel events at different concentrations of full or partial agonists, a new intermediate state (flipped) was proposed. The flipped state was interpreted to correspond to a conformational rearrangement in the extracellular domain upon ligand binding prior to channel opening, for example the wrapping of the C loop around the ligand as proposed for C loop capping. It was also shown that the difference between full and partial agonist is not the equilibrium of the gating step, but rather of the transition between the resting ligand bound state and the flipped state.

Allosteric modulators

As previously described, pLGICs are allosteric proteins that exist in several conformations or states. The various conformations are occupied according to the differences in free energy by a Boltzman distribution. The receptors thus form a dynamic system of changing conformations. An allosteric modulator may have a high affinity for one or several of these states and bind to these once they are formed. Thereby the relative free energy of the states changes and the native equilibrium of conformations are biased towards the conformations bound by the allosteric modulator. This stabilization of a conformation can lead to multiple structural changes compared to the native protein and modify several properties of the receptor. Due to the coupling between different parts of the molecule, the binding site of the modulator can be remote from the site that is functionally affected by the modulation and there is no need for a direct interaction as the modulation is transmitted through the protein.

Allosteric modulators can act in two different ways on pLGICs. They can change the affinity of the receptor to the agonist by influence the equilibrium of the transition between the closed and the open state once the ligand is bound to the receptor. Depending on the compound, these effects can be positive or negative. Positive modulators are therefore also called allosteric potentiators, whereas negative modulators are termed allosteric inhibitors.

As previously seen, a change of either the affinity or efficacy shifts the EC_{50} and it requires further investigations to determine if the allosteric modulator is influencing the affinity of the agonist, the efficacy of gating or both of it. Regardless of the origin of the displacement of the dose response curves in the presence of antagonist, this

shift can be used to determine the pA_2-value and thereby the affinity of the modulator in a similar way as in the case of competitive inhibition.

One difference to competitive antagonism is that the effect of allosteric modulator is saturable. Therefore, the Schild equation is modified for allosteric modulators using a cooperativity factor α (*64*).

$$\log(DR-1) = \log([B](1-\alpha)) - (\log \alpha[B] + pA_2)$$

A negative modulator has α<1 which will cause a shift of the dose response curve to higher agonist concentrations, whereas a positive modulator has α>1, resulting in a shift to lower concentrations of agonist. This also means that at theoretically infinite concentration of the modulator, the apparent affinity to the agonist will saturate at $\frac{K_D}{\alpha}$. For allosteric inhibitors, the magnitude of α is inversely proportional to the ability to act like a competitive inhibitor. The adapted Schild equation for allosteric modulators becomes the Schild equation of competitive inhibitors if α is very small. Therefore in the case of allosteric inhibitors, if α is small and the tested inhibitor concentration range cannot reach saturation, it is possible to use the standard Schild plot for the determination of the affinity of the inhibitor without introducing a large error.

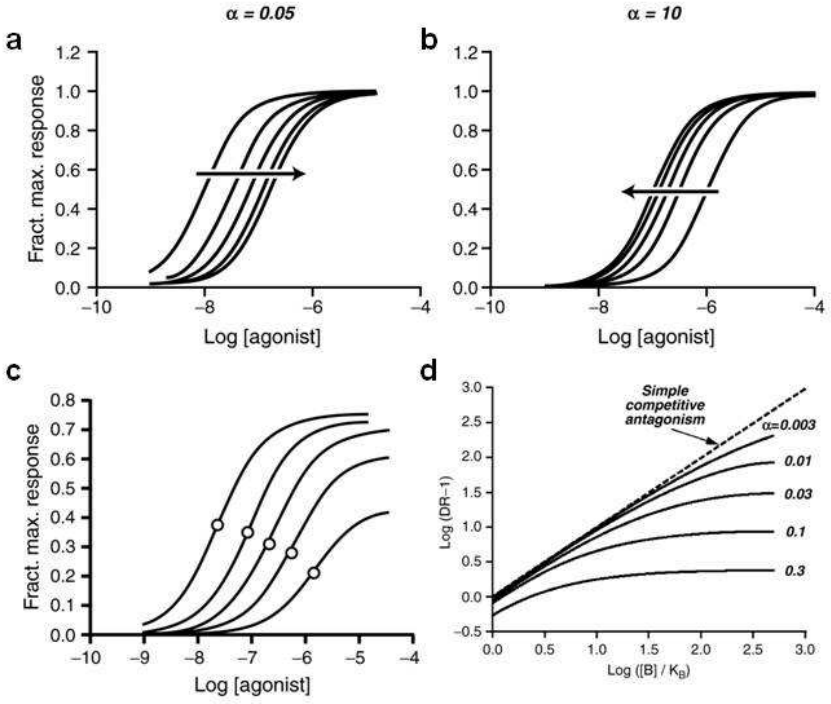

Figure 13 Effects of different allosteric modulators on the agonist dose response curves at increasing modulator concentrations. (a) Negative allosteric modulators shift the dose response curve to higher agonist concentrations whereas positive allosteric modulators cause a shift to lower agonist concentrations. The saturation of the effect is a hallmark of allosteric modulation. In the case of insurmountable allosteric inhibition (c), also the maximum response decreases next to the shift of the dose response curves. (d) Schild plot of allosteric inhibitors depicting the influence of the cooperativity factor α. If α is small, the saturation of inhibition is only apparent at very high concentrations of the antagonist and the inhibition appears to be competitive.

The modified Schild equation above was developed for surmountable allosteric modulators that reduce the affinity of the receptor to the agonist. If the allosteric modulator is not affecting the affinity to the agonist but the efficacy of the receptor

itself, a reduction of the maximum response occurs next to the displacement of the dose response curve. The Schild method can also be used in this case to measure the potency of such an insurmountable allosteric antagonist, but the pA_2-value of the Schild regression is then related to the true K_B by following expression:

$$pK_B = pA_2 - \log\left(1 + \frac{2\alpha[A]}{K_D}\right)$$

In the case of an allosteric inhibitor in combination with a highly efficacious agonist, the ratio $\frac{[A]}{K_D}$ is small and together with the low cooperativity factor α, the impact of the insurmountable property is diminished. Therefore, the pA_2-value of the Schild regression is a very good estimate for the true dissociation constant of an allosteric insurmountable inhibitor.

Several allosteric modulators of pLGICs have been discovered and characterized. All of them have distinct binding sites in the in the receptor, distant from the agonist binding site.

Benzodiazepines are widely used therapeutic compounds that potentiate GABARs. Benzodiazepines bind to a site in the extracellular domain located in the interface of the γ- and α-subunit, topologically equivalent to the ligand binding site. Benzodiazepines cannot activate the channel on their own but they allosterically increase the apparent affinity of the receptor to its agonist GABA which is binding to its binding site in the β- and α-subunit interface (*66*).

Also alcohols and general anesthetics are known to modulate different pLGICs and their effects depend on receptor type and subunit composition. Ethanol has been shown to potentiate AChRs and $5HT_3$Rs whereas longer alcohols have an inhibiting effect. In contrast, all alcohols have a potentiating effect on GlyRs and GABARs. Similar to long chain alcohols, general anesthetics are inhibitors of AChRs but potentiate GABARs and GlyRs (*67*). The binding site of both alcohols and general anesthetics is located in the transmembrane domain. For the AChR and $5HT_3$R, residues of the M2 helix were identified to be critical for the potentiation by ethanol (*68*) and anesthethics (*69*). Recently it was found that GLIC is also inhibited by the general anesthetics Propofol and Desflurane. In contrast to previous studies, both anesthetics were found to bind from the lipid bilayer to a cavity located between M1 and M4. Desflurane was found deeply buried in the cavity and to hydrophobically interact with all four transmembrane helices. Propofol on the other hand was found sandwiched between M1 and M4, not interacting with M2 and M3 (*70*).

Ivermectin is a macrocyclic lactone from the family of the avermecins that are produced by certain bacteria. Ivermectin is an allosteric potentiator of GluCl, the glutamate activated pLGIC of invertebrates. GABARs and GlyRs are also affected by ivermectin but they are about thousand fold less sensitive than GluCls. Mutational studies of the ligand binding site of GluCl could decrease the response to glutamate but failed to affect the response to ivermectin and therefore showed that the binding sites of glutamate and ivermectin do not overlap (*71*).Certain isoforms of GlyRs and GABARs can even be activated by ivermectin only (*72*, *73*).

The question about the binding site and the mechanism of potentiation was finally resolved with the structure of a GluCl from *C.elegans*. It was shown that ivermectin binds in the transmembrane domain between the M3 of the principal and the M1 of the complimentary subunit. It inserts deeply into the subunit interface where it forms a hydrogen bond with a serine on M2 and it interacts closely with the M2M3 loop. By comparing the structure of GluCl to GLIC and ELIC, it was hypothesized that ivermectin is activating GluCl by separating M1 and M3 by 3Å and thereby pulling top of the M2 away from the center of the pore. This movement is thought to open the gate by adopting a conductive conformation with a pore structure very similar to GLIC (*13*).

Next to these big organic compounds, small inorganic cations such as calcium, magnesium and zinc are known to modulate the function of pLGICs. The effect is dependent of the receptors type, as AChRs are potentiated by calcium ions whereas $5HT_3$Rs are inhibited (*74–76*). AchRs and $5HT_3$R are also potentiated by zinc ions where GlyRs and GABARs are inhibited (*77–79*). These studies have postulated different binding sites for the interaction with divalent cations, either located in the pore of the channel or the extracellular domain in the interface between the subunits. The calcium interaction site for the potentiation of AChRs was found to consist of a glutamate in the loop F as the potentiation was lost upon a mutation to glutamine (*50*, *80*). The inhibition of $5HT_3$Rs by calcium was found to be associated to the ligand binding site and to appear as competitive inhibition (*81*). The equivalent sites in loop F as identified in the AChR were also mutated in the $5HT_3$ receptor but the mutants still showed modulation by divalent cations. A mutation of an aspartate at the extracellular mouth of the pore to alanine was found to abolish the modulation by calcium. Therefore it was concluded that the interaction site for divalent cations in the $5HT_3$Rs is located in the pore (*82*, *83*). Mutational analysis of GABARs revealed that the binding site of zinc is located in the extracellular domain between the subunits and is formed by histidines and glutamates. Interestingly, this site is located at a similar position as proposed for the AchRs (*79*).

Although it is believed that the regulation of pLGICs by divalent cations plays an important role in the physiology of these receptors, and despite the fact that the effect has been described in different studies, the underlying mechanism is still poorly understood.

Aim of the work

The function of pLGICs is well understood and very detailed models of receptor function were developed, but the formulation of a molecular mechanism was impossible for a long time due to a lack of high resolution structures. The first mechanisms were proposed using the 4Å EM-structure of the AChR and the crystal structures of the AChBPs. These mechanisms based on the information collected from many different sources, because it was still not possible to obtain high resolution structural and the corresponding functional data from the same native receptor. This only changed with the high resolution structures of the two prokaryotic homologues ELIC and GLIC and the eukaryotic GluCl.

The structure of ELIC has offered the first insights at high resolution into the architecture of pLGICs. In combination with the two structures of GLIC and GluCl, ELIC has contributed to the comprehension of selective ion conduction, but our mechanistic understanding of the gating process is still poorly understood. Both GLIC and GluCl suffer from certain drawbacks if used as model systems. The activation of GLIC is not dependent on the binding of small molecular agonist but on the protonation state of the receptor itself, a ligand recognition mechanism not found in eukaryotic pLGICs. The structure of GluCl was solved from a truncated homopentamer of the α-subunit, which is only partially activatable by its native agonist glutamate and requires the allosteric modulator ivermectin for full activation. The use of GluCl for functional studies might thus be limited. Therefore, ELIC remained an attractive model system for pLGICs where detailed structural and functional studies could be carried out on the same protein. Moreover, its compactness and the possibility to produce milligram amounts of protein, makes ELIC accessible for spectroscopic studies and calorimetry. Unfortunately, nothing was known about the function of ELIC at the beginning of this thesis.

The first aim of this thesis was to identify molecules that act as agonists on ELIC and to characterize the functional properties of ELIC with respect to channel opening, agonist binding and ion permeation. Next to establishing ELIC as a model system for the pLGIC family, a second goal was to stabilize the open state of the protein to make it accessible for the structure determination of ELIC in a conducting conformation. The first question was successfully addressed with results described in the first publication about the ligand activation of ELIC. The second question proved to be challenging and has so far not yet been successfully approached.

The second aim of this thesis was raised during the work with ELIC. It was realized that divalent cations are very potent in reducing the current elicited by ELIC. Divalent cations are known to be important modulators of pLGICs. Due to the high functional similarity of ELIC to eukaryotic receptors, the goal of this second project was to identify the origin of this inhibition and to elucidate its mechanism using both structural and functional assays. The study has revealed insight into the mechanism of inhibition by divalent cations and is described in the second publication.

Results

Ligand Activation of the Prokaryotic Pentameric Ligand-Gated Ion Channel ELIC

ELIC was initially identified as a prokaryotic member of the pLGIC family based on sequence conservation. Its structure, which was recently determined at high resolution, is highly conserved compared to eukaryotic receptors, and thus confirmed the close relationship between pro- and eukaryotic channels. In contrast to our structural knowledge, little is known about the physiological role of ELIC in bacteria. Thus it was difficult to deduce which molecules could trigger ELIC activation. This major drawback had to be overcome before ELIC becomes accessible to detailed structure-function investigations.

The first publication in this thesis summarizes the results on the identification of ELIC agonists and the initial biophysical characterization of the channel. Different expression systems in combination with various electrophysiological methods were investigated for their suitability for agonist screening. Transiently transfected HEK 293 cells showed robust surface expression of ELIC and could be used to measure ELIC mediated currents in a planar patch clamp setup. Also the reconstitution of purified ELIC in liposomes and their fusion to an artificial bilayer was tested. Both systems turned out to be inappropriate for agonist screening, as the application of different compounds led to a loss of the patch or resulted in rupture of the bilayer. Therefore, a more robust system, the expression of ELIC in *X.laevis* oocytes was combined with two-electrode voltage-clamp for agonist screening.

A library of compounds was assembled based on the available structural information on the ligand binding pocket (Figure 14). The structural alignment revealed that the binding pockets of AChBP and ELIC are of similar size, even though sequence alignments showed a stronger conservation of ELIC to the GABARs and GlyRs. Further, it was known from earlier structural investigations that inorganic monovalent cations bind to the ligand binding pocket, thus implying that the agonist should be cationic as well (*10*). The library thus contained about 250 organic cations of similar size as known neurotransmitters.

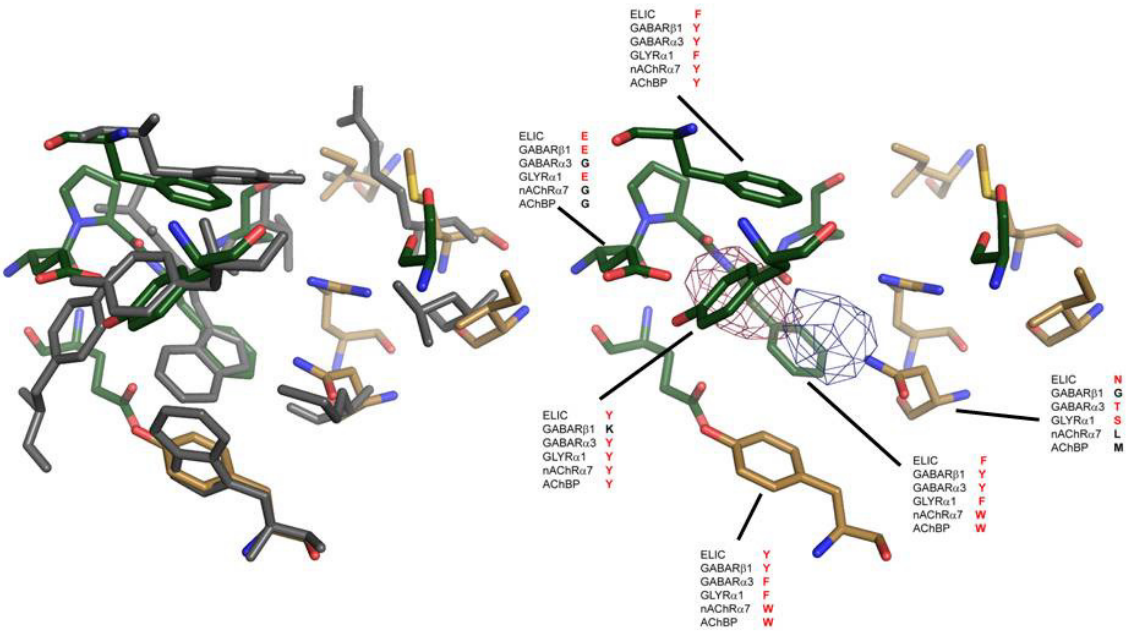

Figure 14 (left) The superposition of the ligand binding sites of AChBP (gray) and ELIC (principal side green, complementary side orange) reveals a pocket that is similar in size and conserved in its chemical character. (right) The ligand binding site of ELIC binds inorganic monovalent cations. The red and blue mesh shows the anomalous difference densities of the coordinated Tl^+ and Cs^+ ions respectively. The conservation of the ligand binding residues is indicated by the corresponding amino acids of selected eukaryotic pLGICs. The strong conservation to GABARs and GlyRs is evident.

Several molecules of this library were found to evoke currents in ELIC expressing oocytes. The potency of these molecules was quantified by the measurement of dose response relationships. Both the apparent affinities and the maximal evoked currents of all agonists were determined and compared to cysteamine, the most potent of the identified ligands. X-ray crystallography was used to identify the agonist binding site of ELIC. In addition, the biophysical properties of ELIC, its ion selectivity and single channel conductance as well as activation and deactivation kinetics were determined by patch clamp electrophysiology and recording of reconstituted protein in artificial bilayers.

The results place ELIC in the branch of the cation-selective pLGICs. As all the functional properties of ELIC are similar to the eukaryotic receptors, the results from investigations performed on ELIC are representative for pLGICs.

OPEN ACCESS Freely available online PLoS BIOLOGY

Ligand Activation of the Prokaryotic Pentameric Ligand-Gated Ion Channel ELIC

Iwan Zimmermann, Raimund Dutzler*

Department of Biochemistry, University of Zurich, Zurich, Switzerland

Abstract

While the pentameric ligand-gated ion channel ELIC has recently provided first insight into the architecture of the family at high resolution, its detailed investigation was so far prevented by the fact that activating ligands were unknown. Here we describe a study on the functional characterization of ELIC by electrophysiology and X-ray crystallography. ELIC is activated by a class of primary amines that include the neurotransmitter GABA at high micro- to millimolar concentrations. The ligands bind to a conserved site and evoke currents that slowly desensitize over time. The protein forms cation selective channels with properties that resemble the nicotinic acetylcholine receptor. The high single channel conductance and the comparably simple functional behavior make ELIC an attractive model system to study general mechanisms of ion conduction and gating in this important family of neurotransmitter receptors.

Citation: Zimmermann I, Dutzler R (2011) Ligand Activation of the Prokaryotic Pentameric Ligand-Gated Ion Channel ELIC. PLoS Biol 9(6): e1001101. doi:10.1371/journal.pbio.1001101

Academic Editor: David E. Clapham, Harvard Medical School, United States of America

Received March 17, 2011; **Accepted** May 31, 2011; **Published** June 21, 2011

Funding: The research leading to these results has received funding from a grant from the Swiss National Science Foundation (grant no. 31003A_124799) to RD. The funders had no role in study design, data collection and analysis, decision to publish, or preparation of the manuscript.

Competing Interests: The authors have declared that no competing interests exist.

Abbreviations: AChBP, acetylcholine binding protein; nAChRs, nicotinic acetylcholine receptors; pLGICs, pentameric ligand-gated ion channels

* E-mail: dutzler@bioc.uzh.ch

Introduction

The pentameric ligand-gated ion channels (pLGICs) constitute a large family of ionotropic neurotransmitter receptors that are ubiquitously expressed in the animal kingdom. In vertebrates the family encompasses cation selective serotonin and nicotinic acetylcholine receptors (nAChRs) and anion selective GABA and glycine receptors [1]. All family members share a conserved molecular architecture and a similar functional behavior. The proteins act as gated ion channels that are closed in their resting state and that open a selective ion conduction pore upon the binding of a ligand to a site located on an extracellular domain [2–6]. These properties are shared by close prokaryotic homologues that are encoded in the genome of certain bacterial species [7–9]. The X-ray structures of two prokaryotic pLGICs from the plant pathogen *Erwinia chrysanthemi* (or *Dickeya dadantii*, ELIC) [10] and the cyanobacterium *Gloebacter violaceous* (GLIC) [11,12] have recently revealed first structural insight into the family at high resolution. While both structures are similar overall, distinct conformational differences in the ligand binding domain and the transmembrane pore domain indicate that they represent different functional states of the protein, with ELIC showing a non-conducting and GLIC a conducting state (Figure S1).

The functional properties of GLIC, which is opened by a decrease of the extracellular pH, have been investigated by electrophysiology [13]. The protein forms cation selective channels with slow opening kinetics and currents that are stable over an extended period of time. The latter property differs from most eukaryotic pLGICs that quickly inactivate after opening [14–16]. The analogous ion permeation properties and the sensitivity to the same set of open channel blockers underline the close structural relationship of the ion conduction pore between GLIC and the nAChR [13,17], which is also manifested in the sequence conservation of this region (Figure S1G). Although, based on sequence similarity and an initial functional characterization [10], ELIC is also expected to belong to the same group of cation selective channels, it has so far been impossible to investigate its detailed properties since the stimulus for its activation was unknown.

ELIC shows a non-conducting conformation of the pore [10,18], whose correspondence to the resting state of eukaryotic pLGICs is currently unclear [7,19]. The structural similarity of its extracellular part to the acetycholine binding protein (AChBP), a soluble protein that closely resembles the ligand-binding domain of nAChRs, however, suggests a conserved mode for ligand interactions (Figure 1, Figure S2) [10,20]. Structures of the AChBP in complex with different agonists of the nAChR have provided a detailed picture of this process and have helped to rationalize previous biochemical studies [3,21–23]. The ligand binding site is placed in a pocket at the interface of adjacent subunits of the pentameric protein. The two halves of the pocket are termed "principal" and "complementary side," respectively, depending on the subunit in which the contributing residues are located. On each subunit residues from different regions of the molecule line the ligand binding pocket. Their location was named according to early experiments (Figure S2A) [24]. Based on this nomenclature the principal side contains the regions A, B, and C and the complementary site the regions D, E, and F. The conserved residues include several aromatic side chains, which provide delocalized electrons to stabilize the positively charged quaternary ammonium group (Figure S2C) [25,26]. The structural similarity between ELIC and AChBP extends to the

Author Summary

Electrical signal transduction at chemical synapses of nerve and muscle cells is initiated by the binding of neurotransmitters to their receptors, which function as gated ion channels that open a selective ion conduction path in the ligand-bound state. The pentameric ligand-gated ion channels constitute a very important family of neurotransmitter receptors that includes, amongst others, the nicotinic acetylcholine receptor. While most pLGICs are expressed in higher eukaryotes, there are few family members found in bacteria. These bacterial channels share the overall structural features of the family and are thus expected to function by similar mechanisms, but although the channel from the bacteria *Erwinia chrysanthemi* has revealed first structural insight into the family at high resolution, its functional characterization was impossible since activating ligands were not known. In our study we have identified ligands activating ELIC and we have located their binding by X-ray crystallography. Ligand binding causes the transition into an open state, which, as in eukaryotic receptors, is only transient and which slowly inactivates in the presence of the ligand. By single channel analysis we found that, similar to the acetylcholine receptor, ELIC forms cation selective channels. With known ligands ELIC has become an important model system to study the general mechanisms of the family.

ligand binding site, which also in ELIC contains conserved aromatic positions that surround a pocket of about the same volume (Figure 1, Figure S2). It was thus assumed that ELIC might be opened by a ligand of similar size and chemical properties [10].

Here we have investigated the activation of ELIC by small molecular ligands by X-ray crystallography and different electrophysiological techniques. Our study has identified a class of primary amines that open the channel by a strongly cooperative process. Although the open state is comparably stable the channels desensitize with slow kinetics. An X-ray structure of ELIC in complex with a ligand shows electron density in the consensus binding site, thus suggesting that the mechanism of activation is conserved. The open channel of ELIC mediates the permeation of cations with a large single channel conductance and selectivity properties that resemble other cation selective members of the family.

Results

Activation of ELIC

To identify ligands that activate ELIC we have expressed the protein in *Xenopus laevis* oocytes and investigated the response to potential agonists by the two-electrode voltage-clamp technique. Based on the volume and chemical properties of the proposed ligand binding region and the presence of positively charged ions bound to this site, we reasoned that parts of the agonists might have a cationic character [10]. We have thus selected a set of cationic and zwitterionic compounds with an approximate size of neurotransmitters for screening. Our library included different natural products such as amino acids and their derivatives, metabolites, and related synthetic substances (Figure S3A). Among the investigated molecules, only those containing a primary amino moiety at one end of a linear two- to four-atom-long carbon chain showed an activating response on ELIC-mRNA injected oocytes when added to the extracellular solution in low millimolar concentrations (Figure 2). The same compounds did not have any effect on water-injected control oocytes. Besides alkylamines all ligands contain atoms with lone electron pairs on the other end of the carbon chain. The size of the agonist is dependent on its chemical nature. For amino alcohols strong activation is obtained for amino-butanol and amino-propanol (Figure 2). The response to brominated amines is shifted towards shorter chain-lengths, with bromoethylamine and bromopropylamine both opening the channel. Ethylamine and propylamine activate the channel while the effects of butylamine and the branched isopropylamine are weak (Figure 2, Figure S3B). Among aminothiols, cysteamine is the most efficacious, while the response to homocysteamine is small. Different polyamines from diaminoethane to putrescine, but not cadaverine, activate ELIC in a state where one of the two amino groups is deprotonated. Due to the shift of one of its pK_a values, the short diamine aminoethane is thus already active at neutral conditions, while a significant effect by the natural product putrescine is only observed at higher pH (Figure 2, Figure S3B). Remarkably also the neurotransmitter GABA shows an activating

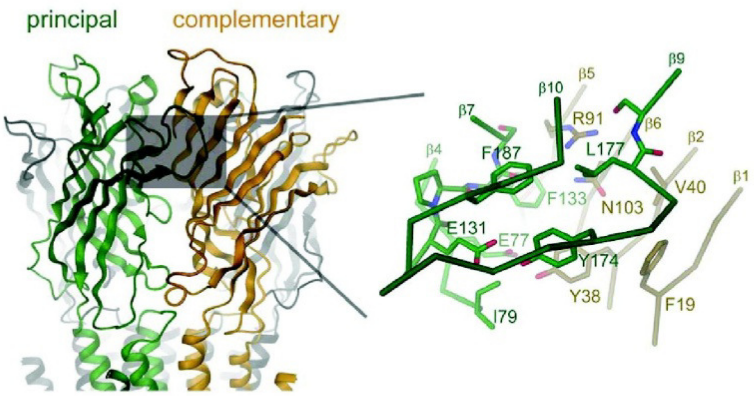

Figure 1. Ligand binding region of ELIC. Left: ribbon representation of the ligand binding domain of ELIC. The subunits contributing to the principal and complementary side of the binding region are colored in green and orange, respectively. The binding site is marked by a grey box. Right: zoom into the binding site. The protein is shown as Cα-trace with residues lining the binding pocket shown as stick model. The residues and secondary structure elements are labeled. Structures displayed in Figures 1, 3, and 5 were prepared with DINO (www.dino3d.org).
doi:10.1371/journal.pbio.1001101.g001

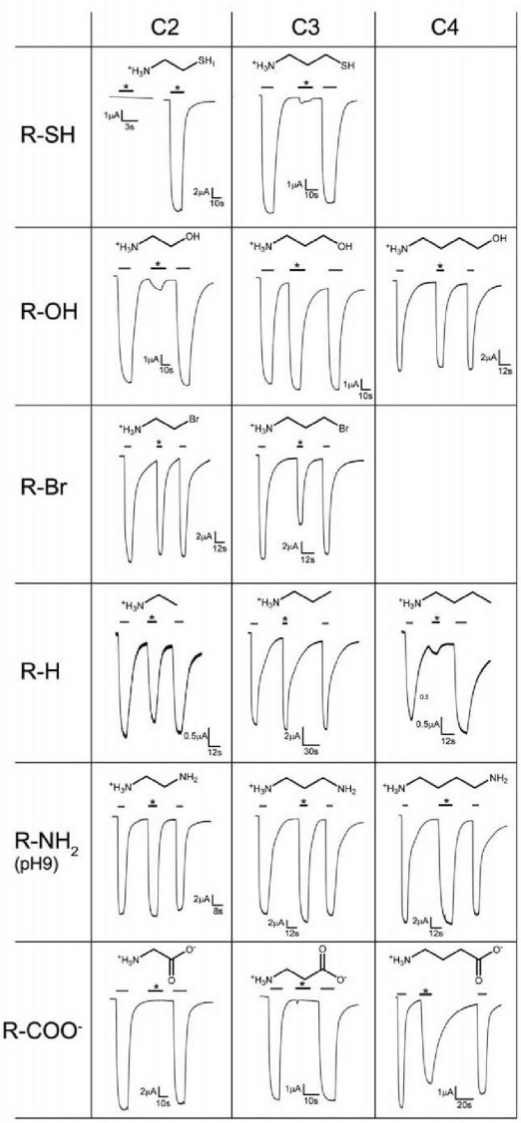

Figure 2. Current response of ELIC to different ligands. The chemical structures of the ligands are shown above the traces. Currents were recorded from oocytes at −60 mV with the two electrode voltage clamp technique. Top left: the response to 2 mM cysteamine is shown for water-injected control oocytes and for oocytes expressing ELIC. The application of the ligand is indicated (bar, *). All other traces show the response to agonists in comparison to the response to cysteamine. Agonists were applied to the outside in a concentration of 10 mM. The activation by cysteamine (grey bar, 2 mM) is followed by the application of a different agonist (black bar, *, 10 mM) and another activation by cysteamine (grey bar, 2 mM). Ligands are grouped according to their chemical properties and length of the aliphatic chains.
doi:10.1371/journal.pbio.1001101.g002

response at low mM concentrations, while the response to the shorter beta-alanine and glycine is absent (Figure 2).

The strongest response at low ligand concentration is evoked by cysteamine, the decarboxylation product of the amino acid cysteine. We have thus used this molecule as an agonist in most subsequent experiments. At the pH of the recording solution, the majority (>96%) of the sulfhydryl groups ($pK_a = 8.4$) are protonated and ligands thus carry a positive net-charge. Stable currents over a period of seconds were obtained upon addition of high micromolar concentrations of cysteamine to the extracellular medium (Figure 3A). At longer incubations with the ligand, however, the currents decayed, which is indicative for a slow desensitization of the channel (Figure S4A). The channel shows a steep voltage-independent activation with an EC_{50} of 365 µM and a Hill coefficient of 2.7, which points at a strongly cooperative process. To follow the time-course of activation and deactivation, we have investigated excised outside-out patches in response to fast solution exchange. A similar phenotype of currents as previously seen in two-electrode voltage clamp recordings, although with faster kinetics of desensitization, was also observed for macroscopic currents in a patch clamp experiment (Figure 3B, Figure S4B). At 5 mM cysteamine, channel activation and deactivation can be approximated by exponential functions with time constants in the ms range ($\tau_{act} = 20 \pm 5$ ms, $n = 19$, $\tau_{deact} = 53 \pm 7$ ms, $n = 19$, all errors are s.d.). As expected for ligand-gated channels, the activation but not the deactivation rates are dependent on the ligand concentration (Figure S4C). Since the observed time constants are within the range required for solution exchange, the values are upper limits for the processes and might even proceed with somewhat faster kinetics.

Other agonists activate ELIC in a similar cooperative process as cysteamine, although at higher concentrations (Figure 3C). A ranking of the ligands with respect to their potency is shown in Table 1. In most investigated cases, the responses at saturating ligand concentrations were comparable to cysteamine, thus suggesting that the corresponding maximum open probabilities of the channel are close (Figure 2, Table 1). GABA opens the channel with an EC_{50} of 2.4 mM, which is higher than that observed for other ligands. At a fixed pH, the potency of diaminoalkanes decreases with increasing chain length, partly reflecting the protonation state of the molecule. Although at pH 8.0 the EC_{50} of putrescine is high, it significantly decreases at higher pH values and it is similar to cysteamine if only the fraction of molecules is considered where one of the two amino groups is uncharged (Figure 3D).

The Ligand Binding Pocket

The chemical nature of the activating ligands as short unbranched primary amines and the response of ELIC to the neurotransmitter GABA mirror the structural conservation in the ligand binding pocket (Figure 1, Figure S5). In its center the binding site is framed by aromatic residues that are found in all members of the family, but among different pLGICs the relationship is closest to inhibitory neurotransmitter receptors such as GABA and glycine receptors [2,27–29]. It is thus noteworthy that the gene encoding for ELIC (protein_id: ADN00343.1) has been annotated as a GABA receptor homologue. On the principal side the conserved residues include Glu131 and Phe133 on β-7 (loopB), Tyr 174 on β-9, and Phe187 on β-10 (loopC). On the complementary side, Tyr38 on β-2 (loop D) and Asn103 on β-6 are conserved. The differences in other residues lining the pocket likely account for the unique agonist specificity of ELIC when compared to eukaryotic receptors.

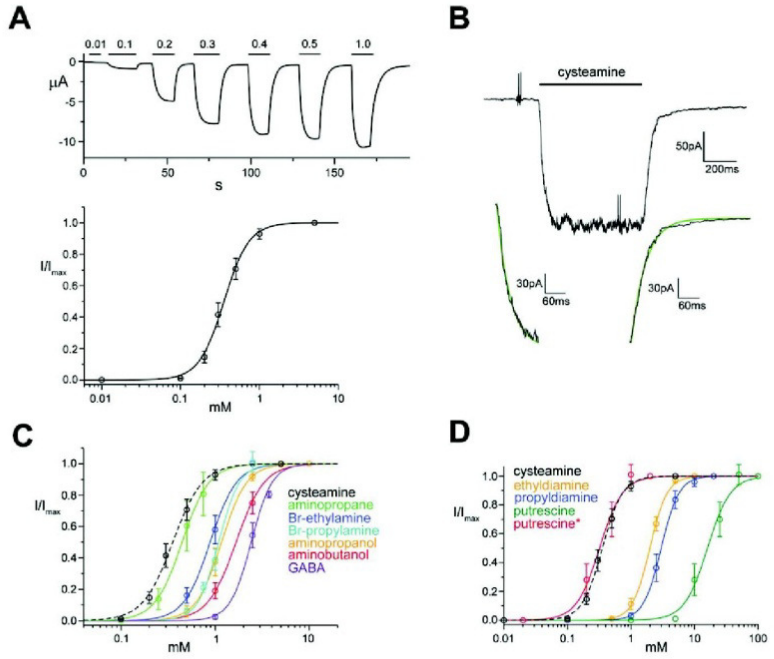

Figure 3. Ligand activation of ELIC. (A) The current response upon application and washout of cysteamine was recorded at −60 mV with the two-electrode voltage clamp technique. The application of cysteamine at the respective concentration is indicated above (black bar). The relative open probability (I/I_{max}) plotted as a function of the ligand concentration is shown below. The currents were normalized to the maximum at saturating ligand concentration (i.e., 5 mM). The average of 10 oocytes and their standard deviations are shown. The solid line shows a fit to a Hill equation with a coefficient of 2.7. (B) Activation and deactivation kinetics. Macroscopic currents from a membrane patch in the outside-out configuration were recorded at −60 mV in response to a fast exchange into solutions containing 5 mM cysteamine. The fit of the current increase upon application of the ligand and the decrease upon washout to a single exponential function is shown below. (C) Dose response curves for the activation of ELIC by different agonists. Currents were recorded with the two electrode voltage clamp technique at −60 mV. The solid lines show fits to a Hill equation. The dose response curve for cysteamine (black, dashed line) is shown for comparison. (D) Dose response curves for the activation of ELIC by diamines. Currents were recorded with the two electrode voltage clamp technique at −60 mV and pH 8. The solid lines show fits to a Hill equation. The red trace (putrescine*) shows a fit to the fraction of putrescine at pH 8 that carries a single positive charge. The dose response curve for cysteamine (black, dashed line, measured at pH 7) is shown for comparison.
doi:10.1371/journal.pbio.1001101.g003

In an attempt to locate bound agonists we have soaked bromopropylamine into crystals of ELIC and we have collected data at the anomalous absorption edge of bromine. The overall structure of the protein was not visibly affected by this procedure. Despite the comparably low resolution of the data, strong peaks in anomalous difference Fourier maps in all binding pockets of the two the channels in the asymmetric unit reveal the presence of bound ligands (Figure 4A). When placing bromopropylamine into these sites the primary amino group is located close to the two carboxyl groups of Glu77 and Glu131 of the principal subunit and the bromide moiety is found close to the residues Asn103 and Arg91 at the complementary side.

To investigate the role of residues surrounding the bound ligand for channel activation, we have mutated single residues to alanine and we have measured activation with the two-electrode voltage-clamp technique (Table 2). For many mutants there was no response to the addition of cysteamine. This was the case for all investigated residues of the principal site, such as Glu77 and Glu131, that may interact with the primary amino group and hydrophobic and aromatic residues (i.e., Phe187, Phe133, Tyr174, Ile79) that surround the aliphatic carbon atoms of the ligand. The effect of mutations on the complementary side, in contrast, was diverse and in some cases less drastic. The mutations of Phe19 on β-1 and Val40 on β-2 shifted the activation towards higher agonist concentrations (Figure 4B). The mutations of two residues that were found close to the bromine position in the crystal structure had opposite effects: While the mutation of Asn103 did not show an activating response, the truncation of a nearby Arg91 increased the apparent affinity for the ligand as reflected in a 4-fold decrease of the EC_{50} for cysteamine and a smaller 2-fold decrease for aminopropanol (Figure 4B,C). The detection of bound ligands in an X-ray structure and the strong effect of mutations in the same region emphasize the role of the ligand binding site for channel activation and demonstrate that the general agonist-binding mode that has been thoroughly characterized for the AchBP is also conserved in ELIC.

The Role of Aromatic Pore Residues for Channel Activation

In contrast to the extracellular domain, the pore of ELIC resembles cation selective members of the family that include nAChRs, serotonin receptors, and the prokaryotic channel GLIC

Table 1. Dose-response relationships of different agonists of ELIC.

	EC_{50}/mM	n	pH_{EC50}	$I_{max}/I_{max}^{cysteamine}$*	$pH_{I/I}$
cysteamine	0.365	2.7	7.0	1	7.0
aminopropane	0.446	3.0	7.0	0.99±0.02	7.0
bromoethylamine	0.885	3.1	7.0	0.94±0.04	7.0
bromopropylamine	1.1	3.9	7.0	0.71±0.03	7.0
aminopropanol	1.2	3.2	7.0	1.00±0.014	7.0
aminobutanol	1.7	2.9	7.0	0.98±0.03	7.0
GABA	2.4	3.9	7.0	0.79±0.09	7.0
diaminoethane	2.0	3.2	8.0	1.07±0.06	9.0
diaminopropane	3.0	3.1	8.0	1.08±0.03	9.0
putrescine	16.0	2.4	8.0	1.03±0.07	9.0
putrescine$^+$	0.23	2.4	8.0		

$^+$concentration of monovalent putrescine.
*Averages and s.d. of six measurements.
doi:10.1371/journal.pbio.1001101.t001

(Figure S1G). In cation selective pLGICs, three layers of hydrophobic side-chains provide an overall apolar character to the extracellular half of the pore region while the following two layers of polar residues and a layer of negatively charged residues render the intracellular half hydrophilic [7,30]. In a recent study, it was suggested that interactions between aromatic residues (i.e., Phe246) of the outer hydrophobic layer would stabilize the closed conformation of ELIC [31]. To investigate the role of this aromatic group for channel opening, we have mutated it to alanine and studied the mutant by X-ray crystallography and electrophysiology. The structure of the mutant F246A was determined at 3.3 Å resolution and shows a conformation that is, apart from the side chain truncation, virtually identical to WT (Figure 4D, Table 3). In electrophysiological recordings we found that the EC_{50} of cysteamine activation of F246A was shifted towards higher concentrations (Figure 4E). This shift is due to a mutation of a residue located remote from the ligand binding site and thus likely reflects a decreased efficacy of the channel. Our results thus do not provide any evidence that the ring of phenylalanine residues, which is unique to ELIC, would stabilize the pore in an unusual non-conducting conformation.

The Conduction Properties of the Ion Channel Pore

To characterize the ion conduction properties of ELIC, we have investigated single channel currents by patch-clamp and by fusion of reconstituted protein to artificial lipid bilayers (Figure 5, Figure S6). In recordings of patches excised from *Xenopus* oocytes expressing low levels of ELIC in the outside-out configuration, the opening of single channels upon addition of cysteamine can be observed (Figure 5A). These channels show an ohmic behavior in a broad voltage range with a single channel conductance (g) of 84 pS (Figure 5B). At high ligand concentrations, the initially strong channel activity decreases over time due to the desensitization of the channel. At prolonged incubation with the ligand, thus, bursts of activity alternate with long closures (Figure 5A). Within the bursts the channels are predominantly in an open state that is only interrupted by brief closures, which is consistent with a high efficacy of the ligand [32]. The openings recorded from ELIC, which was overexpressed and purified from *E. coli* and reconstituted into planar lipid bilayers, show a channel with very similar behavior (Figure 5C). Channel activity is evoked upon addition of the ligand to either side of the bilayer, thus indicating that the reconstituted channels are oriented in both ways. As for patch clamp recordings also in bilayers, long periods of closures are interrupted by burst of openings. In bilayers, and less frequently in patches, we have also observed the occasional transition of the open channel to a subconductance of about 80% of the current amplitude (Figure S6A). A similar subconductance was previously described for the nAChR [33]. At corresponding ion concentrations the conduction properties of reconstituted ELIC in planar lipid bilayers are very similar as observed in patch clamp recordings of the channel expressed in *Xenopus laevis* oocytes (for the main conductance level g = 96 pS), thus emphasizing that the functional behavior of the protein is largely independent of its expression host (Figure 5B). In gradients of NaCl, single channel currents reverse at the Nernst potential of Na^+, thus indicating that the channel is cation selective and the permeability to anions is negligible (Figure 5D). Under asymmetric conditions with the same concentrations of different monovalent salts on either side of the membrane, the currents reverse at 0 mV, showing that there is no measurable discrimination between monovalent cations (Figure 5E). This functional behavior resembles the ion selectivity of the nAChR [34,35] and it matches the behavior of the protein described for macroscopic currents obtained at high protein-to-lipid ratio in the absence of the ligand [10]. The single channel conductance linearly increases with the ion concentration and does not show any saturation at high concentrations (Figure 5F). To characterize the conduction behavior of divalent ions, we have replaced the monovalent cations at the "intracellular side" with different concentrations of divalent cations and we have activated the channel by addition of agonists to the "extracellular side." The IV curve in this case shows weak rectification with a lower slope conductance at positive voltages where divalent ions permeate the channel from the intracellular side (Figure 5G). This behavior is observed for different divalent cations such as Ca^{2+} and Ba^{2+} (Figure S6C). In contrast to monovalent ions, the concentration dependence of the Ca^{2+} conductance is shallow and nearly saturates already at low ion concentration (Figure 5H). This property was previously observed in nAchRs, where divalent ions in general interact stronger with the channel than their monovalent counterparts [36–38]. In all cation selective members of the family, a conserved negatively charged residue at the intracellular pore entry termed the "intermediate ring of charge" plays an important role for ion conductance, selectivity, and the interaction with divalent ions (Figure S1G) [39,40]. In the mutant E229A, the charge corresponding to this ring of residues is removed. When investigated in planar lipid bilayers after addition of ligand to the "extracellular side," a large effect on ion conductance is apparent. The currents show pronounced rectification with a strong decrease of the conductance at positive voltages (Figure 5I). The mutant is less selective and also permits the conduction of small anions. This behavior is manifested in recordings from solutions where chloride is replaced by the larger anion glucuronate, which for steric reasons does not permeate the channel. In such cases, the conductance of the mutant E229A is strongly decreased, whereas the WT protein is hardly affected (Figure S6D). The distinct permeation properties place ELIC within the cation selective branch of the family. The relative stability of the open state and the high single channel conductance additionally make it an attractive model for detailed biophysical investigations.

Discussion

Although the prokaryotic pLGIC ELIC has provided the first structural insight into this family of ligand-gated ion channels at

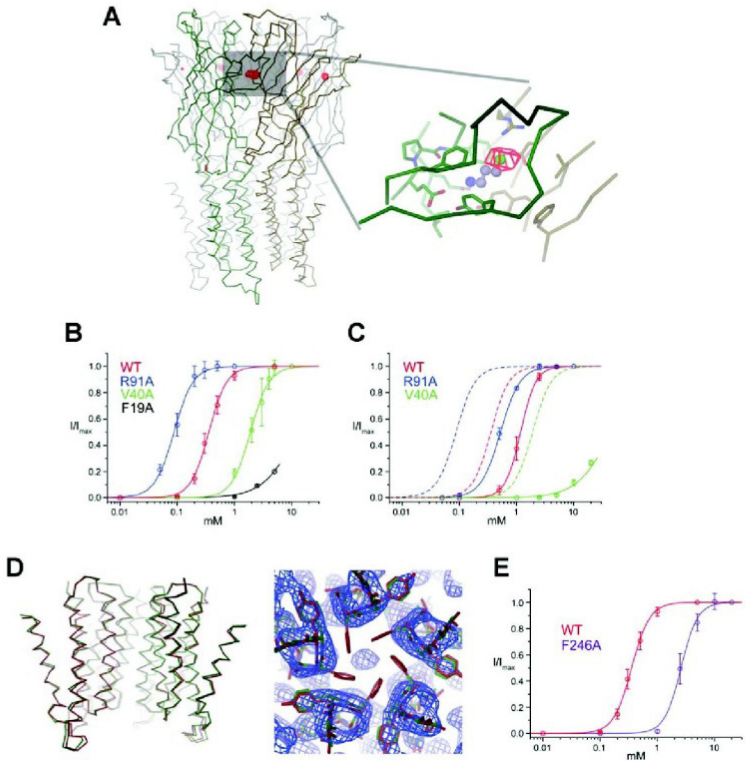

Figure 4. Ligand binding and mutagenesis. (A) Anomalous difference map of ELIC in complex with bromopropylamine. One of two pentamers of ELIC in the asymmetric unit of the crystal and a zoom into a single binding pocket are shown. The subunits of the principal and complementary side are colored in green and orange, respectively. The anomalous difference map calculated at 5.0 Å and contoured at 4.5 σ is shown as red mesh. The ligand binding region is indicated by a grey box. A model of bromopropylamine is shown in ball and stick representation. (B) Activation of ligand binding site mutants by cysteamine. Dose response curves from currents recorded with the two-electrode voltage clamp technique are shown. The solid lines show fits to a Hill equation. (C) Activation of ligand binding site mutants by aminopropanol. The solid lines show fits to a Hill equation, and dashed lines in the same color show the activation of the respective mutants by cysteamine. (D) Structure of the mutant F246A. Left: Superposition of Cα traces of the pore region of WT (red) and the mutant F246A (green). The view is from within the membrane; the front subunit is removed for clarity. Right: 2Fo-Fc electron density (calculated at 3.3 Å and contoured at 1 σ, blue mesh) of the pore region of the mutant F246A superimposed on the refined structure (green). The WT structure (red is shown for comparison). The view is from the extracellular side. The missing electron density for the aromatic side chains is apparent. (E) Activation of the pore mutant F246A by cysteamine. Dose response curves from currents recorded with the two-electrode voltage clamp technique are shown. The solid lines show fits to a Hill equation. The WT is shown for comparison.
doi:10.1371/journal.pbio.1001101.g004

Table 2. Dose-response relationship of activation of ELIC point mutants.

	cysteamine		aminopropanol	
	EC_{50}/mM	n	EC_{50}/mM	n
WT	0.365	2.7	1.2	3.2
R91A	0.087	2.6	0.511	2.45
V40A	1.9	2.6	>10	
F19A	>10		—	
F246A	2.59	3.0	n.d.	

doi:10.1371/journal.pbio.1001101.t002

high resolution, its functional characterization was so far prevented by the fact that activating ligands were unknown. In this study we have identified agonists of ELIC from a library of molecules that were selected based on the chemical features of the ligand binding site, we have located a bound ligand in a crystal structure, and we have characterized the functional properties of the channel by electrophysiology.

ELIC is activated by a set of primary amines that include alkylamines, aminothiols, aminoalcohols, bromoamines, diamines, and the neurotransmitter GABA. Quaternary amines, such as acetylcholine, in contrast, are ineffective. The chemical properties of the agonists underline the conservation of the ligand binding pocket that is closer to GABA and glycine receptors than to nAChRs and AChBPs (Figure S5). As is the case for other pLGICs [41,42], ligand activation in ELIC is a cooperative process and appears to involve the binding of at least three molecules to

Table 3. Data collection and refinement statistics.

	ELIC 5 mM bromopropylamine	ELIC F246A
Data collection		
Space group	$P2_1$	$P2_1$
Cell dimensions		
a, *b*, *c* (Å)	105.2, 266.7, 110.6	105.4, 266.2, 110.9
α, β, γ (°)	90.0, 110.1, 90.0	90.0, 110.7, 90.0
Resolution (Å)	40–4.0	40–3.3
R_{merge}*	9.2 (85.2)	7.1 (76.4)
$I/\sigma I$*	9.8 (1.8)	15.1 (2.0)
Completeness (%)*	99.5 (99.4)	99.0 (95.9)
Redundancy*	3.5	3.5
Refinement		
Resolution (Å)	20–4.0	15–3.3
Number of reflections	48,130	83,739
R_{work}/R_{free}	29.5/29.5	23.9/26.1
Number of atoms		
Protein	n/a	24,960
R.m.s. deviations		
Bond lengths (Å)	n/a	0.01
Bond angles (°)	n/a	1.5

*Values in parentheses are for highest resolution shell.
doi:10.1371/journal.pbio.1001101.t003

maximally activate the protein. However, unlike its eukaryotic counterparts [43], all agonists activate ELIC with comparably low apparent affinity at high μM to mM concentrations. While it is still not known whether the ligand activating ELIC in a biological context is among the characterized molecules, it is noteworthy that several of the agonists are breakdown products of amino acids, two of which, putrescine and GABA, may play a role in the natural environment of the bacteria, which as pathogens degrade the roots of plants. It may thus not be a coincidence to find the gene of a putative amino acid decarboxylase in the direct vicinity of the gene encoding for ELIC on the bacterial chromosome (Figure 6A). This protein, which might be involved in the processing of the ligand, was annotated as glutamate decarboxylase, thus suggesting that, despite its low potency, GABA is among the likely candidates for natural ligands.

The macroscopic opening and closing kinetics of ELIC is in the millisecond time range. Although the rates are slow compared to most eukaryotic family members [44,45], they are similar to the previously investigated activation and deactivation rates of GLIC [13]. In contrast to most eukaryotic pLGICs [15], the evoked currents are stable for several hundred milliseconds, but they slowly decay, due to the transition into a desensitized state. This behavior is consistent with long periods of closures separating bursts of channel openings upon prolonged exposure to saturating concentrations of the ligand observed in single channel traces. Within the bursts, the open probability of the channel is high, which is indicative for a high efficacy of the investigated ligands [32,46]. The detailed kinetic characterization of gating based on single channel recordings will be the subject of future investigations.

It is currently still unclear whether the crystal structure of ELIC, which shows a non-conducting conformation of the channel obtained in the absence of ligands, is closer to the resting or the desensitized state of the channel. Consequently, its relationship to the resting state of eukaryotic receptors is also unknown [19,47]. A previous hypothesis that the observed conformation would be induced by strong interactions of aromatic phenylalanine residues at the extracellular pore entry [31], however, could not be substantiated since the mutation to alanine did not change the overall structure and instead stabilized the closed state of the channel as indicated by a decrease in the potency of the agonist. This observation is unexpected, as hydrophobic interactions generally play an important role in the stabilization of protein structures.

In an allosteric model of channel activation, the binding of the ligand shifts the equilibrium between the open and closed channel towards the open state [48,49]. For that purpose, the agonist has to bind with higher affinity to the open state of the channel. In this respect, it is interesting to compare the conformation of the ligand binding domain of ELIC with a hypothetical conformation of the domain in the open state that was generated by a rigid body transformation to the structure of GLIC (Figure 6B). In this hypothetical conformation, the binding site has contracted and is no longer accessible to the solvent. While the site is still large enough to accommodate the different ligands, their interaction with the protein would likely be stronger, thus fulfilling an important requirement for ligand activation.

With respect to its ion conduction properties, ELIC is closely related to nAChRs, serotonin receptors, and GLIC [13,34,37,50,51]. ELIC is a cation selective channel that is essentially impermeable for anions. It does not discriminate between different monovalent cations and allows the permeation of divalent cations, which appear to interact stronger with the protein. The single channel conductance of ELIC is high; it is about 10 times higher than observed in GLIC [13], and it is comparable to the fastest conducting members of the family [39,52,53]. While a detailed understanding of this property will require more experimental data, it is still interesting to compare the pore geometry of GLIC and a hypothetic open state of ELIC that is based on the conformation of the pore forming helix observed in GLIC (Figure 6B). Despite the similarity of the protein backbone, the pore geometries of ELIC and GLIC would differ in such a model due to the different size of the side-chains of pore-lining residues. While the bulky Phe246 and Leu239 at the extracellular half of the pore of ELIC would result in a smaller pore diameter, the constricting intracellular diameter, which might be the main determinant for the conductance, could be larger (Figure 6B). Part of this larger pore diameter is caused by the location of the conserved Glu229 at the intracellular pore entry that is shifted by one residue in GLIC.

With known agonists, ELIC has now become amenable for detailed structural and functional investigations. A fundamental question of ionotropic receptors concerns the mechanisms by which the binding of ligands induces channel activation over a large distance in a different part of the protein. ELIC is well suited to study the details of this process: Its large conductance will allow investigations of ion conductance and gating on a single channel level, which will additionally be facilitated by its comparably simple functional properties. Its high expression level and biochemical stability make it a suitable candidate for spectroscopy, and finally, knowledge of the ligand opens up the possibility to obtain structural information of a conducting conformation of the protein.

Materials and Methods

Protein Expression and Purification

ELIC and the mutants F246A and E229A were expressed and purified as described [10]. *E. coli* BL21DE3 containing a vector

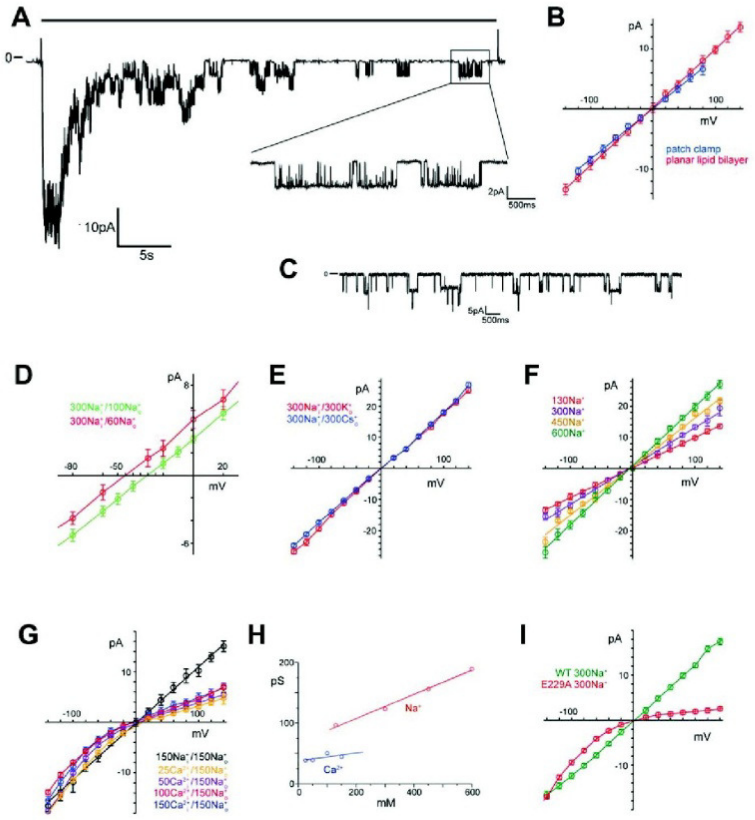

Figure 5. Single channel recording of ELIC. (A) Patch clamp recordings of ELIC expressed in *Xenopus oocytes* in the outside-out configuration at −60 mV. The agonist (5 mM cysteamine) was applied by a fast solution exchange (black bar above). The decrease of channel activity over time is due to desensitization. The magnified trace shows activity of a single channel. Recordings were filtered at 1 kHz. (B) Current-voltage relationships recorded from single channels of ELIC expressed in *Xenopus oocytes* in a patch clamp experiment (blue) and of reconstituted protein in artificial lipid bilayers (red). The errors are standard deviations (s.d.) obtained from fits to current amplitude histograms. (C) Current trace from a planar lipid bilayer containing at least two channels recorded at −100 mV in the presence of 2 mM cysteamine (recordings were filtered at 200 Hz). (D) Current voltage relationships of ELIC in asymmetric concentrations of NaCl measured in the presence of 2 mM cysteamine. The currents reverse at the Nernst potential of Na^+. The compartment with lower ion concentration corresponds to the "extracellular side." Data shown in panels D–G and I were measured from single channels in planar lipid bilayers. The errors are s.d. obtained from fits to current amplitude histograms. Channels were activated by addition of 2 mM cysteamine to both compartments unless stated differently. (E) Current voltage relationships in asymmetric conditions containing equivalent amounts of different monovalent salts. (F) Current voltage relationships of single channel currents at different concentrations of NaCl. (G) Current voltage relationships in asymmetric salt conditions. The "extracellular side" contains 150 mM NaCl, and the "intracellular side" contains different concentrations of $CaCl_2$ (25–150 mM). Channels were activated by addition of 2 mM cysteamine to the "extracellular side" only. Data from symmetric concentrations of NaCl (150 mM, black) are shown for comparison. (H) Concentration dependence of the single channel conductance of Na^+ and Ca^{2+} currents. (I) Current-voltage relationships of the mutant E229A in symmetric concentrations of NaCl. Channels were activated by addition of 2 mM cysteamine to the "extracellular side." Data from the WT channel (green) are shown for comparison.
doi:10.1371/journal.pbio.1001101.g005

encoding for a fusion protein consisting of the pelB signal sequence, a His_{10} tag, maltose binding protein, a HRV 3C protease site, and ELIC were grown in M9 minimal medium at 37°C to an OD of 1.0 and subsequently cooled to 20°C. Expression was induced by addition of 0.3 mM IPTG overnight. All the following steps were carried out at 4°C. The protein was extracted from isolated membranes in a buffer containing 1% n-Undecyl-β-D-Maltoside (UDM, Anatrace, Inc.) and purified by Ni-NTA chromatography (Qiagen). The purified MBP-ELIC-fusion protein was digested with HRV 3C protease to cleave the His_{10}-MBP protein. His_{10}-MBP and 3C were subsequently removed from solution by binding to Ni-NTA resin. ELIC was concentrated and subjected to gel filtration on a Superdex 200 column (GE Healthcare). The protein peak corresponding to the ELIC pentamer was pooled and concentrated to 10 mg/ml and used for crystallization. For reconstitution into liposomes, an additional anion exchange purification step (POROS HQ, Applied Biosystems) was introduced prior to gel filtration.

Crystallization and Structure Determination

The purified protein was crystallized in sitting drops at 4°C. Protein containing additional 0.5 mg/ml *E. coli* polar lipids (Avanti

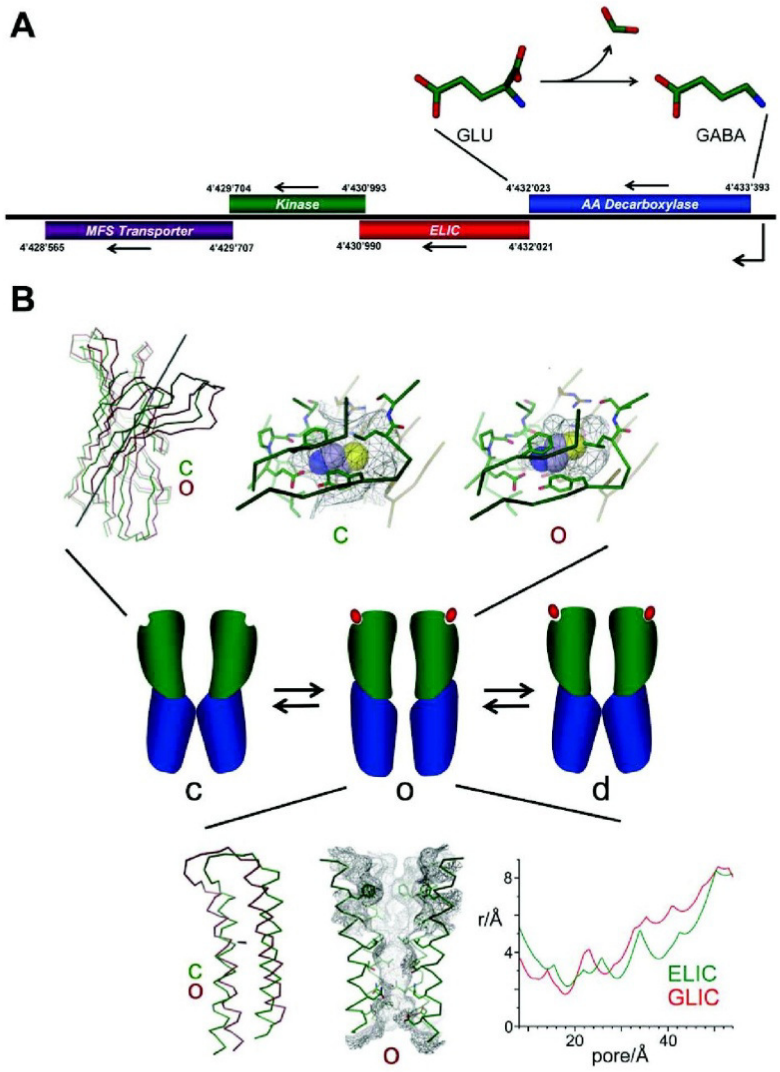

Figure 6. Biology and hypothetical mechanisms. (A) Localization of ELIC on the genome of *Erwinia chrysanthemi*. Open reading frames residing on the same operon and their respective positions on the gene are shown. The arrows indicate the direction of transcription. The annotation is based on sequence homology. The reaction catalyzed by the annotated glutamate decarboxylase (AA Decarboxylase) is shown above. (B) Potential conformational transitions during ligand activation. Upon ligand binding the channel changes from a resting state (c) to an open state (o) followed by a transition to a desensitized state (d). (Top) Comparison of the binding pocket of ELIC in a non-conducting conformation with a hypothetical structure of the region in a conducting state. The model of the conducting state (red) was generated by independent counterclockwise rigid-body rotations of the ligand binding domain of ELIC (green) by about 12° around the axis indicated in the figure. The rotation axis was obtained from a least square fit of conserved regions of the ligand binding domain of ELIC on the equivalent regions of GLIC. The binding sites of both states are shown. The ligand binding pockets are displayed as grey mesh. A model of cysteamine (shown as CPK representation) was placed into the binding site in a similar binding mode as observed in the structure of ELIC in complex with bromopropylamine. (Bottom) Hypothetical structure of the pore region in a conducting conformation. The conducting state of the pore region (red) was constructed by a rigid body rotation of the α2-α3 helix pair of a subunit of ELIC (green) by 12° in a counterclockwise direction around an axis that is indicated in the figure. The model of the pore region of this conformation is displayed as Cα trace. Side chains of pore forming helices are shown as sticks. The solvent accessible surface is shown as grey mesh. The front subunit is removed for clarity. The pore radii of GLIC (green, with the side chains of Glu 221 pointing away from the channel axis) and the hypothetical conducting conformation of ELIC as calculated with the program HOLE [61] are shown (the cytoplasm is on the left side).
doi:10.1371/journal.pbio.1001101.g006

Polar Lipids, Inc.) was mixed in a 1:1 ratio with reservoir solution (100 mM ADA pH 6.5, 200 mM $NaLiSO_4$, and 10% (w/v) PEG4000). Bromopropylamine was soaked into the crystals by incubation with solutions containing 5 mM of the ligand. The crystals were cryoprotected by transfer into solutions containing 30% glycerol. All datasets were collected on frozen crystals on the X06SA beamline at the Swiss Light Source (SLS) of the Paul Scherrer Institut (PSI) on a PILATUS detector (Dectris). The data were indexed, integrated, and scaled with XDS [54] and further processed with CCP4 programs [55]. The structure of the F246A mutant at 3.3 Å was determined by Molecular Replacement using the structure of ELIC as the search model. The model was rebuilt in O [56] and refined maintaining strong 10-fold NCS constraints in PHENIX [57]. The structures of the WT protein in complex with bromopropylamine at 4.0 Å was improved by rigid body refinement in CNS [58]. R and R_{free} were monitored throughout. R_{free} was calculated by selecting 5% of the reflection data in thin slices that were selected for the initial dataset of ELIC and that were omitted in refinement (Table 3).

Reconstitution and Planar Lipid Bilayer Experiments

ELIC was reconstituted into *E. coli* polar lipids that were solubilized in reconstitution buffer (450 mM KCl, 25 mM citric acid, 25 mM phosphoric acid, pH 7.0) containing 35 mM CHAPS. The protein was added at a protein-to-lipid ratio of 1 to 10 µg/mg with a final lipid concentration of 15 mg/ml. The detergent was removed by dialysis, and liposomes were frozen in liquid nitrogen and stored at −80°C. Liposomes containing ELIC were fused to bilayers formed from POPE/POPG lipids (in molar ratio of 1:3, Avanti) and recorded in a horizontal planar lipid bilayer system as previously described [59]. Electrodes were connected to the respective bath solutions via salt bridges. Solutions were prepared using 10 mM HEPES as buffer. NaCl and NaOH were added to reach desired Na^+ concentration. Solutions containing K^+ ions were prepared in a similar way but using KOH and KCl instead. Cs^+ solutions were prepared in 10 mM Tris. For all solutions pH was adjusted to 7.0 with HCl. Low salt solutions contained equivalent concentrations of mannitol to correct the osmotic pressure. Currents were recorded with an Axopatch amplifier 200B (Axon Instruments, Inc.). Data were sampled at 100 µs, filtered at 1,000 Hz, and analyzed using Clampfit (Axon Instruments, Inc.).

Two Electrode Voltage Clamp Recording

Constructs containing the gene of either the WT channel or point mutants preceded by the signal sequence of the chicken α7nAchR were cloned into the pTLN vector for expression in *X. laevis* oocytes [60]. After linearization of the plasmid DNA by MluI, capped complementary RNA was transcribed with the mMessage mMachine kit (Ambion) and purified with the RNeasy kit (Qiagen). For expression, 1–50 ng of RNA was injected into defolliculated oocytes. Two-electrode voltage clamp measurements were performed one day after injection at 20°C (OC-725B, Warner Instrument Corp.). Currents were recorded in bath solutions containing 10 mM HEPES (pH 7), 130 mM NaCl, and the respective ligands. Cysteamine containing solutions were supplemented with 1 mM DTT.

Patch Clamp Recording

Membrane patches of *X. laevis* oocytes were recorded in the excised outside-out configuration 2–3 d after injection of mRNA with an Axopatch 200B amplifier (Axon Instruments) at 20°C. Data were sampled at 100 µs, filtered with 1,000 Hz, and analyzed using Clampfit (Axon Instruments, Inc.). Bath solutions contained 10 mM HEPES (pH 7.0), 150 mM NaCl, 0.5 mM $BaCl_2$, and the respective ligands. The electrodes had a resistance of 2–3 MΩ. Pipette solutions contained 150 mM NaCl, 1 mM EGTA, 5 mM MgCl, and 10 mM HEPES at pH 7.0. Bath electrodes were placed in 1 M KCl solution connected to the bath solution by Agar bridges. The agonists were applied to the patch using a stepper motor (SF77B Perfusion fast step, Warner).

Accession Code

The coordinates of the ELIC mutant F246A have been deposited with the Protein Data Bank under code 2yks.

Supporting Information

Figure S1 Pore geometries of pentameric ligand-gated ion channels. (A) ELIC and GLIC pentamers were superimposed by a least square fit of the α1 helices. The Cα traces of single subunits of the superimposed structures (ELIC, orange; GLIC, green) are shown. The structures are viewed from within the membrane. The rotation axes describing the main movements in the extracellular and pore domains are indicated. (B) View of the superimposed α2–α3 helix pairs of a single subunit. The color coding is as in (A). The rotation axis is indicated. (C) View of the superimposed α2–α3 helix pairs of the ELIC and GLIC pentamers from within the membrane. The front subunit is removed for clarity. (D) View of the superimposed α2–α3 helix pairs of ELIC and the structure of the nAChR, which was determined by electron crystallography at 4.0 Å resolution. (E) View of the α2 helices of ELIC defining the pore region. The front subunit is removed for clarity. The molecular surface is shown as white mesh. (E) View of the α2 helices of GLIC defining the pore region. The front subunit is removed for clarity. The molecular surface is shown as white mesh (G) Sequence alignment of the pore regions of ELIC, GLIC, the human α7 nicotinic acetylcholine receptor (nAChR), and the α3 subunit of the human GABA-receptor (GABAR). Conserved residues of cation selective channels that are lining the pore region are highlighted (yellow, hydrophobic; green, hydrophilic; red, negatively charged). A conserved proline residue in the α2–α3 linker is highlighted in grey.
(TIF)

Figure S2 Comparison of the ligand binding domains of ELIC and the AChBP. (A) Cα trace of the AChBP. The regions A–F that constitute the ligand-binding site are shown in unique colors and labeled. The secondary structure elements are indicated. (B) Stereo view of the AChBP superimposed on the ligand binding domain of ELIC and the AChBP. The proteins are shown as Cα traces. The principle and complementary sides are shown in green and orange, respectively. The light colors correspond to the AChBP. (C) Ligand binding site of the AChBP. Bound carbamylcholine is shown in magenta. Selected residues of the binding pocket and the secondary structure elements are labeled. (D) Ligand binding site of ELIC. Selected residues of the binding pocket and the secondary structure elements are labeled. (E) Stereo view of the superimposed structures of the binding regions of ELIC and the AChBP.
(TIF)

Figure S3 Library of potential agonists. (A) List of molecules used for screening of agonists. (B) Current response of ELIC to isobutylamine and putrescine at pH 7.0. Currents were recorded from *Xenopus laevis* oocytes at −60 mV with the two electrode voltage clamp technique. Traces show the response to agonists in comparison to the response to cysteamine. Agonists were applied to the outside in a concentration of 10 mM. The activation by

cysteamine (grey bar, 2 mM) is followed by the application of the respective agonist (black bar, *, 10 mM) and another activation by cysteamine (grey bar, 2 mM).
(TIF)

Figure S4 Activation, deactivation, and desensitization of ELIC. (A) Decay of currents in two-electrode voltage clamp recordings. *Xenopus laevis* oocytes expressing ELIC were incubated in solutions containing 5 mM cysteamine for an extended amount of time (black bar). The voltage was clamped to the reversal potential and the fraction of open channels was assayed by brief steps to −60 mV. (B) Activation and desensitization of macroscopic currents measured from excised outside-out patches. Solutions containing either no ligand or 5 mM cysteamine (black bar) were applied by fast solution exchange. The currents decay over time in the presence of ligand, but full channel activity was recovered after washout and incubation of the patch in the absence of ligand. (C) Activation and deactivation kinetics obtained from macroscopic currents measured from outside-out patches in response to application and washout of cysteamine. Solutions were exchanged using a stepper motor (SF77B Perfusion fast step, Warner). Currents were fitted to a single exponential function. The activation time constant decreased with increasing ligand concentration as expected for a ligand-gated channel. Averages from nine independent measurements are shown. The deactivation time constant was independent of the ligand concentration. Averages of 27 independent measurements are shown. All errors are standard deviations (s.d.).
(TIF)

Figure S5 Conservation of the ligand-binding site. (A) Sequence alignment of sections of the extracellular domain constituting the ligand-binding site. Strongly conserved residues are colored in red. Residues lining the ligand-binding site are highlighted (green, aromatic residues conserved in all pLGICs; red, positions conserved in ELIC, GABA, and glycine receptors; yellow, residues in ELIC that are not conserved). (B) Structure of the ligand-binding region of ELIC. The conservation of residues is indicated.
(TIF)

Figure S6 Single channel analysis. (A) Single channel trace of ELIC recorded in planar lipid bilayers. The voltage was clamped to 100 mV. Channel activity was induced by addition of 2 mM cysteamine. The trace shows the occasional transition of the open channel to a subconductance of about 80% of the maximum current amplitude. (B) Single channel traces of ELIC expressed in *Xenopus laevis* oocytes recorded in excised outside-out patches (left) and of reconstituted protein recorded in planar lipid bilayers (right). The current histograms of the respective traces and a fit to a Gaussian are shown. (C) Current-voltage relationships in asymmetric salt solutions. The "extracellular side" contained 150 mM NaCl, and the "intracellular side" contained 150 mM of either $CaCl_2$ or $BaCl_2$. Channels were activated by addition of 2 mM cysteamine to the "extracellular side." (D) Current-voltage relationships of the mutant E229A in symmetric concentrations of either 300 mM NaCl or 300 mM Na-glucuronate (NaGlc). Channels were activated by addition of 2 mM cysteamine to the "extracellular side." Data from the WT channel are shown for comparison. Data shown in panels C and D were measured from single channels in planar lipid bilayers. The errors are s.d. obtained from fits to current amplitude histograms.
(TIF)

Acknowledgments

We thank the staff of the X06SA beamline for support during data collection, Alwin Reiter and Dirk Trauner for providing a sample of homocysteamine, and members of the Dutzler lab for help in all stages of the project. Data collection was performed at the X06SA beamline at the Swiss Light Source of the Paul Scherrer Institute.

Author Contributions

The author(s) have made the following declarations about their contributions: Conceived and designed the experiments: IZ RD. Performed the experiments: IZ. Analyzed the data: IZ RD. Wrote the paper: IZ RD.

References

1. Hille B (2001) Ion channels of excitable membranes, third edition. Sunderland, MA: Sinauer Associates Inc.
2. Miller PS, Smart TG (2010) Binding, activation and modulation of Cys-loop receptors. Trends Pharmacol Sci 31: 161–174.
3. Thompson AJ, Lester HA, Lummis SC (2010) The structural basis of function in Cys-loop receptors. Q Rev Biophys 43: 449–499.
4. Sine SM, Engel AG (2006) Recent advances in Cys-loop receptor structure and function. Nature 440: 448–455.
5. Karlin A (2002) Emerging structure of the nicotinic acetylcholine receptors. Nat Rev Neurosci 3: 102–114.
6. Lester HA, Dibas MI, Dahan DS, Leite JF, Dougherty DA (2004) Cys-loop receptors: new twists and turns. Trends Neurosci 27: 329–336.
7. Hilf RJ, Dutzler R (2009) A prokaryotic perspective on pentameric ligand-gated ion channel structure. Curr Opin Struct Biol 19: 418–424.
8. Tasneem A, Iyer LM, Jakobsson E, Aravind L (2005) Identification of the prokaryotic ligand-gated ion channels and their implications for the mechanisms and origins of animal Cys-loop ion channels. Genome Biol 6: R4.
9. Corringer PJ, Baaden M, Bocquet N, Delarue M, Dufresne V, et al. (2010) Atomic structure and dynamics of pentameric ligand-gated ion channels: new insight from bacterial homologues. J Physiol 588: 565–572.
10. Hilf RJ, Dutzler R (2008) X-ray structure of a prokaryotic pentameric ligand-gated ion channel. Nature 452: 375–379.
11. Hilf RJ, Dutzler R (2009) Structure of a potentially open state of a proton-activated pentameric ligand-gated ion channel. Nature 457: 115–118.
12. Bocquet N, Nury H, Baaden M, Le Poupon C, Changeux JP, et al. (2009) X-ray structure of a pentameric ligand-gated ion channel in an apparently open conformation. Nature 457: 111–114.
13. Bocquet N, Prado de Carvalho L, Cartaud J, Neyton J, Le Poupon C, et al. (2007) A prokaryotic proton-gated ion channel from the nicotinic acetylcholine receptor family. Nature 445: 116–119.
14. Feltz A, Trautmann A (1982) Desensitization at the frog neuromuscular junction: a biphasic process. J Physiol 322: 257–272.
15. Auerbach A, Akk G (1998) Desensitization of mouse nicotinic acetylcholine receptor channels. A two-gate mechanism. J Gen Physiol 112: 181–197.
16. Sakmann B, Patlak J, Neher E (1980) Single acetylcholine-activated channels show burst-kinetics in presence of desensitizing concentrations of agonist. Nature 286: 71–73.
17. Hilf RJ, Bertozzi C, Zimmermann I, Reiter A, Trauner D, et al. (2010) Structural basis of open channel block in a prokaryotic pentameric ligand-gated ion channel. Nat Struct Mol Biol 17: 1330–1336.
18. Cheng X, Ivanov I, Wang H, Sine SM, McCammon JA (2009) Molecular-dynamics simulations of ELIC-a prokaryotic homologue of the nicotinic acetylcholine receptor. Biophys J 96: 4502–4513.
19. Miyazawa A, Fujiyoshi Y, Unwin N (2003) Structure and gating mechanism of the acetylcholine receptor pore. Nature 423: 949–955.
20. Sixma TK, Smit AB (2003) Acetylcholine binding protein (AChBP): a secreted glial protein that provides a high-resolution model for the extracellular domain of pentameric ligand-gated ion channels. Annu Rev Biophys Biomol Struct 32: 311–334.
21. Brejc K, van Dijk WJ, Klaassen RV, Schuurmans M, van Der Oost J, et al. (2001) Crystal structure of an ACh-binding protein reveals the ligand-binding domain of nicotinic receptors. Nature 411: 269–276.
22. Celie PH, van Rossum-Fikkert SE, van Dijk WJ, Brejc K, Smit AB, et al. (2004) Nicotine and carbamylcholine binding to nicotinic acetylcholine receptors as studied in AChBP crystal structures. Neuron 41: 907–914.
23. Hansen SB, Sulzenbacher G, Huxford T, Marchot P, Taylor P, et al. (2005) Structures of Aplysia AChBP complexes with nicotinic agonists and antagonists reveal distinctive binding interfaces and conformations. Embo J 24: 3635–3646.
24. Sine SM (2002) The nicotinic receptor ligand binding domain. J Neurobiol 53: 431–446.
25. Zhong W, Gallivan JP, Zhang Y, Li L, Lester HA, et al. (1998) From ab initio quantum mechanics to molecular neurobiology: a cation-pi binding site in the nicotinic receptor. Proc Natl Acad Sci U S A 95: 12088–12093.
26. Dougherty DA, Stauffer DA (1990) Acetylcholine binding by a synthetic receptor: implications for biological recognition. Science 250: 1558–1560.

27. Cromer BA, Morton CJ, Parker MW (2002) Anxiety over GABA(A) receptor structure relieved by AChBP. Trends Biochem Sci 27: 280–287.
28. Sigel E, Baur R, Kellenberger S, Malherbe P (1992) Point mutations affecting antagonist affinity and agonist dependent gating of GABAA receptor channels. EMBO J 11: 2017–2023.
29. Lummis SC (2009) Locating GABA in GABA receptor binding sites. Biochem Soc Trans 37: 1343–1346.
30. Imoto K, Methfessel C, Sakmann B, Mishina M, Mori Y, et al. (1986) Location of a delta-subunit region determining ion transport through the acetylcholine receptor channel. Nature 324: 670–674.
31. Gonzalez-Gutierrez G, Grosman C (2010) Bridging the gap between structural models of nicotinic receptor superfamily ion channels and their corresponding functional states. J Mol Biol 403: 693–705.
32. Colquhoun D, Hawkes AG (1982) On the stochastic properties of bursts of single ion channel openings and of clusters of bursts. Philos Trans R Soc Lond B Biol Sci 300: 1–59.
33. Colquhoun D, Sakmann B (1985) Fast events in single-channel currents activated by acetylcholine and its analogues at the frog muscle end-plate. J Physiol 369: 501–557.
34. Adams DJ, Dwyer TM, Hille B (1980) The permeability of endplate channels to monovalent and divalent metal cations. J Gen Physiol 75: 493–510.
35. Lewis CA, Stevens CF (1983) Acetylcholine receptor channel ionic selectivity: ions experience an aqueous environment. Proc Natl Acad Sci U S A 80: 6110–6113.
36. Nutter TJ, Adams DJ (1995) Monovalent and divalent cation permeability and block of neuronal nicotinic receptor channels in rat parasympathetic ganglia. J Gen Physiol 105: 701–723.
37. Bertrand D, Galzi JL, Devillers-Thiery A, Bertrand S, Changeux JP (1993) Mutations at two distinct sites within the channel domain M2 alter calcium permeability of neuronal alpha 7 nicotinic receptor. Proc Natl Acad Sci U S A 90: 6971–6975.
38. Dani JA, Eisenman G (1987) Monovalent and divalent cation permeation in acetylcholine receptor channels. Ion transport related to structure. J Gen Physiol 89: 959–983.
39. Imoto K, Busch C, Sakmann B, Mishina M, Konno T, et al. (1988) Rings of negatively charged amino acids determine the acetylcholine receptor channel conductance. Nature 335: 645–648.
40. Konno T, Busch C, Von Kitzing E, Imoto K, Wang F, et al. (1991) Rings of anionic amino acids as structural determinants of ion selectivity in the acetylcholine receptor channel. Proc Biol Sci 244: 69–79.
41. Lester HA, Changeux JP, Sheridan RE (1975) Conductance increases produced by bath application of cholinergic agonists to Electrophorus electroplaques. J Gen Physiol 65: 797–816.
42. Rayes D, De Rosa MJ, Sine SM, Bouzat C (2009) Number and locations of agonist binding sites required to activate homomeric Cys-loop receptors. J Neurosci 29: 6022–6032.
43. Akk G, Sine S, Auerbach A (1996) Binding sites contribute unequally to the gating of mouse nicotinic alpha D200N acetylcholine receptors. J Physiol 496 (Pt 1): 185–196.
44. Maconochie DJ, Zempel JM, Steinbach JH (1994) How quickly can GABAA receptors open? Neuron 12: 61–71.
45. Corradi J, Gumilar F, Bouzat C (2009) Single-channel kinetic analysis for activation and desensitization of homomeric 5-HT(3)A receptors. Biophys J 97: 1335–1345.
46. Lape R, Colquhoun D, Sivilotti LG (2008) On the nature of partial agonism in the nicotinic receptor superfamily. Nature 454: 722–727.
47. Wilson G, Karlin A (2001) Acetylcholine receptor channel structure in the resting, open, and desensitized states probed with the substituted-cysteine-accessibility method. Proc Natl Acad Sci U S A 98: 1241–1248.
48. Colquhoun D (1998) Binding, gating, affinity and efficacy: the interpretation of structure-activity relationships for agonists and of the effects of mutating receptors. Br J Pharmacol 125: 924–947.
49. Changeux JP, Bon F, Cartaud J, Devillers-Thiery A, Giraudat J, et al. (1983) Allosteric properties of the acetylcholine receptor protein from Torpedo marmorata. Cold Spring Harb Symp Quant Biol 48(Pt 1): 35–52.
50. Thompson AJ, Lummis SC (2003) A single ring of charged amino acids at one end of the pore can control ion selectivity in the 5-HT3 receptor. Br J Pharmacol 140: 359–365.
51. Corringer PJ, Bertrand S, Galzi JL, Devillers-Thiery A, Changeux JP, et al. (1999) Molecular basis of the charge selectivity of nicotinic acetylcholine receptor and related ligand-gated ion channels. Novartis Found Symp 225: 215–224; discussion 224–230.
52. Hansen SB, Wang HL, Taylor P, Sine SM (2008) An ion selectivity filter in the extracellular domain of Cys-loop receptors reveals determinants for ion conductance. J Biol Chem 283: 36066–36070.
53. Bormann J, Rundstrom N, Betz H, Langosch D (1993) Residues within transmembrane segment M2 determine chloride conductance of glycine receptor homo- and hetero-oligomers. EMBO J 12: 3729–3737.
54. Kabsch W (1993) Automatic processing of rotation diffraction data from crystals of initially unknown symmetry and cell constants. J Appl Cryst 26: 795–800.
55. CCP4 (1994) Collaborative computational project Nr. 4. The CCP4 suite: programs for X-ray crystallography. Acta Crystallogr D 50: 760–763.
56. Jones TA, Zou JY, Cowan SW, Kjeldgaard M (1991) Improved methods for building protein models in electron density maps and the location of errors in these models. Acta Crystallogr A 47(Pt 2): 110–119.
57. Adams PD, Grosse-Kunstleve RW, Hung LW, Ioerger TR, McCoy AJ, et al. (2002) PHENIX: building new software for automated crystallographic structure determination. Acta Crystallogr D Biol Crystallogr 58: 1948–1954.
58. Brunger AT, Adams PD, Clore GM, DeLano WL, Gros P, et al. (1998) Crystallography & NMR system: a new software suite for macromolecular structure determination. Acta Crystallogr D Biol Crystallogr 54: 905–921.
59. Nimigean CM, Miller C (2002) Na+ block and permeation in a K+ channel of known structure. J Gen Physiol 120: 323–335.
60. Lorenz C, Pusch M, Jentsch TJ (1996) Heteromultimeric CLC chloride channels with novel properties. Proc Natl Acad Sci U S A 93: 13362–13366.
61. Smart OS, Neduvelil JG, Wang X, Wallace BA, Sansom MS (1996) HOLE: a program for the analysis of the pore dimensions of ion channel structural models. J Mol Graph 14: 354–360, 376.

Supplementary Figures

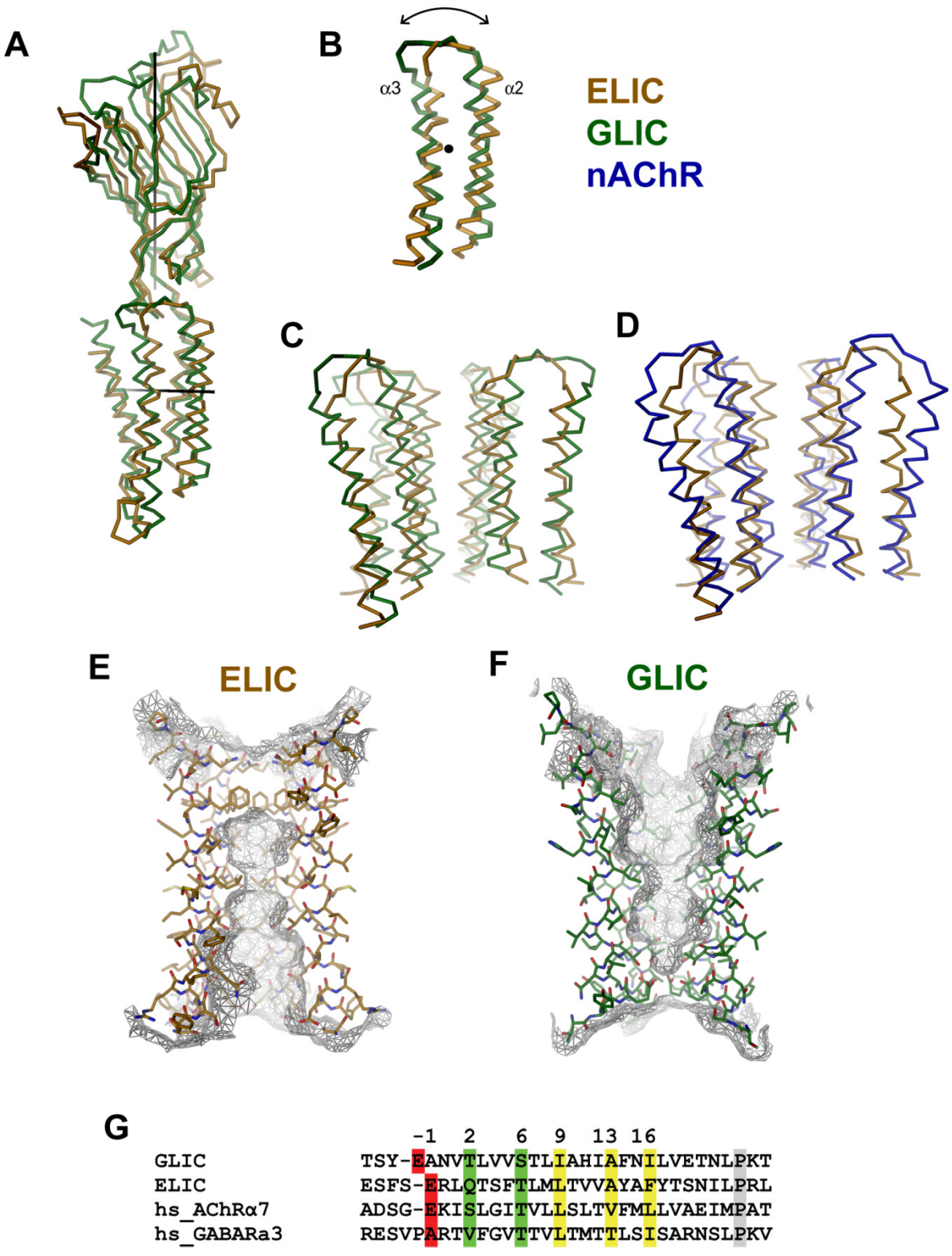

Supplementary Figure 1

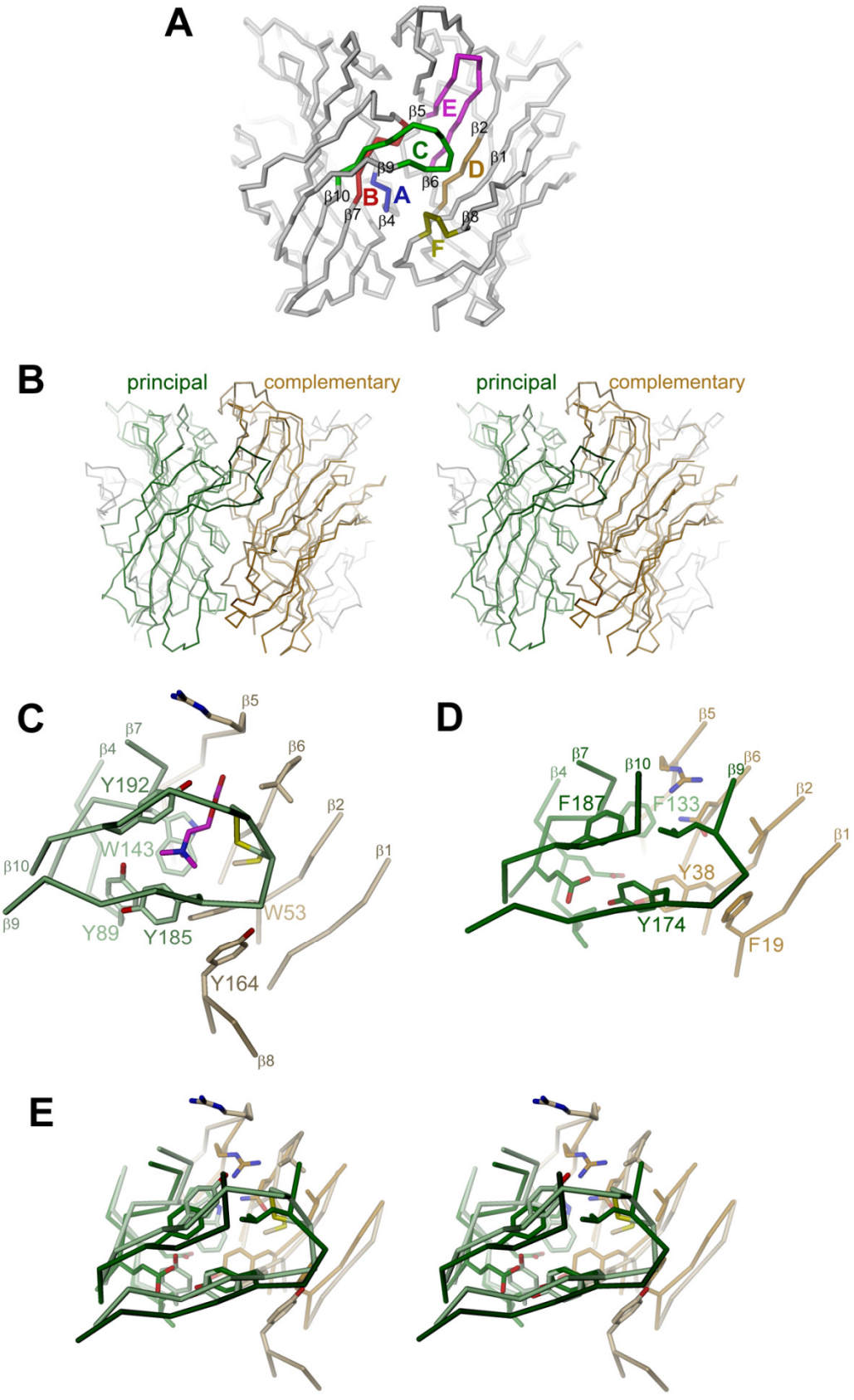

Supplementary Figure 2

A

Primary amines: 3-Amino-4-hydroxybenzoic acid, 2-Aminobenzimidazole, 4-Amino-2-hydroxybenzoic acid, 3-Bromopropylamine, 3-Amino-1-propanol, 4-Aminobutyric acid, E-4-Amino-2-butenoic acid, Ethanolamine, Butylamine, 4-Amino-1-butanol, Ethylamine, Propylamine, 3-Methyl-2-butylamine, Isobutylamine, R-(+)-α-Amino-γ-butyro-lactone (cycloserine), Glycineamide, β-Alanine, 4-Amino-L-phenlalanine, DL-5-Hydroxylysine Succinamide, 6-Aminocaproic acid, Benzylamine, 3-(Methylthio)propylamine, 4-Bromoaniline, (S)-(-)-Methioninol, DL-Ornithine, (+/-)-3-Amino-1,2-propanediol, L-Citrulline, 4-Aminobenzamide, 2-Chloroethylamine, 3-Chloropropylamine, 2-Fluoroethylamine, 4-Aminopyridine, Muscimol, Adenine, Taurine, 4-Aminobenzoic acid, Homocysteamine, Cysteamine, Serotonin, Tryptamine, 3-amine-2,3-dihydrobenzoic acid, (+/-)-2-Amino-1-phenylethanol, Histamine, (-)-Norepinephrine, Agmantine, Aminoacetonitril

Secondary amines: Benzimidazole, Purin, 6-Ethylthiopurine, 2-Imidazolidone, 2-Methl-2imidazoline, Piperazine, (-)-Epinephrine, (-)-Phenylephrine

Teritary amines: Nicotineamide**,** Nicotine

Quarternary amines: (2-Bromoethyl)trimethylammonium, N,N,N-Trimethylanilinium, Carbamoylcholine, 1-Butyl-1-methylpyrrolidinium, Acetylcholine, Choline, L-Carnitine, Betaine, 3-(Bromopropyl)trimethylammonium, (2-Aminoethyl)trimethylammonium, 1,1-Dimethyl-4-phenylpiperazine, Acetylthiocholine

Polyamines: Spermidine, Spermine, 1,3-Diaminopropane, 1,4-Diaminobutane, 1,2-Diaminoethane, Methylenediamine, Cadaverine, m-Phenylendiamine, o-Phenylenediamine, p-Phenylenediamine

Guanidinium derivatives: Debrisoquine, 1-(3-Chlorophenyl)biguanide, 4-Guanidinobutyric acid, 2-Guanidinobenzimidazole, Glycocyamine, Creatine, L-Canavanine, 4-Guanidinobenzoic acid

Biogenic aminoacids: Glycine, Alanine, Valine, Leucine, Isoleucine, Methionine, Proline, Phenylalanine, Tryptophane, Serine, Threonine, Asparagine, Glutamine, Tyrosine, Cysteine, Lysine, Arginine, Histidine, Aspartate, Glutamate

Other compounds: Bromoacetic acid, 2,3-Butanediol, 3-Guanidinopropionic acid, 1,3-Propanediol

B

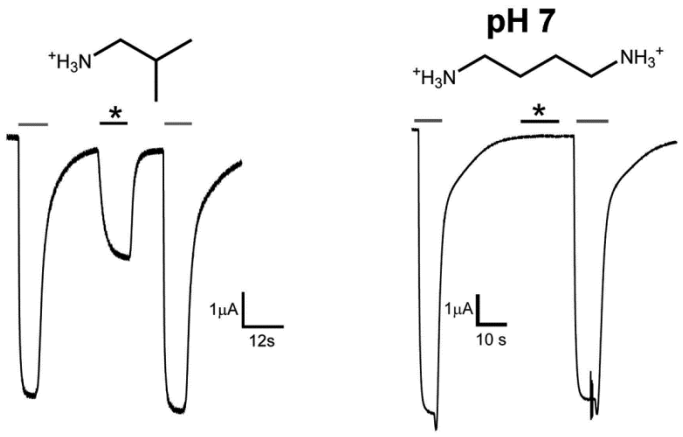

Supplementary Figure 3

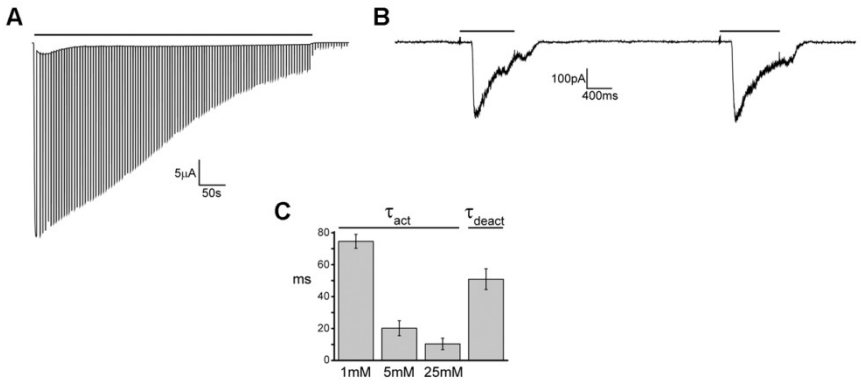

Supplementary Figure 4

A

```
                β1          β2          β4          β5          β6
hs_GABARρ1  VGVDVQVESL...MTLYLRHYW...WVPDMFFVH...NVMLRVQPDG...LYSLRV
hs_GABARβ1  VGMNIDIASI...LTMYFQQAW...WVPDTYFLN...NRMIRLHPDG...LYGLRI
hs_GABARα3  VKTDIYVTSF...IDVFFRQTW...WTPDTFFHN...NKLLRLVDNG...LYTMRL
mm_GLYRα1   VSCNIFINSF...VNIFLRQQW...WKPDLFFAN...NKLLRISRNG...LYSIRI
RDL         VGVTMYVLSI...LDFYFRQFW...WVPDTFFVN...NEFIRVHHSG...TRSIRL
ELIC        VSVSIFINKI...VDGYIVAQW...WVPALEFIN...NKRLMLFPDG...IYNARF
hs_nAChRα7  VYFSLNLLQI...TNIWLQMSW...WKPDILLYN...N--VLVNPSG...QYLPPG
AChBP       VSVSLKFINI...VVFWQQTTW...WVPDLAAYN...PQLARVVSDG...LYMPSI

                β7          β9          β10
hs_GABARρ1  QTCSLEIESYAYT...HTTTKLAFYSST...GWYNRLYINFTLRRH
hs_GABARβ1  QNCTLEIESYGYT...VDYKLITKKVVF...GSYPRLSLSFKLKRN
hs_GABARα3  HACPLKFGSYAYT...YDLLGHVVGTEI...GEYVVMTTHFHLKRK
mm_GLYRα1   QTCIMQLESFGYT...KEEKDLRYCTKH...GKFTCIEARFHLERQ
RDL         QLCHIEIESFGYT...LG-HRQRATEIN...GNYSRLACEIQFVRS
ELIC        QQFVLELEPFSYN...THISDIRYDHLS...NEFSRITVRIDAVRN
hs_nAChRα7  QHCKLKFGSWSYG...GKRSERFYECCK...EPYPDVTFTVTMRRR
AChBP       ATCRIKIGSWTHH...QKKNSVTYSCCP...EAYEDVEVSLNFRKK
```

B

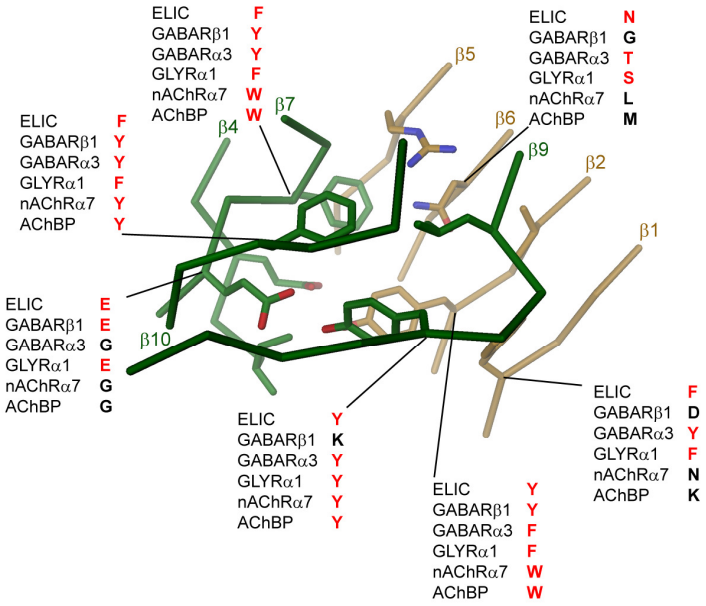

Supplementary Figure 5

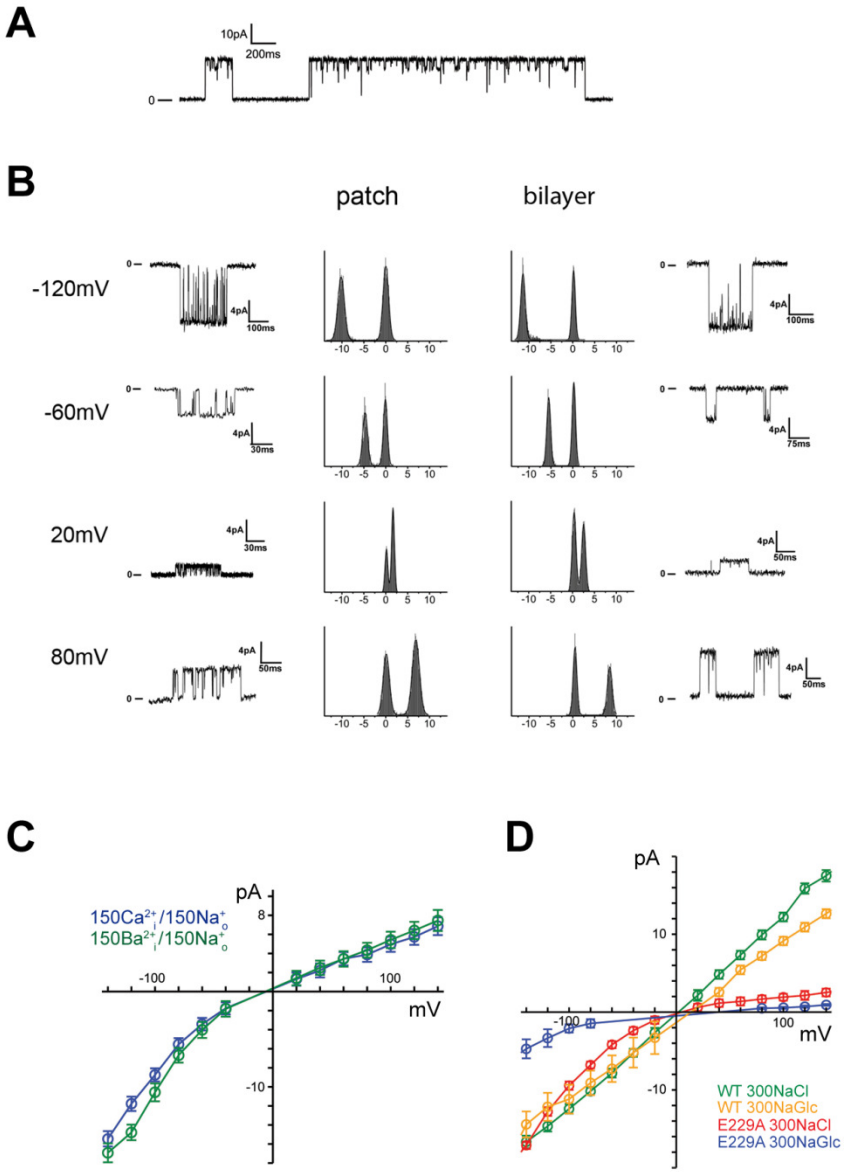

Supplementary Figure 6

Inhibition of the Prokaryotic Ligand-Gated Ion Channel ELIC by Divalent Cations

Almost all eukaryotic pLGICs are modulated by different divalent cations, either in a positive or a negative manner. Even though the physiological context of this modulation is not entirely understood, it is believed to play an important role in regulating the synaptic response. During an initial biophysical characterization of ELIC, it was realized that calcium ions inhibit the ion permeation. In experiments, where agonist and divalent cations are co-applied to the activated receptor, a decrease of the current is observed (Figure 15). Dose response relationships can be used to determine the potency of the inhibitor. However, all inhibitors behave similar in such experiments, irrespective of their mechanism of action and it is thus impossible to distinguish between pore blockers, competitive or allosteric inhibitors. To clarify the mechanism of the modulation of ELIC by divalent cations, different electrophysiological experiments were combined with X-ray crystallography.

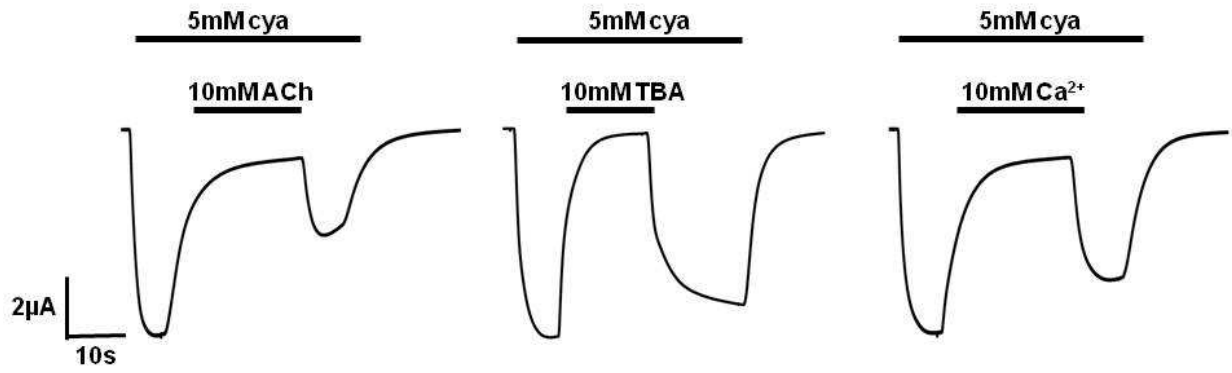

Figure 15 2EVC traces of a *X.laevis* oocyte expressing ELIC clamped at -40mV. In each experiment, ELIC is activated by 5mM cysteamine (cya) followed by the co-application of different inhibitors. These are the competitive inhibitor ACh, the pore blocker TBA and the divalent cation Ca^{2+}. The difference in current before and after the application of the inhibitors is due to the desensitization of ELIC. In this experiment, the phenotype of the inhibition is indistinguishable between the different kinds of inhibitors.

A detailed investigation by electrophysiology revealed a complex behavior of ELIC in the presence of divalent cations. With increasing calcium concentrations, the dose response curve shifts to higher agonist concentrations. This effect was not found to saturate, even at high concentrations. Additionally, it was noticed that the maximal evoked current is not affected at low concentrations of divalent cations, where the inhibition is surmountable. At higher concentrations, however, the maximal current is decreased and the inhibition is no longer surmountable. The different effects could be interpreted by two distinct mechanisms, acting at low and high concentrations of divalent cations. This behavior resembles the effect of calcium on $5HT_3$ receptors and it suggests that divalent cations act by a conserved mechanism of inhibition which can be deduced in ELIC by a combination of structural and functional investigations.

In our study, we found that divalent cations act as negative allosteric modulators of ELIC by decreasing the efficacy of channel gating. Even though three different binding sites for divalent cations were identified by X-ray crystallography, only one of them is functionally important and accounts for all the facets the complex pattern of inhibition. Interestingly, the divalent cation binding sites of several eukaryotic receptors were mapped to positions similar to the identified site in ELIC. It implies that the same location in the receptors is responsible for either positive or negative allosteric modulation.

OPEN ACCESS Freely available online

PLOS | BIOLOGY

Inhibition of the Prokaryotic Pentameric Ligand-Gated Ion Channel ELIC by Divalent Cations

Iwan Zimmermann[1], Alessandro Marabelli[2], Carlo Bertozzi[1], Lucia G. Sivilotti[2], Raimund Dutzler[1]*

1 Department of Biochemistry, University of Zürich, Zürich, Switzerland, **2** Department of Neuroscience, Physiology and Pharmacology, University College London, London, United Kingdom

Abstract

The modulation of pentameric ligand-gated ion channels (pLGICs) by divalent cations is believed to play an important role in their regulation in a physiological context. Ions such as calcium or zinc influence the activity of pLGIC neurotransmitter receptors by binding to their extracellular domain and either potentiate or inhibit channel activation. Here we have investigated by electrophysiology and X-ray crystallography the effect of divalent ions on ELIC, a close prokaryotic pLGIC homologue of known structure. We found that divalent cations inhibit the activation of ELIC by the agonist cysteamine, reducing both its potency and, at higher concentrations, its maximum response. Crystal structures of the channel in complex with barium reveal the presence of several distinct binding sites. By mutagenesis we confirmed that the site responsible for divalent inhibition is located at the outer rim of the extracellular domain, at the interface between adjacent subunits but at some distance from the agonist binding region. Here, divalent cations interact with the protein via carboxylate side-chains, and the site is similar in structure to calcium binding sites described in other proteins. There is evidence that other pLGICs may be regulated by divalent ions binding to a similar region, even though the interacting residues are not conserved within the family. Our study provides structural and functional insight into the allosteric regulation of ELIC and is of potential relevance for the entire family.

Citation: Zimmermann I, Marabelli A, Bertozzi C, Sivilotti LG, Dutzler R (2012) Inhibition of the Prokaryotic Pentameric Ligand-Gated Ion Channel ELIC by Divalent Cations. PLoS Biol 10(11): e1001429. doi:10.1371/journal.pbio.1001429

Academic Editor: David E. Clapham, Harvard Medical School, United States of America

Received June 6, 2012; **Accepted** October 12, 2012; **Published** November 20, 2012

Funding: The research leading to these results has received funding from a grant from the Swiss National Science Foundation (grant no. 31003B_141180) to RD and a grant from BBSRC (BB/J005312/1) to LGC. AM is supported by a UCL Impact studentship. The funders had no role in study design, data collection and analysis, decision to publish, or preparation of the manuscript.

Competing Interests: The authors have declared that no competing interests exist.

Abbreviations: $5HT_3R$, serotonin receptor; GABAR, gaba receptor; GlyR, glycine receptor; nAChR, nicotinic acetylcholine receptor; pLGIC, pentameric ligand-gated ion channel

* E-mail: dutzler@bioc.uzh.ch

Introduction

The pentameric ligand-gated ion channels (pLGICs) are ionotropic neurotransmitter receptors, which are activated by the binding of ligands to specific sites of the protein. The family includes both cation-selective channels, such as nicotinic Acetylcholine- (nAChRs) and Serotonin receptors ($5HT_3Rs$), and anion-selective channels, such as GABA- (GABARs) and Glycine receptors (GlyRs) [1]. Despite these differences in ion selectivity, the overall molecular architecture and the mechanism by which ligands open the ion conduction path are conserved [2–8]. pLGIC subunits form either homo- or hetero-pentamers that consist of at least two functional units, an extracellular ligand-binding region and a transmembrane pore [9,10]. Agonists open the channel by binding to a conserved site in the extracellular domain, at the interface between two subunits [11,12]. A homomeric receptor contains five equivalent agonist binding sites, several of which need to be occupied for maximum channel activation and this makes the process highly cooperative [5,13–16]. Agonist binding is accompanied by conformational rearrangements that are transmitted over a distance of tens of angstroms from the extracellular domain, via the domain interface to the pore [17]. These receptors have thus become important model systems for the study of allosteric mechanisms [18]. Many pLGICs are important drug targets and all aspects of their function can be influenced by pharmacological agents. These are a diverse set of molecules that include agonists and competitive antagonists (which act on the agonist binding site itself), pore blockers that inhibit ion conduction, and allosteric modulators that interact with regions distinct from the agonist-binding site. Modulators such as benzodiazepines [19], general anesthetics [20], alcohol [21], and the antiparasite ivermectin [22] can either enhance or inhibit pLGIC activation. pLGIC function is affected also by divalent cations (such as calcium and zinc) in two distinct ways. Cation-selective pLGICs are somewhat permeable to divalents, but the strong interaction between these ions and the pore decreases or blocks conduction in a voltage-dependent manner [23,24]. In addition to that, divalent cations can also modulate channel gating. For instance, calcium potentiates the agonist responses of nAChRs [25–27] and inhibits those of $5HT_3Rs$ [28,29], and zinc can either potentiate or inhibit channel activation, depending on the type of pLGIC and the ion concentration [30–35].

Here we show that both the modulatory and the channel block effects of divalent cations are present also in ELIC, a prokaryotic pLGIC channel whose structure was determined in a nonconducting conformation [36]. Agonists of ELIC include primary amines such as cysteamine, propylamine, and the vertebrate neurotransmitter GABA. In ELIC, these agonists occupy the

Author Summary

Pentameric ligand-gated ion channels (pLGICs) are ionotropic neurotransmitter receptors that mediate electrical signaling at chemical synapses. The pLGIC family includes receptors for acetylcholine, serotonin, GABA and glycine, which share a similar structural organization and activation mechanism: the channels are closed in the absence of ligands and open when neurotransmitters bind to a conserved site in the extracellular domain. In many family members, activation by the neurotransmitter can be affected by modulators (including several drugs in therapeutic use), which bind to different sites on the channel. Channel function can be modulated also by divalent cations, which either potentiate or inhibit pLGICs at physiological concentrations. Here, we analyze this mechanism in the pLGIC ELIC, a prokaryotic family member of known structure. We show that divalent cations such as calcium or zinc inhibit ELIC by occupying an extracellular site remote from the ligand-binding region thereby interfering with gating. Although the site of interaction is not conserved between different family members, we present evidence that regulation of other pLGICs involves the same region. Our study has thus provided insights into a regulatory process that appears to be general for the pLGIC family in both eukaryotes and prokaryotes.

canonical ligand-binding site of the family and open a cation-selective pore with permeation properties similar to those of eukaryotic channels [37]. Here we describe how divalent cations permeate and block the ELIC pore, and how they also inhibit ELIC gating, by binding in the extracellular domain, to a site remote from the ligand-binding region.

Results

Modulation of ELIC Function by Divalent Ions

We have investigated the effects of divalent cations on ELIC by electrophysiology and X-ray crystallography. Divalent cations can influence ELIC function in several different ways depending on concentration (Figure 1). The traces in Figure 1A show that low mM concentrations of the alkaline earth metal ion Ca^{2+} decrease the single channel conductance of ELIC when added to the extracellular medium at negative holding potentials. ELIC single channel currents are progressively reduced by increasing Ca^{2+} concentrations and decrease by approximately 25% of their control amplitude at 5 mM Ca^{2+} (Figure 1C) and by a maximum of about 50% at high Ca^{2+} concentration [37]. This effect is due to tight interactions of divalent ions with the channel pore and has been thoroughly characterized for different pLGIC family members [23,24] including the homologous channel GLIC [38], whose structure was determined by X-ray crystallography in a conducting conformation [39,40].

Low extracellular calcium (greater than 100 μM) produces also a voltage-independent decrease in agonist potency. This effect is detectable at Ca^{2+} concentrations too low to decrease channel conductance and is manifested as a parallel rightward shift in the agonist dose–response curve (Figure 1D, Table S1). A similar effect on agonist binding in the presence of calcium is observed in isothermal titration calorimetry experiments (Figure 1E). Up to 1 mM calcium, the shift in the agonist dose–response curves is truly parallel, as the maximum agonist current does not decrease more than the single channel conductance does (Figure 1B and 1C). This pattern appears to reproduce the effects of competitive antagonists, which bind to the ligand-binding site and reduce its occupancy by the agonist in a surmountable way (e.g., their effect can be overcome by increasing agonist concentration). This resemblance is obvious if the effects of Ca^{2+} are compared with those of the competitive antagonist acetylcholine, which is known to bind to the agonist-binding site of ELIC (Figure 1F) [41]. The Schild plot for acetylcholine [42,43] is linear with a slope of unity and a binding affinity of 1.6 mM (Figure 1G, Table 1). The Schild plot for Ca^{2+} is also linear, with a potency of 260 μM, but a shallower slope of 0.8 (Figure 1G, Table 1).

The similarity between the effect of calcium and that of a competitive antagonist disappears as Ca^{2+} concentrations are increased above 1 mM. The current traces in Figure 1B show that the reduction in agonist potency is now associated with a decrease in the maximum agonist response. This decrease is too big to be explained by the effect of Ca^{2+} on conductance: at 5 mM Ca^{2+} the single channel conductance is reduced by 25% and the maximum agonist response by 55% (Figure 1C). At progressively higher concentrations of the divalent cation, the maximum current response continues to decline and this decrease can be described by a fit to a Langmuir equation with an IC_{50} of 6 mM (Figure 1H). Despite the strong reduction in the maximum currents, the shift in EC_{50} remains linear over a wide concentration range (Figure S1). The pronounced drop in maximum current strongly suggests that at higher concentrations calcium impairs the opening of the channel and reduces agonist efficacy.

Next, we tried to establish whether calcium impairs the maximum rate of ELIC gating (e.g., when the channel is fully bound to the agonist) by measuring the on-relaxation of currents elicited by rapid propylamine applications to outside-out patches from HEK293 cells. Figure 1I shows that increasing Ca^{2+} from 50 to 200 μM does slow the onset of the current elicited by a saturating agonist concentration (20 mM propylamine, red trace) but that this effect is overcome by increasing agonist concentration to 50 mM (green trace). Only minor changes in the time course of deactivation were detected (Table 2). Thus the maximum rate with which the agonist-bound channel opens is unchanged, which is unexpected given the observed change in agonist efficacy. This could be because we could test only low calcium (in high calcium the concentrations of agonist required to saturate channel gating are too high to be experimentally feasible). Alternatively, calcium impairs gating by affecting a step in the channel activation that controls the size of the maximum agonist response, but not the speed of overall gating (see Discussion).

Finally, we found that divalent cations other than Ca^{2+} also affect ELIC responses. In particular, other alkaline earth metal ions, such as Mg^{2+}, Sr^{2+}, and Ba^{2+}, are slightly weaker than Ca^{2+} in inhibiting ELIC (Figure 2A–C and E, Table 1, Table S1), whereas the transition metal ion Zn^{2+} is considerably more potent (i.e., Schild plot x-intercept 8 μM, Figure 2D and E, Table 1, Table S1).

Structural Characterization of Divalent Ion Binding

In order to understand the structural basis of the effects of divalent ions we aimed at identifying the region of interaction by X-ray crystallography. Since the crystal form that was used for the structure determination of ELIC contains high concentrations of sulfate, which forms insoluble salts in the presence of most alkaline earth metal ions, we had to identify novel crystallization conditions compatible with divalent ions. In a broad screen we observed crystals growing in Ba^{2+}-acetate. Ba^{2+} can be readily located in the electron density by its strong anomalous scattering properties, and since it has comparable effects on channel function as Ca^{2+} (Figure 2A, Figure S2A), it is reasonable to assume that it will

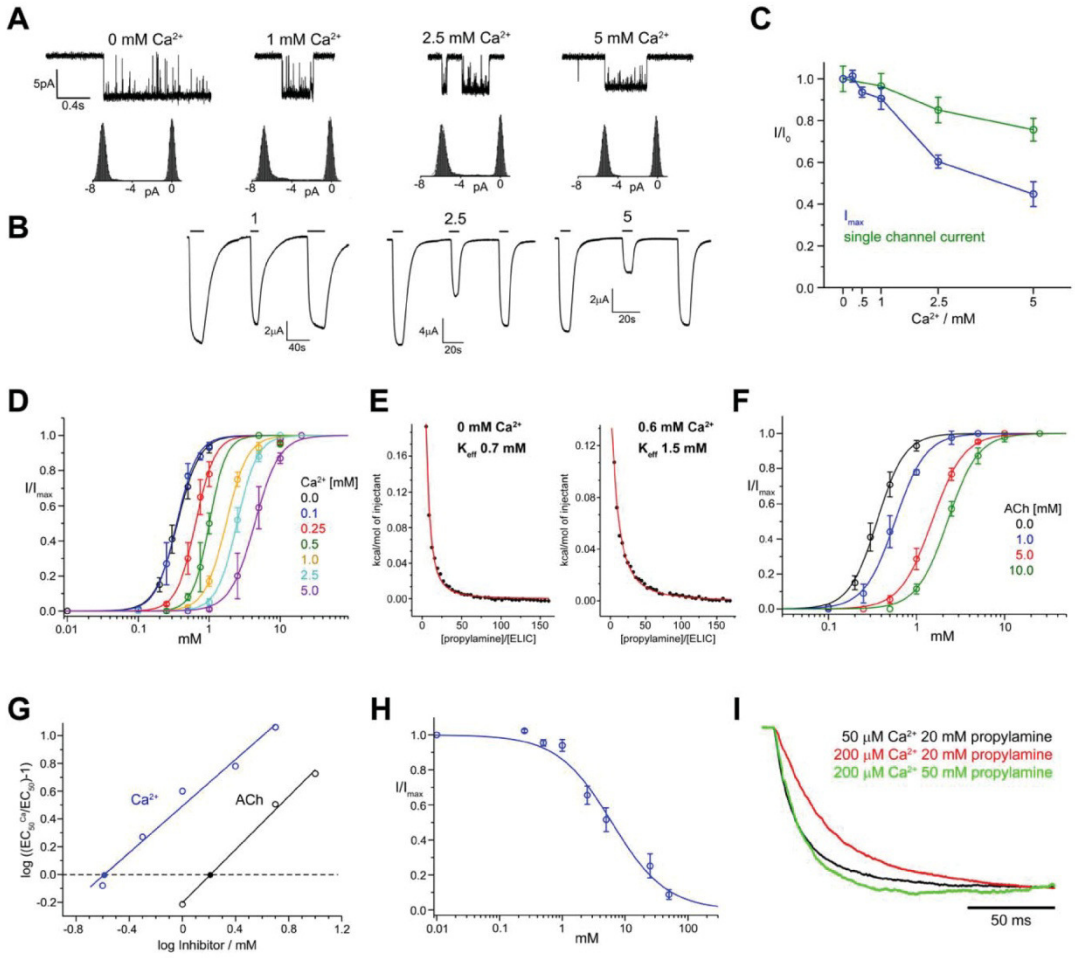

Figure 1. Inhibition of ELIC by calcium. (A) ELIC single channel currents in the presence of different extracellular concentrations of Ca^{2+} and all-points amplitude histograms (recordings were from oocyte outside-out patches at −80 mV holding potential). (B) Maximum ELIC responses to saturating concentrations of the agonist cysteamine in the absence and presence of Ca^{2+}. Currents were measured from oocytes held at −40 mV under two-electrode voltage clamp. Agonist application is indicated by a bar. Responses to cysteamine in the absence of extracellular Ca^{2+} are followed by responses in the presence of Ca^{2+} (concentration in mM as shown) and by recovery application of cysteamine in the absence of Ca^{2+}. (C) Plot of maximum agonist responses and single channel currents at different Ca^{2+} concentrations. The currents are normalized to the control values (in the absence of Ca^{2+}). Maximum cysteamine currents (blue symbols) were measured with the two-electrode voltage clamp technique in oocytes as in panel B. Single channel currents (green symbols) were measured in the outside-out configuration as in panel A. (D) Cysteamine dose–response relationships for ELIC in the presence of different concentrations of Ca^{2+}. (E) Equilibrium cysteamine binding isotherms determined by ITC for ELIC in the absence (left) and presence of Ca^{2+}. Solid curves represent fits to a single-site binding isotherm with Keff = 0.7 mM (no Ca^{2+}) and 1.5 mM (0.6 mM Ca^{2+}), respectively. (F) Cysteamine dose–response relationships for ELIC in the presence of different concentrations of ACh. (G) Schild plot quantifying the inhibition by Ca^{2+} and ACh. EC_{50} values were obtained from fits to data shown in panels (D) and (F). Potencies of the antagonists (pA values) were obtained by linear regression, and the intersection with the *x*-axis is indicated (●). (H) Fraction of the maximum current response at different Ca^{2+} concentrations. The solid line shows a fit to a Langmuir equation with a K_I of 6 mM. The data presented in panels (C), (D), (F), and (H) are averages from at least five oocytes; errors are SD. The solid lines in (D) and (F) show fits to a Hill equation. Currents were recorded at −40 mV. (I) Activation kinetics of macroscopic currents of ELIC activated by propylamine in response to fast solution exchange at different Ca^{2+} concentrations. ELIC was expressed in HEK 293 cells, and currents were recorded from excised patches in the outside-out configuration at −100 mV.
doi:10.1371/journal.pbio.1001429.g001

occupy the same sites in the protein. Crystals of the ELIC/Ba^{2+} complex belong to two different, yet related crystal forms, one similar to the original barium-free form of ELIC that was used for structure determination (space group $P2_1$) and another growing in a higher symmetry space group ($P4_3$) (Table 3). Datasets for both crystal forms were collected to 3.8 Å ($P2_1$) and 3.3 Å ($P4_3$)

Table 1. Schild analysis of inhibition of ELIC.

ELIC	Inhibitor	pA	Slope	K_i^{app} [mM]
WT	ACh	0.21±0.06	1.0±0.1	1.6
WT	Ca^{2+}	−0.57±0.03	0.8±0.05	0.26
WT/BAPTA	Ca^{2+}	−0.69±0.11	1.0±0.3	0.20
WT	Mg^{2+}	−0.36±0.02	0.9±0.01	0.43
WT	Sr^{2+}	−0.07±0.02	0.9±0.02	0.85
WT	Ba^{2+}	−0.07±0.01	1.1±0.03	0.85
WT	Zn^{2+}	−2.16±0.13	1.2±0.01	0.007
R91A	Ca^{2+}	−0.69±0.03	0.7±0.1	0.21
R91A	ACh	−0.77±0.05	0.7±0.1	0.17
R91A	TMA	0.78±0.18	0.8±0.1	6.0
D86A	Ca^{2+}	−0.60±0.11	0.8±0.1	0.25
S84A	Ca^{2+}	−0.83±0.14	0.6±0.2	0.15
N251A	Ca^{2+}	−0.27±0.19	0.9±0.2	0.53
D113A	Ca^{2+}	0.69±0.04	1.0±0.3	4.9
D113N	Ca^{2+}	−0.02±0.08	1.0±0.01	0.95
D158A	Ca^{2+}	0.74±0.01	1.2±0.1	5.4
D158N	Ca^{2+}	0.50±0.17	0.5±0.2	3.2
E150A	Ca^{2+}	0.23±0.12	1.0±0.2	1.7
E150Q	Ca^{2+}	0.09±0.20	0.9±0.3	1.2
D113A/D158A	Ca^{2+}	N/D	N/D	N/D
D113A/D158A	Ba^{2+}	0.81±0.02	0.6±0.02	6.5
D113A/D158A	Zn^{2+}	N/D	N/D	N/D
D113A/D158A	Ach	0.32±0.06	0.8±0.1	2.1
WT/.25 mM Ca^{2+}	Ach	0.06±0.06	0.9±0.1	1.2
WT/.5 mM Ca^{2+}	Ach	0.11±0.09	0.9±0.01	1.3
WT/1 mM Ca^{2+}	Ach	0.35±0.01	1.1±0.01	2.2
WT/1 mM ACh	Ca^{2+}	−0.65±0.01	0.9±0.02	0.22

doi:10.1371/journal.pbio.1001429.t001

resolution and provide equivalent views of the channel and its interaction with divalent cations.

The structures show a conformation of the channel that is overall very similar to the structure of ELIC already described. Strong peaks in the anomalous difference density allow us to detect the presence of Ba^{2+} ions bound to three distinct sites of the protein (Figure 3).

Firstly, a single Ba^{2+} ion per channel is located on the 5-fold axis of symmetry at the extracellular end of the pore and is coordinated by the side-chains of Asn251 (position 20′ of the second transmembrane domain in the numbering system developed for the nAChR, Figure 3A–C). Throughout the article we will refer to this site as S_{pore}.

There are two additional sets of binding sites for Ba^{2+} in the structure shown in Figure 3B. Both are found at the interface between subunits in the extracellular domain in five symmetry-related locations. One set of sites faces the channel vestibule and will be referred to as S_{in}. The barium ion in S_{in} is coordinated by Ser84 of the principal subunit and Asp86 of the complementary subunit (Figure 3D). Barium ions are bound also to a set of five equivalent sites on the outer rim of the extracellular domain (Figure 3B and E). These sites, which we will call S_{out}, are about 15 Å below the ligand-binding pocket, towards the membrane plane and are formed by the side-chains of acidic amino acids

Table 2. Activation and deactivation kinetics of ELIC.

Ca^{2+} (μM)	Propylamine (mM)	τ_{rise} (ms)	τ_{decay} (ms)	*n*
50	20	16.7±1.5	34.7±5.6	6
200	20	38.5±6.7	23.9±3.1	6
200	50	16.4±2.2	36.7±12.7	6
50	20	19.6±3.1	33.5±6.9	6

doi:10.1371/journal.pbio.1001429.t002

contributed by both subunits. These residues include Asp113 at the end of β6 on the principal side and Glu150 and Asp158 on the loop connecting β8 and β9 on the complementary side (Figure 3A and E). The refined $2F_o$-F_c electron density map of this region indicates a direct interaction of the respective carboxylate groups with the bound ions resembling Ca^{2+}-binding sites observed in other proteins (Figure 3E, Figure S2B and C). Remarkably, in none of the collected datasets did we find any evidence for Ba^{2+} in the ligand-binding pocket itself.

Investigation of the Binding Sites of Divalent Ions by Mutagenesis

The structure of ELIC in complex with Ba^{2+} has revealed the location of three distinct sites for the interaction with divalent cations. If binding to any of these sites is relevant for the inhibition of the channel, we would expect that mutating the interacting residues should affect the functional modulation by divalent ions. Thus we mutated the residues that contact Ba^{2+} in the structure and measured again the effects of Ca^{2+} by two-electrode voltage-clamp electrophysiology (Figures 4 and 5, Table 1).

Given that the effects of low Ca^{2+} concentrations resemble those of competitive antagonists, we tested also whether the agonist binding site can play a role (even though we have no structural evidence that divalents bind there). Our functional data show that the agonist binding site is unlikely to be involved, because Ca^{2+} inhibition is not changed by a mutation here (R91A) that increases agonist potency by 3–4-fold ([37], Figure 4A and F).

We then proceeded to investigate whether the inhibitory effects of Ca^{2+} are produced via binding to the S_{pore} site by truncating the side-chain of the Asn residue in contact with the divalent ion. Our X-ray crystallography data show that the structure of this N251A mutant is on the whole similar to WT but lacks the anomalous difference density in S_{pore}. The structure of this mutant still shows strong density of ions bound to S_{out} (and weaker density for S_{in}), thus suggesting that effects of the mutation are local (Figure 4B). Electrophysiological recording shows that agonists activate WT and mutant N251A channels with similar potency and that the inhibition by Ca^{2+} of these responses is only modestly decreased in N251A (Figure 4C and Schild plots in 4F). This suggests that S_{pore} is not the major site responsible for the Ca^{2+} inhibition.

Figure 4F shows also that mutating the binding residues in another set of divalent ion sites, S_{in} (which face the extracellular vestibule), has little effect on Ca^{2+} inhibition. Mutation S84A (on the principal side) changes neither the potency of the agonist nor the inhibition by Ca^{2+} (Figure 4D). Similarly, in the mutant D86A there is only a modest decrease in agonist potency, and the inhibitory effect of Ca^{2+} is virtually unchanged (Figure 4E and F). Thus we have shown that neither S_{pore} nor S_{in} mediate the functional effects of calcium on channel activation.

In contrast to that, we found that Ca^{2+} modulation is greatly decreased when we change any of the residues that coordinate divalent cations in S_{out}. This is seen both when the residues with

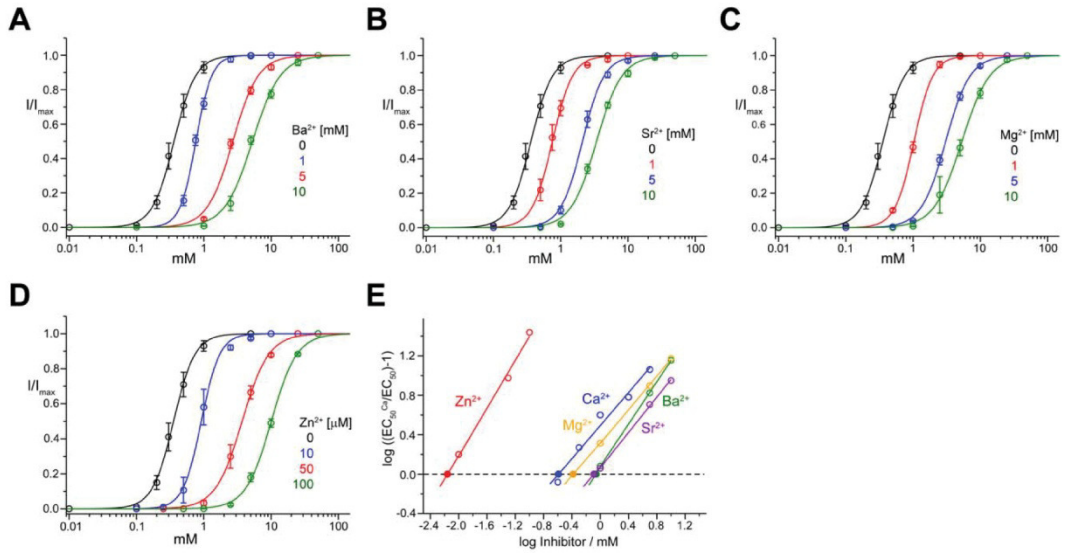

Figure 2. Inhibition of ELIC by different divalent cations. Dose–response relationships of ELIC activated by cysteamine at different concentrations of Ba^{2+} (A), Sr^{2+} (B), and Mg^{2+} (C) and ELIC activated by propylamine at different concentrations of Zn^{2+} (D). (E) Schild plot quantifying the inhibition by different divalent cations. EC_{50} values were obtained from fits to data shown in panels (A–D). Potencies of the Antagonists (pA values) were obtained by linear regression, and the intersection with the x-axis is indicated. The data presented in panels (A–D) are averages from at least 5 oocytes; errors are SD. The solid lines show fits to a Hill equation. Currents were recorded at −40 mV.
doi:10.1371/journal.pbio.1001429.g002

Table 3. Data collection and refinement statistics.

Crystallography	WT Ba^{2+}	WT Ba^{2+}	N251A Ba^{2+}	D113A/D158A Ba^{2+}	WT TMAs
Data collection					
Space group	$P4_3$	$P2_1$	$P2_1$	$P2_1$	$P2_1$
Cell dimensions					
a, *b*, *c* (Å)	100.4, 100.4, 263.7	104.6, 267.5, 109.3	101.5, 268.5, 101.2	103.7, 266.7, 108.8	105.4, 266.8, 110.9
α, β, γ (°)	90, 90, 90	90, 112.6, 90	90, 108.6, 90	90, 112.8, 90	90, 109.6, 90
Resolution (Å)	40-3.3	40-3.8	40-3.7	40-4.4	40-4.0
R_{merge}	12.5 (64.6)	11.9 (69.9)	11.8 (81.0)	12.6 (84.3)	11.0 (81.8)
$I/\sigma I$	12.1 (2.7)	7.6 (2.1)	8.1 (2.1)	8.6 (2.5)	8.0 (1.5)
Completeness (%)	99.4 (96.6)	99.3 (99.0)	96.7 (96.2)	98.6 (97.7)	97.1 (85.6)
Redundancy	6.5 (6.1)	3.4 (3.5)	3.5 (3.6)	4.7 (4.7)	3.1 (3.0)
Refinement					
Resolution (Å)	20-3.3	30-3.8	30-3.7	30-4.4	30-4.0
R_{work}/R_{free}	22.7/25.8	25.5/27.2	24.5/27.4	21.6/23.9	25.6/27.0
Wilson B-factor	90	86	109	107	102
R.m.s. deviations					
Bond lengths (Å)	0.01	0.01	0.01	0.01	0.01
Bond angles (°)	1.2	1.2	1.0	1.3	1.2

Values in parentheses are for highest resolution shell. R.m.s., root mean square.
doi:10.1371/journal.pbio.1001429.t003

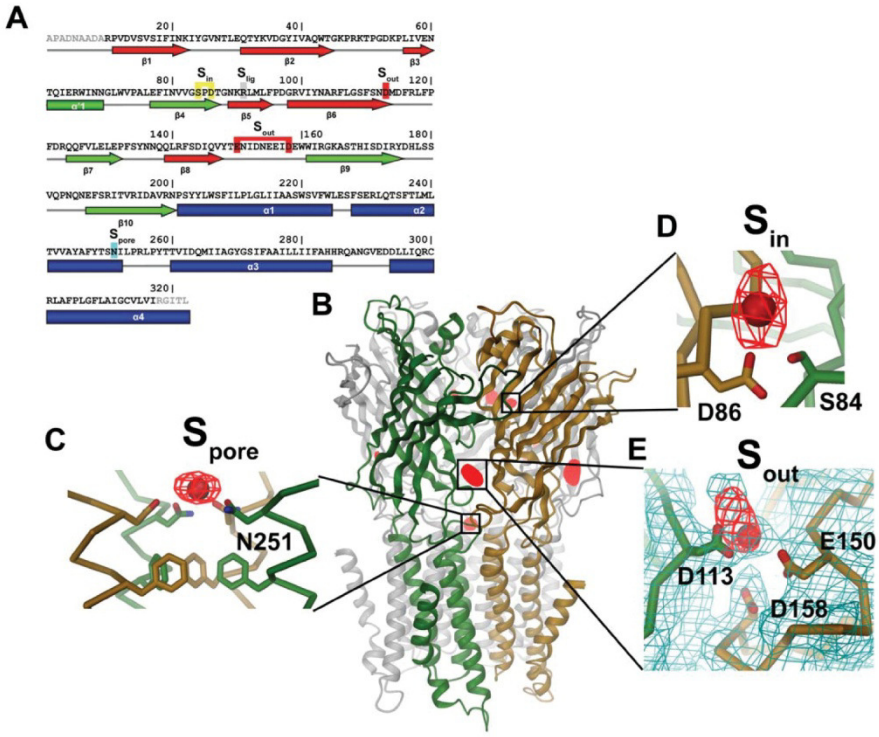

Figure 3. Structure of ELIC in complex with divalent cations. (A) Sequence of ELIC with secondary structure elements indicated below. Residues contributing to ion coordination in different sites are highlighted (S_{in}, yellow; S_{out}, red; S_{pore}, cyan; Arg 91 in the ligand-binding pocket, S_{lig}, grey). (B) Anomalous difference electron density of ELIC in complex with Ba^{2+} superimposed on the structure of the ELIC pentamer (shown as ribbon representation). Ion-binding sites are labeled. Close-up of S_{pore} (C) and S_{in} (D). The protein is shown as Cα-trace with selected side-chains close to Ba^{2+} (red sphere) shown as sticks. (E) Close-up of S_{out}. The protein is shown as Cα-trace with selected side-chains close to Ba^{2+} (red sphere) shown as sticks. The $2F_o$-F_c electron density of a dataset from a crystal of space group $P2_1$ was calculated at 3.8 Å and contoured at 1 σ (shown in cyan). The refined model used to calculate phases did not contain Ba^{2+}-ions. The anomalous difference electron densities shown in (B–E) (red mesh) were calculated from the same dataset at 5 Å and contoured at 5 σ. Crystals of space group $P4_3$ showed a qualitatively similar picture. Structures in Figures 3–7 were prepared with DINO (www.dino3d.org).
doi:10.1371/journal.pbio.1001429.g003

acidic side chains (Asp 113, Glu150, and Asp158) are individually replaced with their uncharged isosteric counterparts (Asn or Gln) and when the acidic side-chains are truncated to Ala (Figure 5, Figure S3). All of these mutations cause a variable but strong decrease in the potency of Ca^{2+}, which suggests that they weaken the interaction with the ion and thus its inhibitory effects (Figure 5E and F). The strongest effect among single mutants is observed for residues Asp113 and Asp158 (Figure 5A, B, and E). Combining these two mutations in the double mutant D113A/D158A virtually abolishes the effects of both calcium and barium on the agonist dose–response curves (Figure 5D, Figure S3E and S3F). Remarkably, and in contrast to our observations in WT, in this double mutant the decrease in I_{max} at high Ca^{2+} concentration appears entirely due to the reduction in single channel conductance (Figure 5G). The binding of Ca^{2+} to S_{out} is thus responsible for both functional effects on the shift of the EC_{50} and the decrease of I_{max}. Figure 5 also shows that mutations in S_{out} shift the EC_{50} towards higher agonist concentrations, an effect that is not surprising given that this region is thought to be important in transducing agonist binding into channel activation (Figure 5A–D, Figure S3, Table S1).

The X-ray structure of the double mutant D113A/D158A in complex with Ba^{2+} is on the whole unperturbed. The double mutation has removed the density of ions bound to S_{out}, while leaving the strong anomalous difference density in S_{pore} unchanged. This confirms that in this mutant divalents fail to modulate channel activation because they cannot bind to the S_{out} site (Figure 5H).

Given that the same mutations abolish also the modulation by Zn^{2+} (Figure 5I), it is very likely that Zn^{2+} inhibits ELIC by binding to the same site. This finding is somewhat unexpected as Zn^{2+} usually interacts with histidine or cysteine residues. However, since the ligand binding domain of ELIC does not contain any cysteines and since mutations of the two histidines, which are both located on β10, did not affect the inhibition by Zn^{2+} (Figure S4), it is likely that the interaction of this transition metal ion with ELIC occurs at this site and therefore deviates from common binding modes.

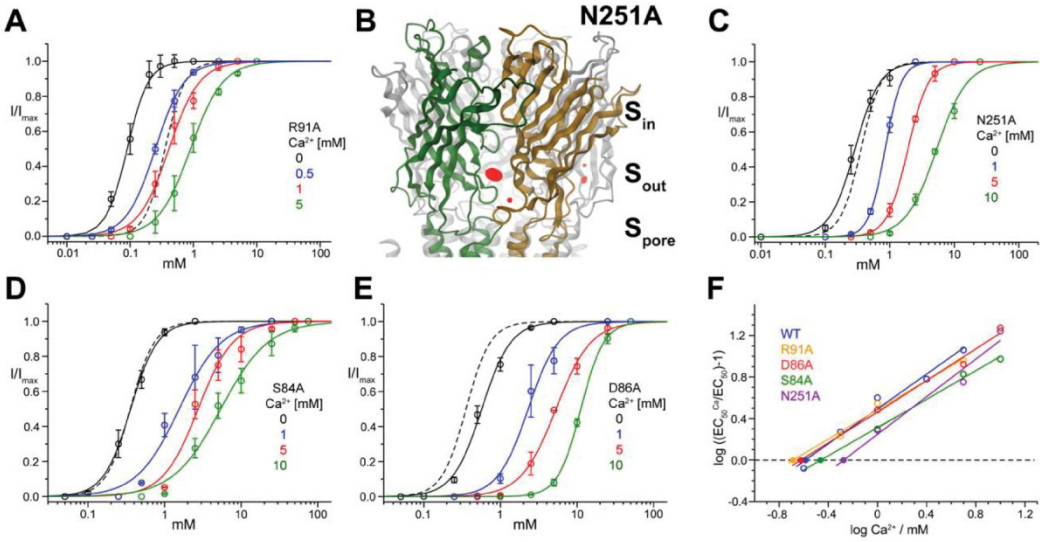

Figure 4. Divalent ion inhibition in mutants of the nonregulatory sites S_{pore} and S_{in}. Dose–response relationships of the ELIC point mutant R91A (A) activated by cysteamine at different concentrations of Ca^{2+}. (B) Anomalous difference electron density (calculated at 5 Å and contoured at 5 σ) from data of the mutant N251A in complex with Ba^{2+} superimposed on a model of ELIC in ribbon representation. Ion-binding sites are indicated. Dose–response relationships of the ELIC point mutants N251A (C), S84A (D), and D86A (E) activated by cysteamine at different concentrations of Ca^{2+}. The data presented in panels (A), (B), (D), and (E) are averages from at least 5 oocytes; errors are SD. The solid lines show fits to a Hill equation. Currents were recorded at −40 mV. A dose–response curve of WT in the absence of Ca^{2+} (dashed line) is shown for comparison. (F) Schild plots quantifying the inhibition of ELIC mutants by Ca^{2+}. EC_{50} values were obtained from fits to data shown in panels (A), (B), (D), and (E). Potencies of the antagonists (pA values) were obtained by linear regression; the intersection with the *x*-axis is indicated (●). WT is shown for comparison.
doi:10.1371/journal.pbio.1001429.g004

Independence of Ca^{2+} and Acetylcholine Inhibition

The results of our mutational analysis strongly suggest that the observed inhibition of ELIC by divalent cations is mediated by the specific interaction with a site that is located at the outer rim of the extracellular domain, at the interface between neighboring subunits. Since this site is distant from the agonist-binding region, we wanted to explore whether there is any direct competition between the effect of divalent ions and that of competitive antagonists binding to the ligand-binding site. Such competitive antagonists include quaternary ammonium compounds such as tetramethylammonium, a weak antagonist (Figure S5), or acetylcholine, which inhibits the channel with higher affinity. The X-ray structure of ELIC in complex with the heavy atom analogue tetramethylarsonium (Figure 6A) and the recently determined structure of ELIC in complex with acetylcholine [41] show that both antagonists bind to the ligand-binding pocket and prevent the binding of the agonist to the same site. The overlap of agonist- and antagonist-binding sites is also reflected in the 10-fold increase in the Schild affinity of acetylcholine in the mutant R91A. This is similar to the increase in agonist potency in the same mutant (Figure 6B and D). In contrast to the mutation in the binding site, the S_{out} double mutant D113A/D158A abolishes the modulatory effect of Ca^{2+} but does not alter the affinity of acetylcholine (WT 1.6 mM, D113A/D158A 2.1 mM), confirming that calcium and acetylcholine act via distinct sites (Figure 6C and F, Table 1).

Finally, in order to probe whether the presence of one antagonist would alter the effect of the other, we have studied the inhibition of ELIC by acetylcholine in the presence of different concentrations of Ca^{2+} and vice versa. In no case did we find any significant change in the potency of either antagonist, which suggests that the inhibitory effects are additive and the two compounds thus act independently (Figure 6E–H).

Discussion

In the present study we have investigated how divalent cations modulate the function of ELIC, a bacterial member of the pLGIC family. ELIC is inhibited by alkaline earth metal ions and by the transition metal ion zinc. The modulation reported here resembles similar effects observed in other family members, where divalent cations act as either positive or negative modulators of gating. Ca^{2+} potentiates channel activity in a subset of nAChRs [26,27], whereas it has an inhibitory effect on $5HT_3$Rs [29]. Like in ELIC, in $5HT_3$Rs calcium shifts the EC_{50} of activation towards higher ligand concentrations [29]. The action of Zn^{2+} appears to be more complex. In some subtypes of GABARs, Zn^{2+} inhibits channel activity [31], whereas in GlyRs, nAChRs, and $5HT_3$Rs, it acts as a potentiator at low concentrations and as an inhibitor at higher concentrations [30,32,33]. These opposing effects are believed to be mediated by the successive occupation of binding sites of different affinity.

Divalent Ions Inhibit ELIC Gating by Binding to S_{out}

X-ray structures of ELIC crystals grown in the presence of barium have allowed us to identify five structurally equivalent

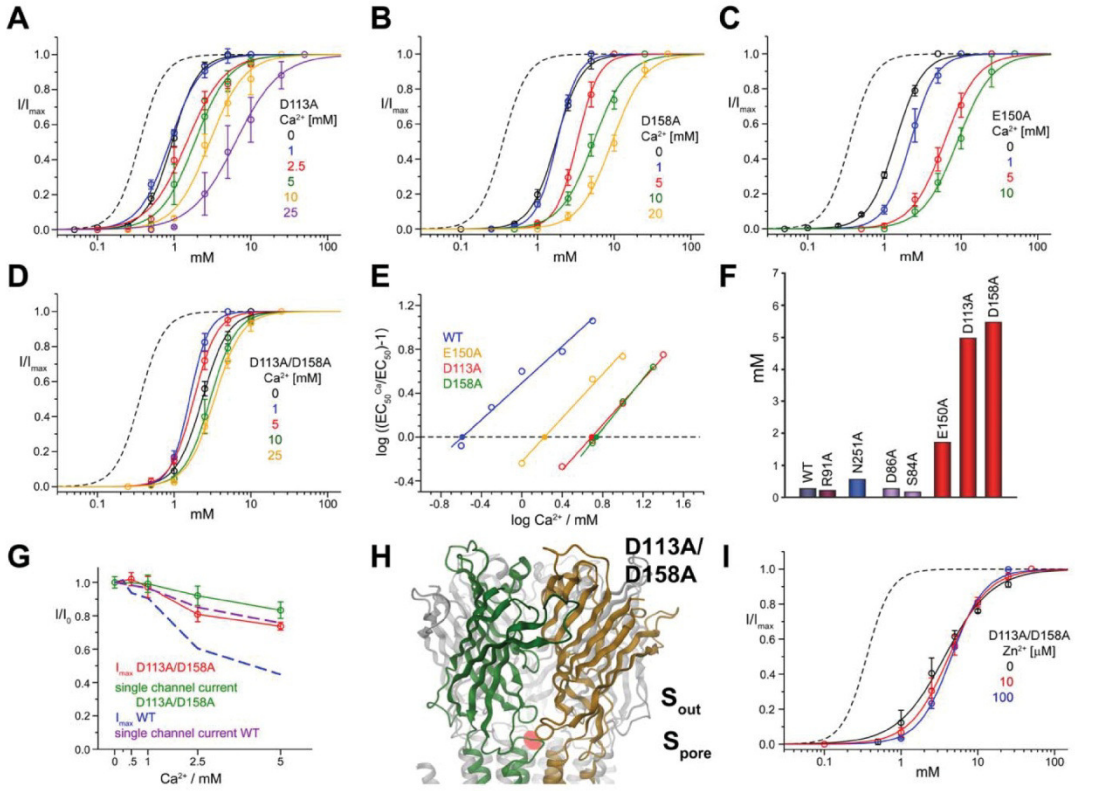

Figure 5. Divalent ion inhibition in mutants of the regulatory site S_{out}. Dose–response relationships of the ELIC mutants D113A (A) and D158A (B), E150A (C), and the double mutant D113A/D158A (D) activated by cysteamine at different concentrations of Ca^{2+} are shown. (E) Schild plots quantifying the inhibition of ELIC mutants by Ca^{2+}. EC_{50} values were obtained from data shown in panels (A–D). Potencies of the antagonists (pA values) were obtained by linear regression; the intersection with the *x*-axis is indicated (●). WT is shown for comparison. (F) Graphical depiction of potencies for Ca^{2+} inhibition in different mutants. (G) Maximum current response of the double mutant D113A/D158A at different Ca^{2+} concentrations. The currents are normalized to the maximum response in the absence of Ca^{2+}. Whole cell currents measured at −40 mV with the two-electrode voltage clamp technique are shown in red (the averages of at least 5 oocytes are shown; errors are SD). Single channel currents from the double mutant D113A/D158A were measured in the outside-out configuration and are shown in green. WT macroscopic and single channel currents are shown as dashed lines for comparison. (H) Anomalous difference electron density (calculated at 5 Å and contoured at 5 σ) from data of the double mutant D113A/D158A in complex with Ba^{2+} is superimposed on a model of ELIC in ribbon representation. Ion-binding sites are indicated. (I) Dose–response relationships of the double mutant D113A/D158A activated by propylamine at different concentrations of Zn^{2+}. The data presented in panels (A–D) and (I) are averages from at least 5 oocytes; errors are SD. The solid lines show fits to a Hill equation. Currents were recorded at −40 mV. A dose–response curve of WT in the absence of Ca^{2+} (dashed line) is shown for comparison.
doi:10.1371/journal.pbio.1001429.g005

binding sites (S_{out}) located at subunit interfaces on the extracellular domain about 15 Å from the agonist-binding region. These are likely to be responsible for the observed inhibition, as mutations at this site have a strong effect on the potency of both Ca^{2+} and Zn^{2+}. The sites resemble regulatory calcium-binding pockets found in other ion channel proteins, where the divalent ions interact with the side chains of acidic residues that are often organized in clusters on the protein sequence (Figure 7A) [44–46]. The interaction found in ELIC is, however, not typical for zinc-binding sites, as these usually contain either histidines or cysteines for ion coordination [47–49], residues that are unlikely to play this role in ELIC (Figure 7A, Figure S4).

While the residues that interact with divalent cations in ELIC are not conserved across pLGICs, there is evidence that equivalent modulatory effects in other pLGICs involve the same (S_{out}) region. In the α7-nAChR, the residue Glu 172, which has been identified as a key residue in the interaction with calcium [50–52], resides on the same loop as Glu 150 and Asp 158 (loop 8) in ELIC. Similarly, histidine and glutamate residues contributing to the interaction with Zn^{2+} in $GABA_A$Rs were mapped to the same location, at the interface between two subunits [53], thus indicating that the Zn^{2+}-dependent inhibition of $GABA_A$Rs may follow a similar mechanism. Residues in the same loop of $5HT_3$Rs have also been proposed to participate to calcium regulation of this receptor [54].

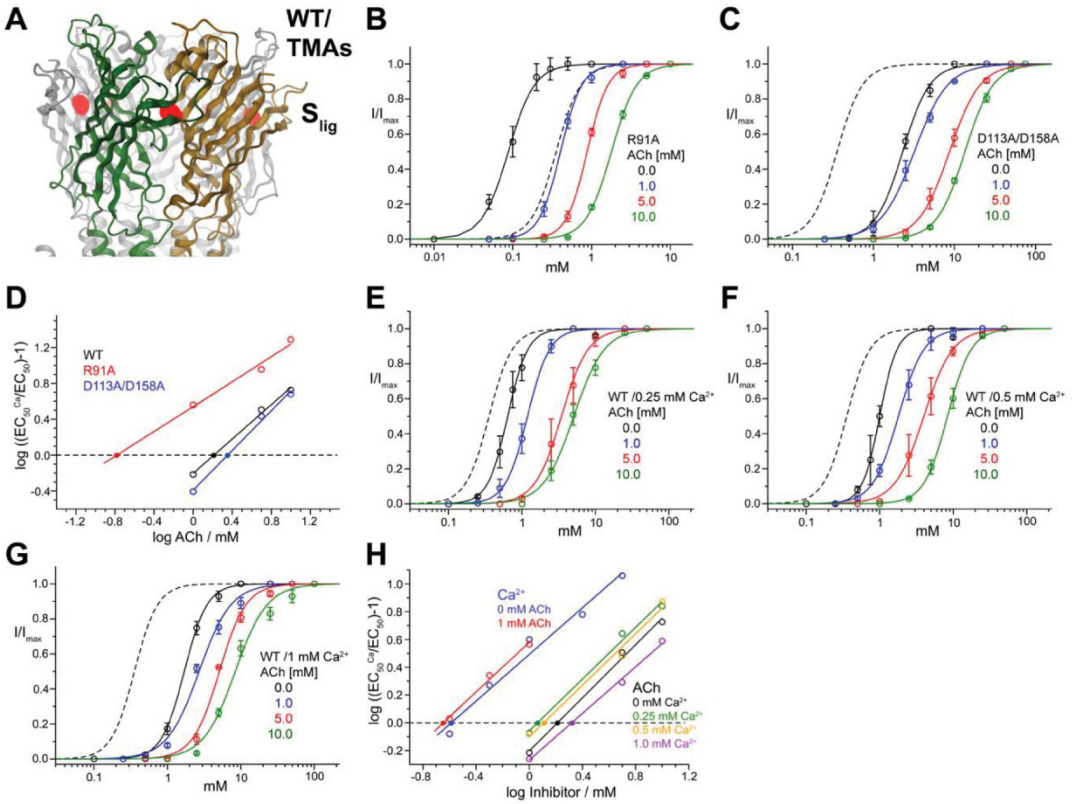

Figure 6. Inhibition by ACh. (A) Anomalous difference electron density (calculated at 5 Å and contoured at 6 σ) from data of WT in complex with TMAs is superimposed on a model of ELIC in ribbon representation. The ligand-binding site is indicated. Dose–response relationships upon activation with cysteamine of the ELIC mutants R91A (B) and the double mutant D113A/D158A (C) at different concentrations of ACh. (F) Schild plots quantifying the inhibition of ELIC mutants by ACh. EC_{50} values were obtained from data shown in panels (B–C). Dose–response relationships upon activation with cysteamine of WT in the presence of either 0.25 (E), 0.5 (F), or 1 mM Ca^{2+} (G). (H) Schild plots quantifying the inhibition of ELIC mutants by ACh in the presence of Ca^{2+}. EC_{50} values were obtained from data shown in panels (E–G). Potencies of the antagonists (pA values) were obtained by linear regression; the intersection with the *x*-axis is indicated (●). The data presented in panels (B–C) and (E–G) are averages from at least 5 oocytes; errors are SD. The solid lines show fits to a Hill equation. Currents were recorded at −40 mV. A dose–response curve of WT in the absence of ACh and Ca^{2+} (dashed line) is shown for comparison.
doi:10.1371/journal.pbio.1001429.g006

Interestingly, a study on the $5HT_3R$ has identified an aspartate residue in the pore domain as an important determinant for calcium-dependent inhibition. The equivalent Asn residue in ELIC coordinates the barium ion in the site S_{pore} [55]. We investigated this site by mutagenesis but did not find any indication for a similar role in the calcium regulation of ELIC. The phenotypic difference may be due to a stronger interaction with a divalent ion in the $5HT_3R$ where the respective residue is an aspartate and thus carries a negative charge (cf., an uncharged asparagine in ELIC).

The Mechanism of Action of Divalent Ions

The effect of calcium and other divalent cations on gating of ELIC results in a complex functional phenotype. At low extracellular calcium concentrations, we see a reduction in agonist potency that resembles competitive inhibition (with a linear Schild plot with a slope near unity). Despite this resemblance, the agonist binding site is not involved in this process and the presence of the antagonist acetylcholine (which binds in the canonical agonist site) has no effect on the action of calcium. Finally, higher calcium concentrations reduce the maximum agonist response (to a greater extent than can be accounted for by a conductance decrease). At first sight, these effects appear to be too complex to be explained by a single microscopic action of divalents (i.e., the binding of Ca^{2+} to the site S_{out}). However, they can all be accounted for, if calcium impairs a single step of ELIC activation, for example channel opening, provided gating is efficient in wild-type ELIC (i.e., the agonist efficacy E is high to start with, Figure 7B). This is a plausible hypothesis, given the high open probability of the single channel activity in Figure 1A.

In first approximation, the relation between maximum open probability P_{max} and efficacy E is:

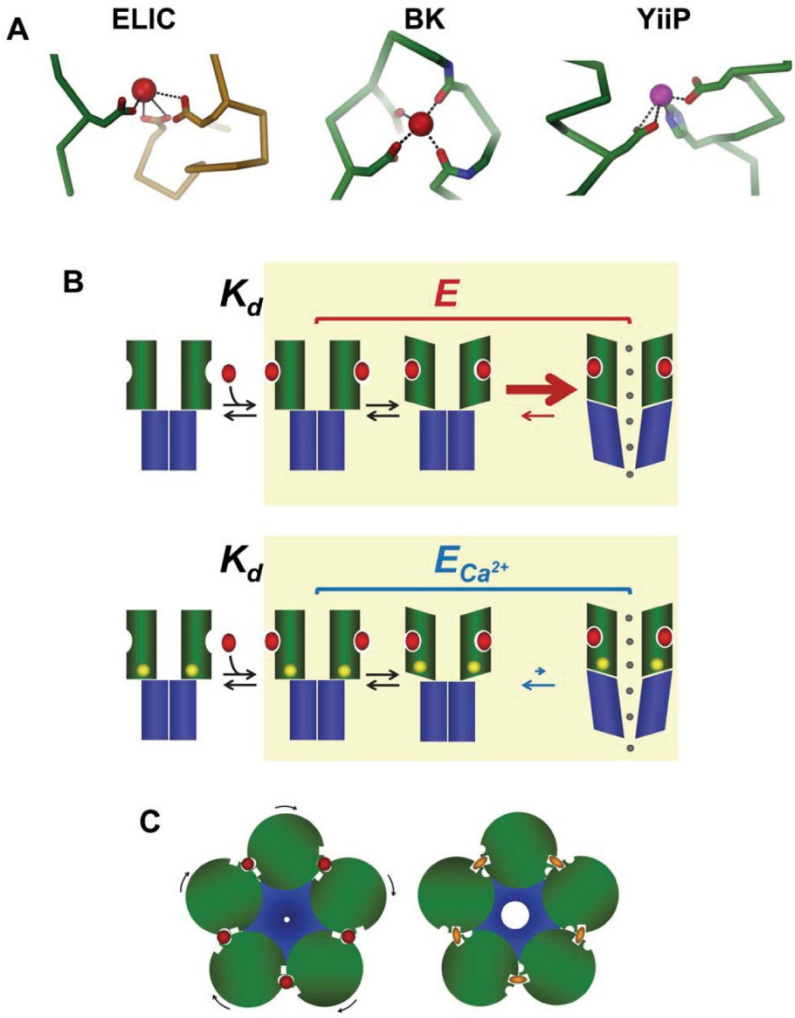

Figure 7. Potential mechanisms. (A) Interactions in the regulatory divalent ion-binding site of ELIC (left) in comparison with a regulatory Ca^{2+} binding site of the BK-channel (middle) and the Zn^{2+}-transporter YiiP (right). (B) Schematic model of a potential mechanism for the inhibitory effect of divalent ions. The two rows show simplified schemes for channel activation in control conditions (top) and in the presence of divalent ions. From left to right, the schemes show that binding of agonist molecules (red ovals) to the extracellular domain (with microscopic affinity K_d) is followed by conformational changes (yellow background) that result in channel opening. Channel gating (described by the efficacy equilibrium constant E) is impaired when the channel is bound to divalent ions (yellow circles, $E_{Ca^{2+}}$). The decrease in agonist efficacy is likely to be due to a change in the rate of opening, as shown by the size of the arrows in the last step of the reaction. (C) Schematic mechanism of how binding sites located on similar places of an oligomeric channel could alternately stabilize the closed or open conformation of the channel.
doi:10.1371/journal.pbio.1001429.g007

$$P_{max} = \frac{E}{E+1},$$

and our observations of an ELIC P_{max} greater than 95% are compatible with values of E that are greater than 20 (as reported for other pLGIC such as nicotinic and glycine receptors). If the value of E is high to start with, the reduction in efficacy produced by divalents must be substantial before a decrease in maximum response becomes apparent. That is why it is seen only at high calcium concentrations. More modest decreases in efficacy, at low calcium concentrations, will cause only a decrease in agonist

potency. This is because agonist EC_{50} is directly affected by the value of E. In the simplest del Castillo-Katz model, EC_{50} is given by:

$$EC50 = \frac{K_d}{E+1},$$

where K_d is the microscopic dissociation constant of the agonist (Figure 7B) [56].

It can also be shown (Text S1) that the effects of calcium and those of a competitive antagonist are expected to be independent, if we model equilibrium channel activation with a simple scheme, where calcium binding impairs gating (by affecting E) and the antagonist binds to the resting form of the channel. This model not only predicts Schild-like behavior for the effect of calcium but suggests also that the Schild intercept is a reasonable estimate for the microscopic affinity of divalents (Text S1).

These conclusions are unchanged if we model channel activation by a more detailed and realistic activation scheme, incorporating an intermediate state between agonist binding and channel opening. The existence of one or more gating intermediate states for channels in the nicotinic superfamily is supported by several lines of evidence. For instance, φ analysis in muscle nicotinic AChRs [57] indicates that blocks of residues move asynchronously in the gating conformational change. In addition to that, mechanisms with reaction intermediates (referred to as flip, primed, or catch-and-hold [13,58–61]) are needed to explain several aspects of the function of the GlyR and the muscle nicotinic AChR, such as agonist efficacy (Figure 7B). In our experiments, the presence of an additional intermediate step that limits the maximum rate of current onset in agonist-bound ELIC channels is required to explain the results of our agonist concentration jumps. This is because we observed that low calcium increased the agonist concentration needed to achieve the maximum rate of current onset, but did not change the limiting rate of channel gating. If activation went through a single conformational step as the channel gates (as in a simple del Castillo-Katz mechanism), this single step would control both the rate of current onset for the agonist-bound channel and the maximum response, and any changes in this would be experimentally detectable (see Text S1).

Conclusions

In our study we have shown how the binding of calcium to a single site remote from the ligand binding pocket modulates the activation of the pLGIC ELIC. Given that divalent ions impair ELIC gating, they are expected to bind more tightly to the resting state of the channel and stabilize it. The location of the divalent binding site at the interface between adjacent subunits is an intriguing mechanism to stabilize distinct states in an allosteric protein, given that these regions are involved in conformational changes (Figure 7C). Thus, occupancy by divalent ions of sites at a similar location in the different pLGICs will result in potentiation or inhibition, depending on whether the equilibrium is shifted towards conducting or nonconducting conformations. Allosteric modulation is important for the pharmacology of pLGICs, as many of pLGIC drugs in therapeutic use act by this mechanism, although by binding to sites distinct from those of divalent ions.

Modulation by divalent ions of pLGICs occurs at concentrations that are physiologically relevant in vertebrates and may regulate the activity of channels in their natural environment [31,62]. It is not known whether such regulation is important for ELIC activity in its natural host *Erwinia chrysanthemi*, but it is remarkable that the observed mechanism has been conserved during evolution.

Materials and Methods

Protein Expression and Purification

ELIC WT and point mutants were expressed and purified as described [36,37]. *E. coli* BL21DE3 containing a vector encoding for a fusion protein consisting of the pelB signal sequence, a His_{10} tag, maltose binding protein, a HRV 3C protease site, and ELIC were grown in M9 minimal medium at 37°C to an OD of 1.0 and subsequently cooled to 20°C. Expression was induced by addition of 0.3 mM IPTG and carried out overnight. All the following steps were performed at 4°C. The protein was extracted from isolated membranes in a buffer containing 1% n-Undecyl-β-D-Maltoside (UDM, Anatrace, Inc.) and purified by Ni-NTA chromatography (Qiagen). The purified MBP-ELIC-fusion protein was digested with HRV 3C protease to cleave the His_{10}-MBP protein. His_{10}-MBP and 3C protease were subsequently removed from solution by binding to Ni-NTA resin. ELIC was concentrated and subjected to gel-filtration on a Superdex 200 column (GE Healthcare). The protein peak corresponding to the ELIC pentamer was pooled and concentrated to 10 mg/ml and used for crystallization.

Crystallization and Structure Determination

The purified protein was crystallized in sitting drops at 4°C. Protein containing additional 0.5 mg/ml *E. coli* polar lipids (Avanti Polar Lipids, Inc.) was mixed in a 1:1 ratio with reservoir solution (50 mM ADA pH 6.5, 50 mM $BaAc_2$, and 10% (w/v) PEG4000). The crystals were cryoprotected by transfer into solutions containing 30% ethyleneglycol. All datasets were collected on frozen crystals on the X06SA beamline at the Swiss Light Source (SLS) of the Paul Scherrer Institut (PSI) on a PILATUS detector (Dectris). The data were indexed, integrated, and scaled with XDS [63] and further processed with CCP4 programs [64]. The structure of WT and mutants in space groups $P4_3$ and $P2_1$ were determined by molecular replacement in PHASER [65] using the ELIC pentamer (2VLO) as a search model. G164, which was not included in the original model (2VLO), was introduced according to the structure of the ELIC acetylcholine complex (3RQW). The absence of this amino acid had only a local effect and did not influence the location of neighboring residues. The model was rebuilt in Coot [66] and refined maintaining strong NCS constraints in PHENIX [67]. R and R_{free} were monitored throughout. R_{free} was calculated by selecting 5% of the reflection data in thin slices that were selected for the initial dataset of ELIC and that were omitted in refinement.

Isothermal Titration Calorimetry

Binding of the agonist propylamine to ELIC in the presence and absence of calcium was measured by isothermal titration calorimetry (ITC) with a MicroCal ITC200 system (GE Healthcare). The syringe was loaded with agonist solution containing 30–37 mM propylamine dissolved in measurement buffer (containing 25 mM Tris-HCl pH8.5, 150 mM NaCl, and in certain experiments 0.6 mM $CaCl_2$). The sample cell was loaded with 300 µl of purified ELIC in measurement buffer containing 0.9 mM UDM at a concentration between 80 and 110 µM. Agonist was applied by sequential injections of 2 µl aliquots followed by a 180 s equilibration period after each injection. The data were recorded at 4°C and analyzed by a fit to a single-site binding isotherm.

Two-Electrode Voltage Clamp Recording

Constructs containing the gene of either the WT or mutant channels preceded by the signal sequence of the chicken α7nAchR were cloned into the pTLN vector for expression in *X. laevis* oocytes [68]. After linearization of the plasmid DNA by MluI, capped complementary RNA was transcribed with the mMessage mMachine kit (Ambion) and purified with the RNeasy kit (Qiagen). For expression, 1–50 ng of RNA was injected into defolliculated oocytes. Two-electrode voltage clamp measurements were performed 1 d after injection at 20°C (OC-725B, Warner Instrument Corp.). Currents were recorded in bath solutions containing 10 mM HEPES (pH 7), 130 mM NaCl, and the indicated concentrations of cysteamine and divalent cations. In case of solutions containing Zn^{2+}, cysteamine was replaced by propylamine. The membrane potential in all dose–response measurements was set to −40 mV. As ELIC is permeable to divalent cations, we tested if endogenous calcium-activated chloride channels affected our measurements. To chelate intracellular calcium ions, the oocytes were incubated for 15 to 30 min in bath solutions lacking divalent ions but containing 10 μM BAPTA-AM. Dose–response curves in the presence of calcium obtained from BAPTA-AM-treated oocytes did not differ from the measurements of the untreated oocytes even at elevated Ca^{2+} concentration (Figure S6). The lack of a significant effect is likely due to the strong outward-rectification of calcium-activated chloride channels, which do not pass significant currents at negative voltages.

Patch Clamp Recording in *X. oocytes*

X. laevis oocytes were transferred to a hyperosmotic solution to manually remove the vitelline layer. Membrane patches were recorded in the excised outside-out configuration 3–5 d after injection of mRNA with an Axopatch 200B amplifier (Axon Instruments) at 20°C. Data were sampled at 100 μs, filtered with 1,000 Hz, and analyzed using Clampfit (Axon Instruments, Inc.). Bath solutions contained 10 mM HEPES (pH 7.0), 150 mM NaCl, and indicated concentrations of ligands and divalent cations. Electrodes had a resistance of 3–5 MΩ. Pipette solutions contained 150 mM NaCl, 10 mM EGTA, 5 mM $MgCl_2$, and 10 mM HEPES at pH 7.0. Bath electrodes were placed in 1 M KCl solution connected to the bath solution by Agar bridges. The agonists were applied to the patch using a stepper motor (SF77B Perfusion fast step, Warner).

Patch Clamp Recording in HEK 293 Cells

Human embryonic kidney 293 cells (American Type Culture Collection-CRL-1573;LGC Promochem) were maintained at 37°C in a 95% air/5% CO_2 incubator in DMEM supplemented with 0.11 g/l sodium pyruvate, 10% (v/v) heat-inactivated fetal bovine serum, 100 U/ml penicillin G, 100 μg/ml streptomycin sulfate, and 2 mM L-glutamine (Invitrogen). Cells (passaged every 2 d, up to 30 times) were plated and transfected by calcium phosphate-DNA coprecipitation [69], with a total amount of DNA of 3 μg/dish (82% ELIC and 18% eGFP DNA, both subcloned in pcDNA3).

Cells were bathed in an extracellular solution containing (mM): 150 KCl, 0.05 or 0.2 $CaCl_2$, and 10 HEPES, pH adjusted to 7.4 with KOH (osmolarity 310 mOsm). Patch pipettes were pulled from thick-walled borosilicate glass (GC150F; Harvard Apparatus) and fire polished to a resistance of 8–12 MΩ. Intracellular solution contained (mM): 150 KCl, 0.5 $CaCl_2$, 5 EGTA, and 10 HEPES, pH adjusted to 7.4 with KOH. Agonist-evoked currents were recorded at 20°C with an Axopatch 200B amplifier (Molecular Devices) from outside-out patches held at −100 mV. Patches were stepped to this holding voltage 0.2 s before the agonist was applied and otherwise held at −40 mV. No correction for junction potential was applied (calculated value 0.2 mV). Currents were filtered at 5 kHz, digitized at 50 kHz with Digidata 1322A, and saved directly on computer with Clampex software (all MDS Analytical Technologies).

All concentration jumps were performed using a piezo stepper (Burleigh instruments) with an application tool made from theta tube glass (Hilgenberg; final tip diameter, 150 μm). Voltage commands for the piezo stepper were 200 ms square pulses conditioned by low-pass eight-pole Bessel filtering (−3 dB frequency 5 kHz) to smooth oscillations. Actual exchange time was estimated by recording the open-tip response to the application of diluted extracellular solution (70% water) after rupture of the patch. Only patches in which the 20%–80% exchange time was faster than 250 μs were included in the analysis.

Agonist solutions were freshly prepared every day from 1 M stock solutions. Propylamine was applied at a concentration known to elicit maximum response (20 mM and 50 mM, for 50 and 200 μM Ca^{2+}, respectively). Traces shown are averages of 5 or 10 individual agonist currents, separated by at least 10 s. Responses were averaged, and the time course of activation and deactivation (between 95% and 5% of the peak current level) was fitted with one exponential component (program Clampfit 9.0).

Accession Code

The coordinates of the $P4_3$ crystal form of ELIC in complex with Ba^{2+} have been deposited with the Protein Data Bank under code 2yn6.

Supporting Information

Figure S1 Dose–response relationships at high Ca^{2+} concentrations. Cysteamine dose–response relationships of ELIC in the presence of different concentrations of Ca^{2+}. Currents were recorded at −40 mV. The data are averages from at least 5 oocytes; errors are SD. The solid lines show fits to a Hill equation. (B) Schild plot quantifying the inhibition by Ca^{2+}. EC_{50} values were obtained from fits to data shown in panel (A). Potencies of the antagonists (pA values) were obtained by linear regression; the intersection with the *x*-axis is indicated (•).
(JPG)

Figure S2 Barium binding. (A) Plot of maximum agonist responses and single channel currents at different Ba^{2+} concentrations. The currents are normalized to the control values (in the absence of Ba^{2+}). Maximum cysteamine currents (blue symbols) were measured with the two-electrode voltage clamp technique. Single channel currents (green symbols) were measured from excised patches in the outside-out configuration. (B, C) Structure of the divalent cation binding site S_{out}. Stereo representations of the binding region in two different crystal forms. The protein is shown as Cα-trace with selected side-chains close to Ba^{2+} (red sphere) shown as sticks. $2F_o$-F_c electron densities are shown as cyan mesh. The refined models used to calculate phases did not contain Ba^{2+}-ions. (B) Space group $P4_3$. The $2F_o$-F_c electron density was calculated at 3.3 Å and contoured at 1 σ. The anomalous difference electron density (calculated at 5 Å and contoured at 5 σ) was obtained from the same dataset. (C) Space group $P2_1$. The $2F_o$-F_c electron density was calculated at 3.8 Å and contoured at 1 σ. The anomalous difference electron density (calculated at 5 Å and contoured at 5 σ) was obtained from the same dataset.
(JPG)

Figure S3 Divalent ion inhibition in mutants of the regulatory site S_{out}. Dose–response relationships of the ELIC mutants D113N (A), D158N (B), and E150Q (C) activated by cysteamine at different concentrations of Ca^{2+} are shown. (D) Schild plots quantifying the inhibition of ELIC mutants by Ca^{2+}. (E) Dose–response relationships of the ELIC double mutant D113A/D158A activated by cysteamine at different concentrations of Ba^{2+} are shown. (F) Schild plot quantifying the inhibition of the ELIC double mutant D113A/D158A by Ba^{2+}. EC_{50} values were obtained from data shown in panels (A–C) and (E). Potencies of the antagonists (pA values) in (D) and (F) were obtained by linear regression; the intersection with the *x*-axis is indicated (•). WT is shown for comparison. The data presented in panels (A–C) and (E) are averages from at least 5 oocytes; errors are SD. The solid lines show fits to a Hill equation. Currents were recorded at −40 mV. A dose–response curve of WT in the absence of Ca^{2+} (dashed line) is shown for comparison.
(JPG)

Figure S4 Divalent ion inhibition in mutants of histidine residues in the extracellular domain. Dose–response relationships of the ELIC mutants H168A (A) and H176A (B) activated by cysteamine at different concentrations of Ca^{2+} are shown. (C) Schild plots quantifying the inhibition of ELIC mutants by Ca^{2+}. EC_{50} values were obtained from data shown in panels (A–B). Potencies of the antagonists (pA values) were obtained by linear regression; the intersection with the *x*-axis is indicated (•). WT is shown for comparison. The data presented in panels (A–B) are averages from at least 5 oocytes; errors are SD. The solid lines show fits to a Hill equation. Currents were recorded at −40 mV. A dose–response curve of WT in the absence of Ca^{2+} (dashed line) is shown for comparison.
(JPG)

Figure S5 Inhibition by tetramethylammonium (TMA). Dose–response relationships of WT (A) and the mutant R91A (B) activated by cysteamine at different concentrations of TMA are shown. A dose–response curve of WT in the absence of TMA (dashed line) is shown for comparison. (C) Schild plots quantifying the inhibition by TMA. EC_{50} values were obtained from data shown in panels (A–B). Potencies of the antagonists (pA values) were obtained by linear regression; the intersection with the *x*-axis is indicated (•). WT is shown for comparison. The data presented in panels (A–B) are averages from at least 5 oocytes; errors are SD. The solid lines show fits to a Hill equation. Currents were recorded at −40 mV.
(JPG)

Figure S6 Ca^{2+} inhibition measured from BAPTA-AM-treated oocytes. Dose–response relationships of WT activated by cysteamine at different concentrations of Ca^{2+} are shown. To chelate intracellular Ca^{2+}, oocytes were incubated in solutions lacking divalent ions but containing 10 μM Bapta-AM. (C) Schild plots comparing the inhibition of ELIC in BAPTA-treated oocytes by Ca^{2+}. EC_{50} values were obtained from data shown in panel (A). Potencies of the antagonists (pA values) were obtained by linear regression; the intersection with the *x*-axis is indicated (•). WT from oocytes treated by standard procedures is shown for comparison. The data presented in panel (A) are averages from at least 5 oocytes; errors are SD. The solid lines show fits to a Hill equation. Currents were recorded at −40 mV.
(JPG)

Table S1 Dose–response relationships of agonists in the presence of different modulators.
(DOC)

Text S1 Supplementary discussion.
(DOCX)

Acknowledgments

We thank the staff of the X06SA beamline for support during data collection, Ilian Jelezarov for help with calorimetry experiments, Alwin Reiter and Dirk Trauner for providing a sample of tetramethyarsonium, and members of the Dutzler lab for help in all stages of the project. Data collection was performed at the X06SA beamline at the Swiss Light Source of the Paul Scherrer Institute.

Author Contributions

The author(s) have made the following declarations about their contributions: Conceived and designed the experiments: RD IZ LGS. Performed the experiments: IZ CB AM. Analyzed the data: RD IZ CB LGS AM. Wrote the paper: RD IZ LGS AM CB.

References

1. Hille B (2001) Ion channels of excitable membranes, third edition. Sunderland, MA: Sinauer Associates Inc.
2. Karlin A (2002) Emerging structure of the nicotinic acetylcholine receptors. Nat Rev Neurosci 3: 102–114.
3. Lester HA, Dibas MI, Dahan DS, Leite JF, Dougherty DA (2004) Cys-loop receptors: new twists and turns. Trends Neurosci 27: 329–336.
4. Sine SM, Engel AG (2006) Recent advances in Cys-loop receptor structure and function. Nature 440: 448–455.
5. Sivilotti LG (2010) What single-channel analysis tells us of the activation mechanism of ligand-gated channels: the case of the glycine receptor. J Physiol 588: 45–58.
6. Miller PS, Smart TG (2010) Binding, activation and modulation of Cys-loop receptors. Trends Pharmacol Sci 31: 161–174.
7. Thompson AJ, Lester HA, Lummis SC (2010) The structural basis of function in Cys-loop receptors. Q Rev Biophys 43: 449–499.
8. Yakel JL (2010) Gating of nicotinic ACh receptors: latest insights into ligand binding and function. J Physiol 588: 597–602.
9. Unwin N (2005) Refined structure of the nicotinic acetylcholine receptor at 4A resolution. J Mol Biol 346: 967–989.
10. Hilf RJ, Dutzler R (2009) A prokaryotic perspective on pentameric ligand-gated ion channel structure. Curr Opin Struct Biol 19: 418–424.
11. Celie PH, van Rossum-Fikkert SE, van Dijk WJ, Brejc K, Smit AB, et al. (2004) Nicotine and carbamylcholine binding to nicotinic acetylcholine receptors as studied in AChBP crystal structures. Neuron 41: 907–914.
12. Sabey K, Paradiso K, Zhang J, Steinbach JH (1999) Ligand binding and activation of rat nicotinic alpha4beta2 receptors stably expressed in HEK293 cells. Mol Pharmacol 55: 58–66.
13. Burzomato V, Beato M, Groot-Kormelink PJ, Colquhoun D, Sivilotti LG (2004) Single-channel behavior of heteromeric alpha1beta glycine receptors: an attempt to detect a conformational change before the channel opens. J Neurosci 24: 10924–10940.
14. Lester HA, Changeux JP, Sheridan RE (1975) Conductance increases produced by bath application of cholinergic agonists to Electrophorus electroplaques. J Gen Physiol 65: 797–816.
15. Rayes D, De Rosa MJ, Sine SM, Bouzat C (2009) Number and locations of agonist binding sites required to activate homomeric Cys-loop receptors. J Neurosci 29: 6022–6032.
16. Beato M, Groot-Kormelink PJ, Colquhoun D, Sivilotti LG (2004) The activation mechanism of alpha1 homomeric glycine receptors. J Neurosci 24: 895–906.
17. Grosman C, Zhou M, Auerbach A (2000) Mapping the conformational wave of acetylcholine receptor channel gating. Nature 403: 773–776.
18. Taly A, Corringer PJ, Guedin D, Lestage P, Changeux JP (2009) Nicotinic receptors: allosteric transitions and therapeutic targets in the nervous system. Nat Rev Drug Discov 8: 733–750.
19. Mohler H (2011) The rise of a new GABA pharmacology. Neuropharmacology 60: 1042–1049.
20. Yamakura T, Bertaccini E, Trudell JR, Harris RA (2001) Anesthetics and ion channels: molecular models and sites of action. Annu Rev Pharmacol Toxicol 41: 23–51.
21. Lobo IA, Harris RA (2008) GABA(A) receptors and alcohol. Pharmacol Biochem Behav 90: 90–94.
22. Hibbs RE, Gouaux E (2011) Principles of activation and permeation in an anion-selective Cys-loop receptor. Nature 474: 54–60.

23. Dani JA, Eisenman G (1987) Monovalent and divalent cation permeation in acetylcholine receptor channels. Ion transport related to structure. J Gen Physiol 89: 959–983.
24. Adams DJ, Dwyer TM, Hille B (1980) The permeability of endplate channels to monovalent and divalent metal cations. J Gen Physiol 75: 493–510.
25. Sine SM, Claudio T, Sigworth FJ (1990) Activation of Torpedo acetylcholine receptors expressed in mouse fibroblasts. Single channel current kinetics reveal distinct agonist binding affinities. J Gen Physiol 96: 395–437.
26. Mulle C, Lena C, Changeux JP (1992) Potentiation of nicotinic receptor response by external calcium in rat central neurons. Neuron 8: 937–945.
27. Vernino S, Amador M, Luetje CW, Patrick J, Dani JA (1992) Calcium modulation and high calcium permeability of neuronal nicotinic acetylcholine receptors. Neuron 8: 127–134.
28. Peters JA, Hales TG, Lambert JJ (1988) Divalent cations modulate 5-HT3 receptor-induced currents in N1E-115 neuroblastoma cells. Eur J Pharmacol 151: 491–495.
29. Niemeyer MI, Lummis SC (2001) The role of the agonist binding site in Ca(2+) inhibition of the recombinant 5-HT(3A) receptor. Eur J Pharmacol 428: 153–161.
30. Palma E, Maggi L, Miledi R, Eusebi F (1998) Effects of Zn2+ on wild and mutant neuronal alpha7 nicotinic receptors. Proc Natl Acad Sci U S A 95: 10246–10250.
31. Smart TG, Xie X, Krishek BJ (1994) Modulation of inhibitory and excitatory amino acid receptor ion channels by zinc. Prog Neurobiol 42: 393–441.
32. Laube B, Kuhse J, Rundstrom N, Kirsch J, Schmieden V, et al. (1995) Modulation by zinc ions of native rat and recombinant human inhibitory glycine receptors. J Physiol 483 (Pt 3): 613–619.
33. Hubbard PC, Lummis SC (2000) Zn(2+) enhancement of the recombinant 5-HT(3) receptor is modulated by divalent cations. Eur J Pharmacol 394: 189–197.
34. Hsiao B, Mihalak KB, Magleby KL, Luetje CW (2008) Zinc potentiates neuronal nicotinic receptors by increasing burst duration. J Neurophysiol 99: 999–1007.
35. Moroni M, Vijayan R, Carbone A, Zwart R, Biggin PC, et al. (2008) Non-agonist-binding subunit interfaces confer distinct functional signatures to the alternate stoichiometries of the alpha4beta2 nicotinic receptor: an alpha4-alpha4 interface is required for Zn2+ potentiation. J Neurosci 28: 6884–6894.
36. Hilf RJ, Dutzler R (2008) X-ray structure of a prokaryotic pentameric ligand-gated ion channel. Nature 452: 375–379.
37. Zimmermann I, Dutzler R (2011) Ligand activation of the prokaryotic pentameric ligand-gated ion channel ELIC. PLoS Biol 9: e1001101. doi:10.1371/journal.pbio.1001101.
38. Hilf RJ, Bertozzi C, Zimmermann I, Reiter A, Trauner D, et al. (2010) Structural basis of open channel block in a prokaryotic pentameric ligand-gated ion channel. Nat Struct Mol Biol 17: 1330–1336.
39. Hilf RJ, Dutzler R (2009) Structure of a potentially open state of a proton-activated pentameric ligand-gated ion channel. Nature 457: 115–118.
40. Bocquet N, Nury H, Baaden M, Le Poupon C, Changeux JP, et al. (2009) X-ray structure of a pentameric ligand-gated ion channel in an apparently open conformation. Nature 457: 111–114.
41. Pan J, Chen Q, Willenbring D, Yoshida K, Tillman T, et al. (2012) Structure of the pentameric ligand-gated ion channel ELIC cocrystallized with its competitive antagonist acetylcholine. Nat Commun 3: 714.
42. Arunlakshana O, Schild HO (1959) Some quantitative uses of drug antagonists. Br J Pharmacol 14: 48–58.
43. Colquhoun D (2007) Why the Schild method is better than Schild realised. Trends Pharmacol Sci 28: 608–614.
44. Yuan P, Leonetti MD, Hsiung Y, MacKinnon R (2012) Open structure of the Ca2+ gating ring in the high-conductance Ca2+-activated K+ channel. Nature 481: 94–97.
45. Wu Y, Yang Y, Ye S, Jiang Y (2010) Structure of the gating ring from the human large-conductance Ca(2+)-gated K(+) channel. Nature 466: 393–397.
46. Schumacher MA, Rivard AF, Bachinger HP, Adelman JP (2001) Structure of the gating domain of a Ca2+-activated K+ channel complexed with Ca2+/calmodulin. Nature 410: 1120–1124.
47. Auld DS (2009) The ins and outs of biological zinc sites. Biometals 22: 141–148.
48. Vallee BL, Auld DS (1990) Zinc coordination, function, and structure of zinc enzymes and other proteins. Biochemistry 29: 5647–5659.
49. Lu M, Chai J, Fu D (2009) Structural basis for autoregulation of the zinc transporter YiiP. Nat Struct Mol Biol 16: 1063–1067.
50. Galzi JL, Bertrand S, Corringer PJ, Changeux JP, Bertrand D (1996) Identification of calcium binding sites that regulate potentiation of a neuronal nicotinic acetylcholine receptor. The EMBO J 15: 5824–5832.
51. Eddins D, Sproul AD, Lyford LK, McLaughlin JT, Rosenberg RL (2002) Glutamate 172, essential for modulation of L247T alpha7 ACh receptors by Ca2+, lines the extracellular vestibule. Am J Physiol Cell Physiol 283: C1454–C1460.
52. Lyford LK, Sproul AD, Eddins D, McLaughlin JT, Rosenberg RL (2003) Agonist-induced conformational changes in the extracellular domain of alpha 7 nicotinic acetylcholine receptors. Mol Pharmacol 64: 650–658.
53. Hosie AM, Dunne EL, Harvey RJ, Smart TG (2003) Zinc-mediated inhibition of GABA(A) receptors: discrete binding sites underlie subtype specificity. Nat Neurosci 6: 362–369.
54. Thompson AJ, Lummis SC (2009) Calcium modulation of 5-HT3 receptor binding and function. Neuropharmacology 56: 285–291.
55. Hu XQ, Lovinger DM (2005) Role of aspartate 298 in mouse 5-HT3A receptor gating and modulation by extracellular Ca2+. J Physiol 568: 381–396.
56. Colquhoun D (1998) Binding, gating, affinity and efficacy: the interpretation of structure-activity relationships for agonists and of the effects of mutating receptors. Br J Pharmacol 125: 924–947.
57. Auerbach A (2005) Gating of acetylcholine receptor channels: brownian motion across a broad transition state. Proc Natl Acad Sci U S A 102: 1408–1412.
58. Mukhtasimova N, Lee WY, Wang HL, Sine SM (2009) Detection and trapping of intermediate states priming nicotinic receptor channel opening. Nature 459: 451–454.
59. Auerbach A (1992) Kinetic behavior of cloned mouse acetylcholine receptors. A semi-autonomous, stepwise model of gating. Biophys J 62: 72–73.
60. Auerbach A (1993) A statistical analysis of acetylcholine receptor activation in Xenopus myocytes: stepwise versus concerted models of gating. J Physiol 461: 339–378.
61. Jadey S, Auerbach A (2012) An integrated catch-and-hold mechanism activates nicotinic acetylcholine receptors. J Gen Physiol 140: 17–28.
62. Amador M, Dani JA (1995) Mechanism for modulation of nicotinic acetylcholine receptors that can influence synaptic transmission. J Neurosci 15: 4525–4532.
63. Kabsch W (1993) Automatic processing of rotation diffraction data from crystals of initially unknown symmetry and cell constants. J Appl Cryst 26: 795–800.
64. CCP4 (1994) Collaborative Computational Project Nr. 4. The CCP4 Suite: Programs for X-ray crystallography. Acta Crystallogr D 50: 760–763.
65. McCoy AJ, Grosse-Kunstleve RW, Adams PD, Winn MD, Storoni LC, Read RJ (2007) Phaser crystallographic software. J Appl Cryst 40: 658–674.
66. Emsley P, Lohkamp B, Scott WG, Cowtan K (2010) Features and development of Coot. Acta Crystallogr D Biol Crystallogr 66: 486–501.
67. Adams PD, Grosse-Kunstleve RW, Hung LW, Ioerger TR, McCoy AJ, et al. (2002) PHENIX: building new software for automated crystallographic structure determination. Acta Crystallogr D Biol Crystallogr 58: 1948–1954.
68. Lorenz C, Pusch M, Jentsch TJ (1996) Heteromultimeric CLC chloride channels with novel properties. Proc Natl Acad Sci U S A 93: 13362–13366.
69. Groot-Kormelink PJ, Beato M, Finotti C, Harvey RJ, Sivilotti LG (2002) Achieving optimal expression for single channel recording: a plasmid ratio approach to the expression of alpha 1 glycine receptors in HEK293 cells. J Neurosci Methods 113: 207–214.

Supplementary Figures

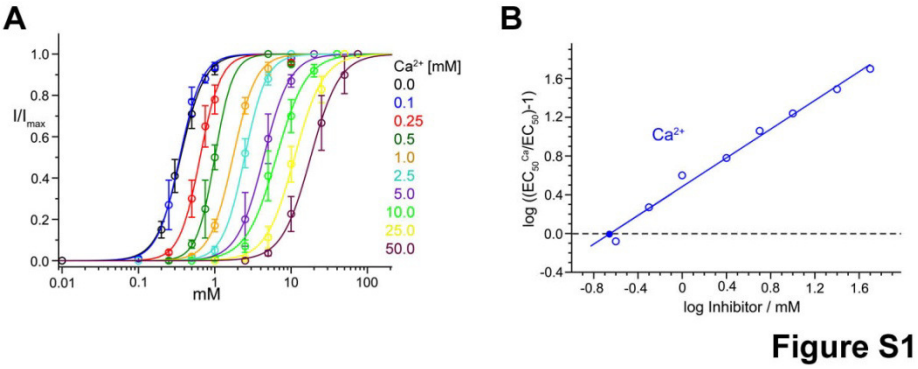

Figure S1

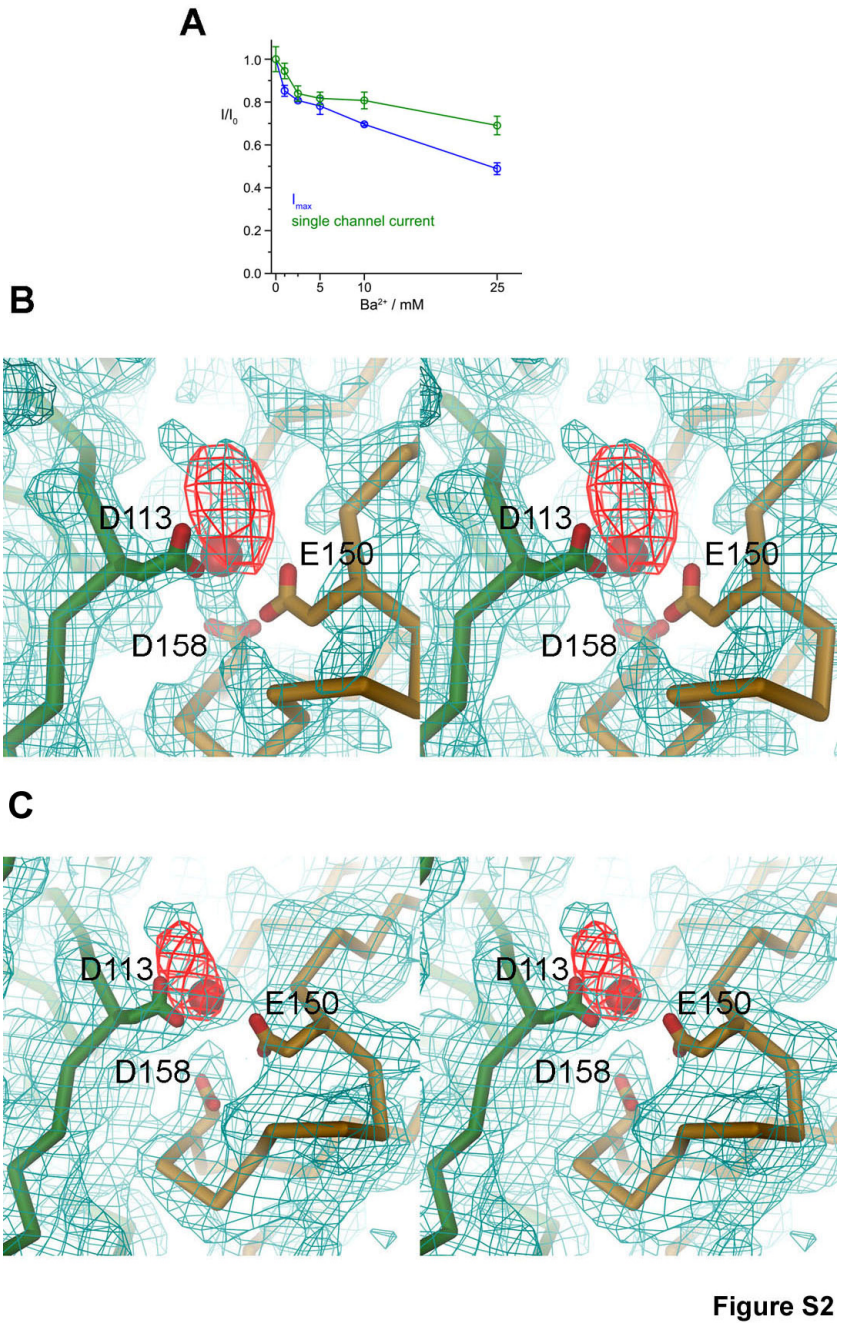

Figure S2

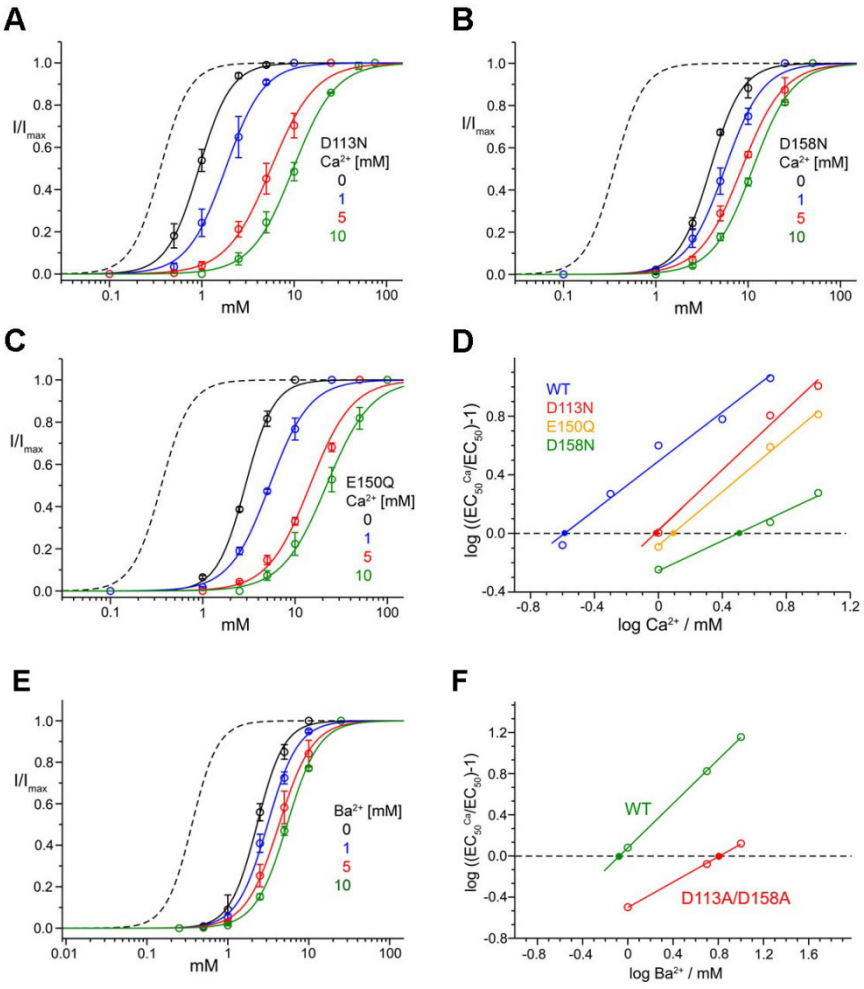

Figure S3

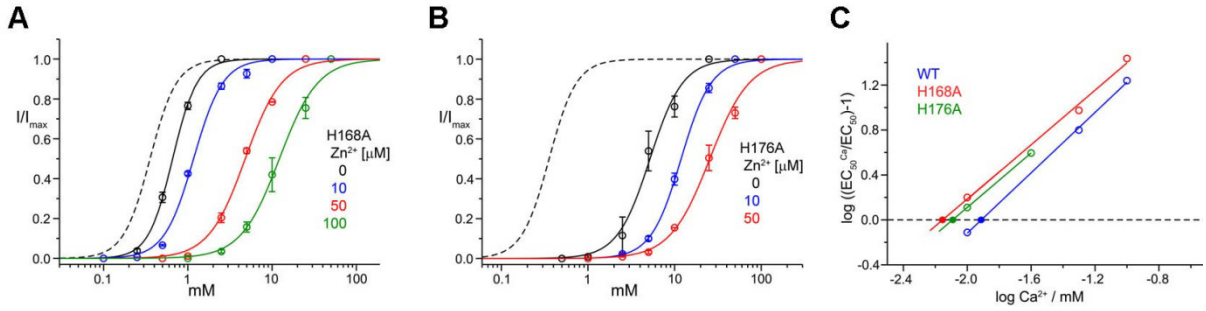

Figure S4

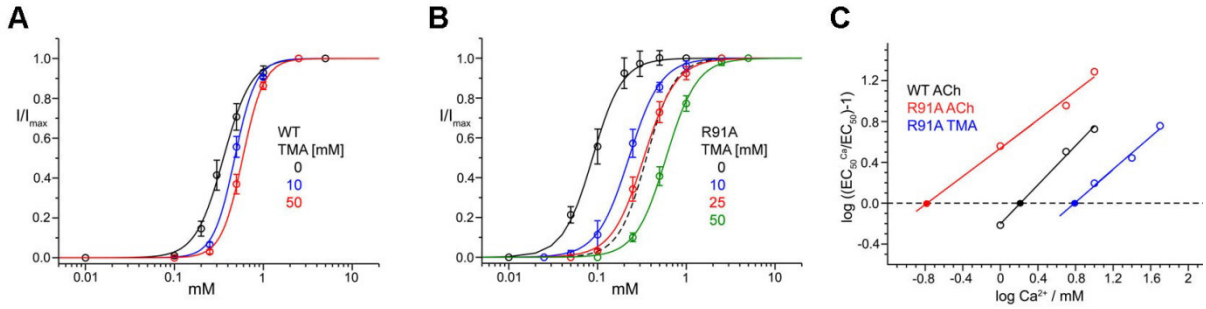

Figure S5

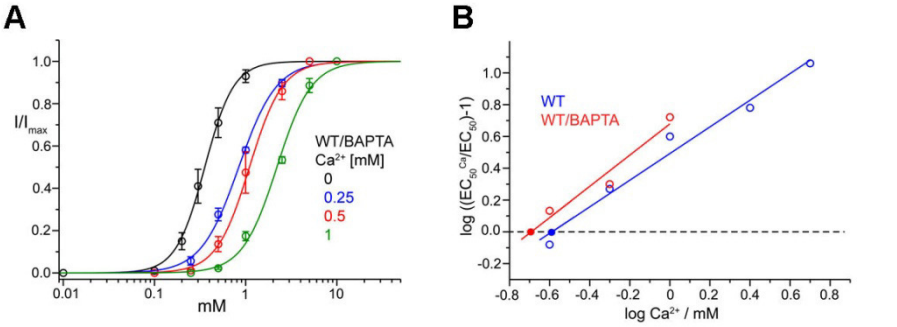

Figure S6

Supplementary Table

Table S1 Dose-response relationships of agonists in the presence of different modulators

		[mM]	EC_{50}^{*}	n			[mM]	EC_{50}^{*}	n
WT	Ca^{2+}	0	0.36	2.8	WT	Ca^{2+}	0.1	0.35	2.9
WT	Ca^{2+}	0.25	0.64	3.2	WT	Ca^{2+}	0.5	1.00	2.9
WT	Ca^{2+}	1.0	1.73	2.9	WT	Ca^{2+}	2.5	2.46	3.0
WT	Ca^{2+}	5.0	4.37	2.5					
WT/BAPTA	Ca^{2+}	0	0.36	2.7	WT/BAPTA	Ca^{2+}	0.25	0.84	2.1
WT/BAPTA	Ca^{2+}	0.5	1.07	2.4	WT/BAPTA	Ca^{2+}	1.0	2.23	2.3
WT	ACh	1	0.57	2.5	WT	ACh	5.0	1.49	2.4
WT	ACh	10.0	2.25	2.5					
WT/0.25Ca^{2+}	ACh	0	0.64	3.2	WT/0.25Ca^{2+}	ACh	1	1.16	1.9
WT/0.25Ca^{2+}	ACh	5	3.46	2.4	WT/0.25Ca^{2+}	ACh	10	5.08	2.1
WT/0.5Ca^{2+}	ACh	0	1.00	3.7	WT/0.5Ca^{2+}	ACh	1	1.83	2.5
WT/0.5Ca^{2+}	ACh	5	4.03	2.2	WT/0.5Ca^{2+}	ACh	10	8.45	2.7
WT/1Ca^{2+}	ACh	0	1.73	2.8	WT/1Ca^{2+}	ACh	1	2.68	2.0
WT/1Ca^{2+}	ACh	5	5.12	2.4	WT/1Ca^{2+}	ACh	10	8.24	1.9
WT	Zn^{2+}	0.01	0.92	3.2	WT	Zn^{2+}	0.05	3.72	2.2
WT	Zn^{2+}	0.1	10.1	2.3					
WT	Ba^{2+}	1	0.76	3.7	WT	Ba^{2+}	5	2.68	2.3
WT	Ba^{2+}	10	5.27	2.3					
WT	Sr^{2+}	1	0.75	2.9	WT	Sr^{2+}	5	2.11	2.7
WT	Sr^{2+}	10	3.41	2.3					
WT	Mg^{2+}	1	1.04	3.1	WT	Mg^{2+}	5	3.05	2.4
WT	Mg^{2+}	10	5.31	2.1					
D86A	Ca^{2+}	0	0.57	2.3	D86A	Ca^{2+}	1	2.30	2.1
D86A	Ca^{2+}	5	5.31	1.9	D86A	Ca^{2+}	10	11.2	2.9
S84A	Ca^{2+}	0	0.36	2.5	S84A	Ca^{2+}	1	1.55	1.6
S84A	Ca^{2+}	5	2.74	1.9	S84A	Ca^{2+}	10	5.43	1.4
N251A	Ca^{2+}	0	0.29	2.3	N251A	Ca^{2+}	1	0.84	3.5
N251A	Ca^{2+}	5	1.90	2.7	S84A	Ca^{2+}	10	5.31	1.8
E150A	Ca^{2+}	0	1.40	2.4	E150A	Ca^{2+}	1	2.20	2.6
E150A	Ca^{2+}	5	6.10	2.0	E150A	Ca^{2+}	10	8.99	1.9
E150Q	Ca^{2+}	0	2.92	2.8	E150Q	Ca^{2+}	1	5.29	2.0
E150Q	Ca^{2+}	5	14.6	1.9	E150Q	Ca^{2+}	10	21.9	1.8
D113A	Ca^{2+}	0	0.95	2.6	D113A	Ca^{2+}	1	0.88	2.2
D113A	Ca^{2+}	2.5	1.46	1.8	D113A	Ca^{2+}	5	1.86	1.9
D113A	Ca^{2+}	10	2.90	1.9	D113A	Ca^{2+}	25	6.37	1.5
D113N	Ca^{2+}	0	0.92	2.5	D113N	Ca^{2+}	1	1.81	2.1
D113N	Ca^{2+}	5	5.59	1.8	D113N	Ca^{2+}	10	9.78	1.9
D158A	Ca^{2+}	0	1.78	2.6	D158A	Ca^{2+}	1	1.79	3.2
D158A	Ca^{2+}	5	3.33	3.1	D158A	Ca^{2+}	10	5.43	2.0
D158A	Ca^{2+}	20	9.38	2.0					
D158N	Ca^{2+}	0	3.88	2.5	D158N	Ca^{2+}	1	5.61	2.1
D158N	Ca^{2+}	5	8.50	1.9	D158N	Ca^{2+}	10	11.2	2.0
113A/158A	Ca^{2+}	0	2.33	2.6	113A/158A	Ca^{2+}	1	1.59	3.5
113A/158A	Ca^{2+}	5	1.81	2.9	113A/158A	Ca^{2+}	10	2.96	2.6

113A/158A	Ca^{2+}	25	3.35	2.4					
113A/158A	Zn^{2+}	0	3.70	1.4	113A/158A	Zn^{2+}	0.01	4.56	2.0
113A/158A	Zn^{2+}	0.1	4.22	1.7					
		[mM]	Ec50	n			[mM]	Ec50	n
113A/158A	Ba^{2+}	1	3.07	2.3	113A/158A	Ba^{2+}	5	3.07	2.1
113A/158A	Ba^{2+}	10	5.42	2.2					
R91A	Ca^{2+}	0	0.09	2.6	R91A	Ca^{2+}	0.5	0.24	1.7
R91A	Ca^{2+}	1	0.41	1.8	R91A	Ca^{2+}	5	0.92	1.7
R91A	ACh	1	0.40	3.2	R91A	ACh	5	0.88	3.3
R91A	ACh	10	1.78	2.7					
R91A	TMA	10	0.23	2.4	R91A	TMA	25	0.33	2.4
R91A	TMA	50	0.59	2.5					
H168A	Zn^{2+}	0	0.67	3.0	H168A	Zn^{2+}	0.01	1.17	2.5
H168A	Zn^{2+}	0.05	4.82	2.1	H168A	Zn^{2+}	0.1	12.2	1.9
H176A	Zn^{2+}	0	5.16	2.3	H176A	Zn^{2+}	0.01	11.9	2.5
H176A	Zn^{2+}	0.025	25.5	1.9					

Propylamine was used as agonist in experiments involving Zn^{2+}, cysteamine in all other cases.

*EC_{50} in mM

Supplementary Discussion

The experimental data we have to explain

By binding to S_{out}, extracellular calcium produces several, apparently disparate effects on functional ELIC responses. These effects are additional to the reduction in single channel conductance and independent of it.

These modulatory effects of calcium include:

1) a reduction in the potency of agonists, which results in a parallel shift to the right of the agonist dose-response curve. This effect appears at low calcium concentration (0.1-1 mM) and is not associated with changes in the agonist maximum response.

2) at higher calcium concentrations (2-5 mM), there is further reduction in agonist potency, and this is associated with a pronounced decrease in the agonist maximum response (about 50% at 6 mM –channel block subtracted).

3) low calcium does not affect how fast ELIC channel open when they are saturated by agonist, but increases the concentration of agonist needed to reach this “limiting” rate of opening.

4) the decreases in agonist potency produced by calcium and those produced by the competitive antagonist acetylcholine are independent, namely they are unaffected by the presence or absence of the other.

The effects of calcium on the agonist dose-response relation can be explained by a decrease in efficacy within a simple del Castillo-Katz activation mechanism

The simplest scheme for the activation of a ligand-gated ion channel was proposed by Jose’ del Castillo and Bernard Katz in 1957[1]. In this scheme

$$A+R \underset{k_{off}}{\overset{k_{on}}{\rightleftharpoons}} AR \underset{\alpha}{\overset{\beta}{\rightleftharpoons}} AR^* \quad (1)$$

activation involves two steps. The first is the binding of the agonist A to the channel R, with microscopic affinity described by the dissociation constant K_d (itself the ratio between the dissociation rate constant k_{off} and the association rate constant k_{on}). The second step is a conformational change, where the agonist-bound resting receptor (AR) opens to the conducting form AR*. The position of the equilibrium between AR and AR* is described by an equilibrium constant E, that reflects agonist efficacy and is the ratio between the opening rate constant β and the closing rate constant α.

More complex schemes are needed to explain all the aspects of channel functional behaviour, and such schemes incorporate the existence of more than one agonist binding site, the possibility of unliganded and partially-liganded openings, intermediate states in the conformational change and desensitisation. Nevertheless, the del Castillo-Katz scheme is sufficient to describe much of basic channel pharmacology (reviewed in ref. [2] and exploring it gives useful insight.

Indeed, if we look only at the ELIC equilibrium responses (ie the agonist dose-response curves), all the effects of calcium can be explained within the del Castillo-Katz mechanism, just by assuming 1) that calcium decreases agonist efficacy E and 2) that full agonist efficacy E is high in ELIC.

The value of efficacy E

The second assumption appears to be quite plausible. In the del Castillo-Katz mechanism, the channel open probability is given by

$$Popen = \frac{E*[A]}{[A]*(E+1)+Kd} \qquad (2)$$

Maximum open probability (P_{open}) is

$$Max\ Popen = \frac{E}{E+1} \qquad (3)$$

and the EC_{50} for the agonist is

$$EC50 = \frac{Kd}{E+1} \qquad (4)$$

Figure 1A shows that cysteamine opens ELIC channels with a high maximum open probability. Our single channel data (Marabelli et al., in preparation) suggest that the maximum P_{open} reaches 98%. From Equation 3, this implies that agonist efficacy is of the order of 50 (50/51= 98%). This value is not dissimilar to that seen for other members of the superfamily, such as the nicotinic ACh receptor and the glycine receptor, when they are activated by full agonists.

The effects of decreasing efficacy

When efficacy E is this high, the effects of a small decrease in E on the maximum agonist response are hard to detect in practice. For instance, a two-fold decrease in E would reduce maximum open probability from 98% to 96% (that is from 50/51 to 25/26).

Even a two-fold decrease in E would however cause a detectable shift in agonist potency, as the agonist EC_{50} would almost double (see equation 4). This is in line with the observations at low calcium concentrations.

It is only when the decrease in E is much larger, and E drops to values below 10, that a decline in the maximum P_{open} becomes noticeable, as the maximum P_{open} falls below 90%. This is in line with our observations at higher calcium concentrations, where more of the calcium binding sites are occupied and calcium can have a greater effect on E.

Thus there is no need to hypothesize that low calcium and high calcium have different microscopic effects: a progressive decrease in agonist efficacy E, more marked at the higher calcium concentrations, is all that is needed to explain our observations.

A more detailed activation mechanism is required to explain the lack of an effect of calcium on the limiting rate of channel gating

In another set of experiments we produced ELIC currents by near-instantaneous applications of agonists ("concentration jumps") to channels in outside-out patches. The time course with which these currents reach their steady-state value depends in principle on all the rate constants in the activation mechanism. However, if agonist is applied at concentrations that are very high and saturate the receptor, it can be shown that these maximum agonist current responses effectively increase as single exponentials with time constant

$$\tau = \frac{1}{\beta+\alpha} \qquad (5)$$

where β is the opening rate constant and α the closing rate constant [3,4].

We already know that efficacy E is high for ELIC. As efficacy is the ratio of β /α, the value of β must be much bigger than that of α (50-fold), and therefore the time constant is influenced mostly by the value of β .

If calcium decreases E (as we have to assume, in order to explain its effects on the agonist dose-response curves), it can do so either by decreasing β or by increasing α. Neither of these effects can be reconciled with our observations, if the del Castillo-Katz scheme is valid for our channel, because we did not observe a change in the limiting rate of gating or in the time course of the current at the end of the agonist pulse (deactivation). From the arguments above, it is clear that if there is a decrease in β, we should see a slowing of the maximum rate of current development and that this should be detectable even for fairly small changes in β. If, on the other hand calcium decreases E by increasing α, the limiting rate of gating would not change (given that β >>α), but speeding the channel closing rate α should result in a faster decline in the current when the agonist pulse ends, that is a speeding up of deactivation, which was not observed either.

Thus it may be that the del Castillo-Katz model is inadequate to explain the action of calcium. Indeed, it could be that activation of the channel requires not a single conformational change, but two. If the rate-limiting step for gating in the agonist jump experiments is not opening, but an earlier, slower step, calcium could still change efficacy and shift agonist potency and maximum responses without affecting the time course of the current in our agonist concentration jumps.

This is because, if reaching this reaction intermediate is slow enough, the agonist limiting relaxation will be dominated by this step, rather than by the opening itself. This explanation is qualitatively plausible because mechanisms incorporating reaction intermediates are necessary to explain the single channel kinetic properties of channels related to ELIC, such as nicotinic ACh receptors and glycine receptors, as shown by our own work and that of the groups of Sine and Auerbach (see main discussion, [5-7].

The simulation below is a proof of principle to show that this explanation is not only qualitatively plausible but also that it can work quantitatively, with at least one set of rate constant values. The solution is certainly not unique, and eq.6 is not proposed as a complete mechanism for the ELIC receptor. Nevertheless the rate constant values used are not unrealistic, as they are not far from our estimates from

mechanism fitting of ELIC single channel data (Marabelli et al., in preparation) or from rate constants estimated from other pLGICs.

The simplest mechanism incorporating a reaction intermediate is

$$A+R \underset{k_{off}}{\overset{k_{on}}{\rightleftharpoons}} AR \underset{b}{\overset{f}{\rightleftharpoons}} AF \underset{\alpha}{\overset{\beta}{\rightleftharpoons}} AF^* \qquad (6)$$

In this minimal "flip" mechanism, there is an additional state AF (for flipped), which is still closed but has changed conformation. The maximum P_{open} becomes

$$Max\ Popen = \frac{EF}{EF+F+1} \qquad (7)$$

For the calculation of the time course of the saturating agonist responses, the mechanism can be simplified by pooling the states separated by a binding step (R and AR) into a single state [R,AR]. This can be done because we have a very high concentration of agonist A, making the association rate, k_{on} [A] very fast. For the same reason, the pooled state [R,AR] is almost entirely made of AR.

The mechanism then becomes

$$[R,AR] \underset{b}{\overset{f}{\rightleftharpoons}} AF \underset{\alpha}{\overset{\beta}{\rightleftharpoons}} AF^* \qquad (8)$$

and has four rate constants: β (open),α (close), f (flip) and b (unflip) and the ratios of these give the equilibrium constants E = β /α and F = f/b. The values of the rate constants are constrained because the maximum P_{open} of the channel is high, suggesting that β >>α and f >=b.

We know also that the risetime of the current produced by the high concentration agonist jump has a time constant of 17-20 ms (this is considerably slower in ELIC than in other pLGICs).

The black trace in Figure SD1A shows the current on-relaxation calculated for this mechanism. This is identical to a single exponential with a time constant of 20 ms (shown for reference as a red dashed curve). The values used in the calculation were β = 50000 s^{-1}, α = 1000 s^{-1}, f = b= 50 s^{-1}. They make E= 50 and F = 1 and imply a maximum P_{open} of 96%.

Let's now assume that we are in the presence of calcium and that calcium has reduced efficacy (by decreasing β) by 5-fold. This would result, as discussed above, in a shift in the agonist potency and in a reduction in the maximum P_{open} (from 96% to 83%; in the model discussed in the next section, where calcium binding is explicit, this would be reached at approximately 1 mM calcium). However, as shown in Figure 1B, even this fairly strong effect of calcium has only a tiny effect on the risetime of the limiting agonist current (the calculated agonist current is shown in black and compared to a reference exponential curve with a time constant of 20 ms, red dashed curve). Note that for the purpose of showing some effect of calcium in the calculation, we have chosen to show the consequences of a reduction in efficacy greater than that likely to prevail in our concentration jump experiments (where we had no effect of calcium on the maximum response).

More detailed mechanisms and the equilibrium effects of calcium

The arguments above show that incorporating an intermediate state that limits the fastest rate of ELIC gating allows us to account for our observations in the agonist jump experiments. This more detailed mechanism can still explain the effects of calcium on the agonist dose-response curves, and in this section we will show that with an appropriate example.

If we incorporate in the flip mechanism the binding of calcium, we obtain

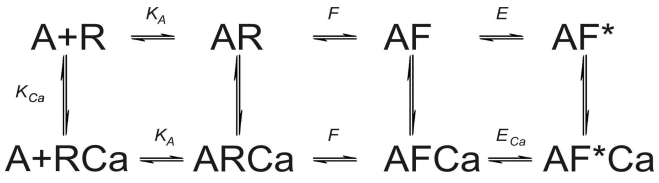

(9)

For clarity, the scheme above shows the names of the equilibrium constants for each step (rather than the rate constants as in schemes 1, 6 and 8). Note that K_A and K_{Ca} are the microscopic dissociation constants for the agonist A and for calcium, respectively. Calcium is assumed to affect only efficacy, which is reduced from E to E_{Ca} in the calcium-bound channel (bottom line of the mechanism).

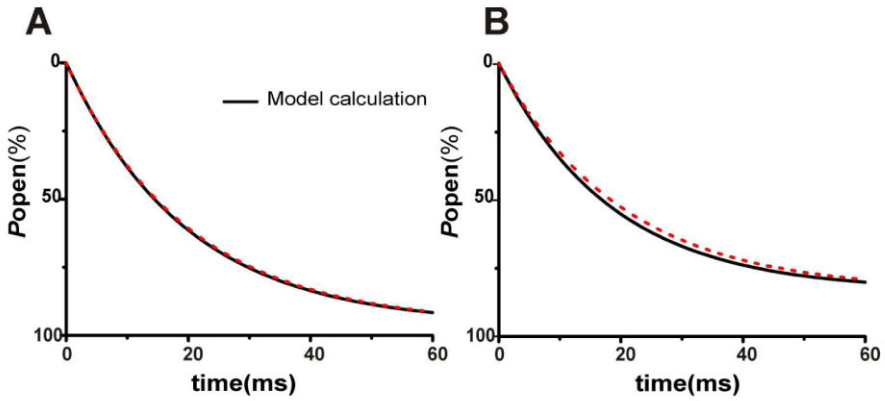

Figure SD1 Calcium can reduce efficacy and the maximum open probability of ELIC without changing the maximum rate of current onset, if this is limited by the channel's slow access to an activation intermediate. The black curves in the graphs are the calculated time course of currents produced by instantaneous applications of saturating agonist concentrations (at time 0, current expressed as open probability). The dashed red curves are single exponentials with time constant of 20 ms and the same maximum values as the currents and are shown for reference. Currents are calculated from mechanism (8). The values used in the control calculation (0 calcium, graph A) were $\beta = 50000\ s^{-1}$, $\alpha = 1000\ s^{-1}$, $f = b = 50\ s^{-1}$. Hence E= 50 and F = 1 (where efficacy E is the equilibrium constant for the final opening step and F is the equilibrium constant for access to the preceding intermediate state) and the maximum P_{open} is 96%. (B) Calcium can reduce the value of β by as much as 5-fold with negligible effects on the time course of current onset. Note that the steady-state value of this maximum current has decreased to a P_{open} value of 83%. The calculations with the more complete models in Figure 2 indicate that this reduction in maximum P_{open} is expected to occur at approximately 1 mM calcium, e.g. a concentration much greater than the one tested in the agonist jump experiments (0.2 mM).

Figure SD2A shows the effect of progressively greater calcium concentrations on the dose-response curves for a full agonist. These effects are calculated from the

scheme above, assuming that calcium reduces efficacy by up to 50-fold (when the channel is fully bound to calcium) and that E = 50 and F = 1. The latter values are chosen because the maximum P_{open} is high in control conditions.

It is clear from the Figure that the lowest calcium concentration (in this example half the calcium dissociation constant) shifts the agonist dose-response curve to the right, without changing the maximum much. Greater calcium concentrations (at least 5-fold the calcium dissociation constant) are required before the maximum response starts to decline. We can also plot the agonist dose-response curves after normalising them to their maximum response. This shows clearly the parallel shift to the right produced by calcium (Figure SD2B).

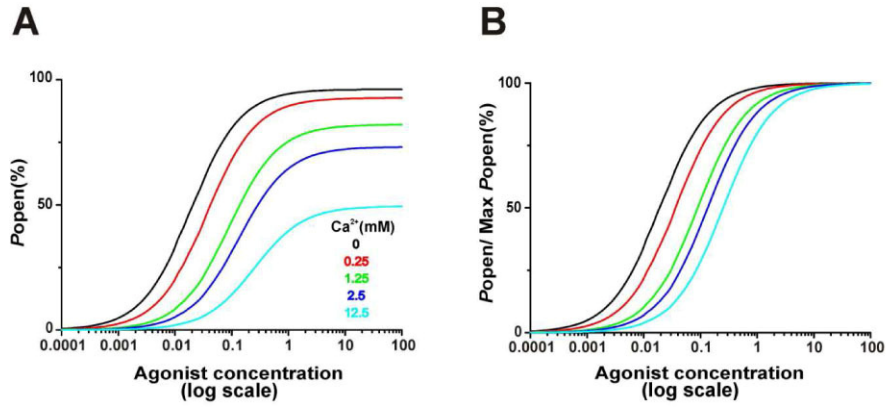

Figure SD2 The decrease in efficacy induced by calcium results in a reduction in agonist potency at low calcium and in an additional decrease in maximum response at high calcium. The graphs show agonist concentration-response curves calculated from mechanism (9). This is a mechanism that incorporates an intermediate state in the activation of the channel. The calculations are based on values of E=50 and F=1. Calcium is assumed to bind to the resting state of the channel with a microscopic affinity of 0.25 mM (in line with the estimate from the Schild plot) and to reduce the value of efficacy by 50-fold when bound to the channel. The agonist concentration is expressed as a multiple of the (unknown) agonist microscopic dissociation constant (K_A in mechanism 9). In Figure SD2A responses are expressed as absolute P_{open} values, and in Figure SD2B as values normalised to the maximum agonist response.

Plotting the effect of calcium as a Schild plot

Schild analysis is used in pharmacology to characterise competitive antagonists, compounds whose binding is mutually exclusive with that of agonists. The dose ratios (e.g. the shifts) produced by the antagonist in the agonist dose-response curves are plotted in a Schild plot, as log(dose ratio-1) against the concentration of antagonist (on a log scale). If the antagonist is competitive, this produces a line with a slope of 1. The intercept between the line and the x-axis estimates the antagonist microscopic dissociation constant, a result that is at the basis of receptor characterization in classical pharmacology [8]. This result holds also for mechanisms that are more complicated than that for which the Schild analysis was originally derived [9]

It may appear surprising that we should see a Schild-like pattern for the effects of calcium, given our hypothesis that calcium acts by impairing gating. However, this behaviour is predicted if we calculate the Schild plot for the effects of calcium from

model (9), with the same assumptions as for the graphs above (namely that calcium reduces efficacy by up to 50-fold when the channel is fully bound to calcium and that E=50 and F=1). This is shown in Figure SD3, where the data calculated from the model are shown by the black curve and are compared with a reference line (dashed red) that has unity slope and intercept equal to the calcium microscopic dissociation constant (set to be 0.25 mM in our model, corresponding to -0.6 on the log scale).

It can be seen that the data follow a Schild-like pattern, particularly at low calcium concentration. Remarkably, the Schild plot intercept for the data is a close approximation of the true calcium dissociation constant.

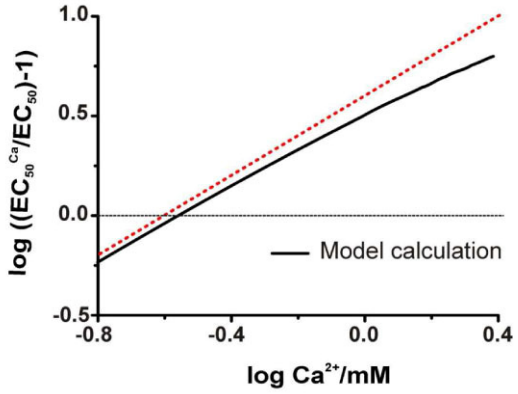

Figure SD3 – The concentration dependence of the effects of calcium is close to a Schild-like pattern, even though calcium does not act as a competitive antagonist. The graph shows (black curve) the effect of calcium calculated from mechanism (9) and plotted as a Schild plot (see text). The dashed red line shown for reference is what a true Schild relation should look like. This is a line with unity slope that crosses the y=0 axis (dashed black horizontal line) at an intercept equal to the calcium affinity (0.25 mM e.g. -0.6 on the log scale). Mechanism (9) incorporates an intermediate state in the activation of the channel and assumes E=50 and F=1. It is also assumes that calcium binds to the resting channel with a microscopic affinity of 0.25 mM and that it reduces the value of efficacy E by 50-fold when bound to the channel. Note that the data calculated with these assumptions are reasonably close to the true Schild line, particularly at low calcium, where the intercept with the y=0 axis is close to the true calcium microscopic binding affinity.

The effects of calcium and those of the competitive antagonist ACh are independent

We can extend model (9) to include binding of the competitive antagonist ACh.

In scheme (10), the antagonist B is modelled to bind to the resting state and to bind in a manner mutually exclusive with the binding of the agonist A, with a dissociation constant K_B

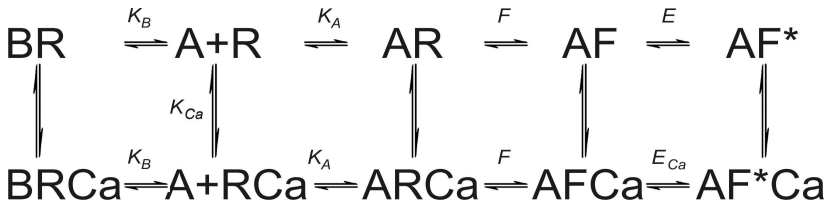

(10)

We can then calculate the dose-response curves for the agonist either in the presence of increasing concentrations of calcium (alone or in the presence of saturating ACh, e.g. 20-fold the ACh dissociation constant) or in the presence of

increasing concentrations of ACh (alone or in the presence of saturating calcium, e.g. 20-fold the calcium dissociation constant). The other assumptions are the same as for mechanism (9) (namely that calcium reduces efficacy by up to 50-fold when the channel is fully bound to calcium, E=50 and F=1). It has been shown more generally [9] that in this sort of mechanism, the effects of blocker B should obey the Schild equation if the microscopic affinity of B is not changed by the other ligand (here calcium).

The graphs below (Figure SD4) show that the effects of calcium and ACh are independent of each other. This is shown by the fact that calcium produces exactly the same reductions in agonist potency, seen as rightward shifts in the normalised agonist dose-response curves, whether or not high ACh concentrations are present (Figure SD4A and SD4B, respectively). The same applies to ACh (shown alone in Figure SD4C and in the presence of high calcium in Figure SD4D).

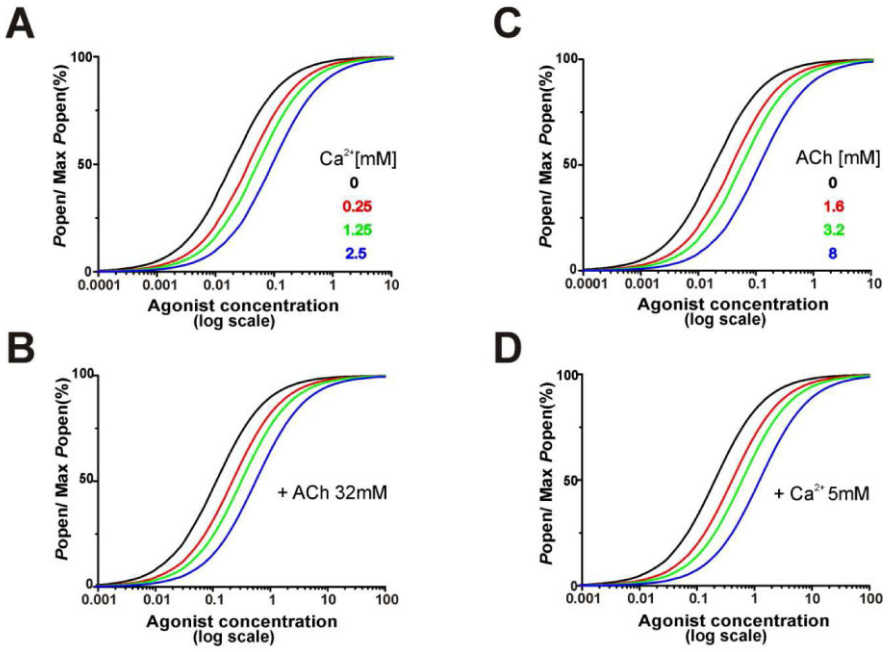

Figure SD4 – The effects of calcium and those of the competitive antagonist ACh are independent. The graphs show agonist concentration-response curves calculated from mechanism (10). This is a mechanism that incorporates an intermediate state in the activation of the channel and assumes that the antagonist ACh can bind only to the resting state of the channel, and that ACh binding and agonist binding are mutually exclusive. The calculations are based on values of E=50 and F=1. In the model, calcium is assumed to bind to the resting state of the channel with a microscopic affinity of 0.25 mM (in line with the estimate from the Schild plot) and to reduce the value of efficacy by 50-fold when bound to the channel. ACh is assumed to bind to the resting state of the channel with a microscopic affinity of 1.6 mM (from our experimental estimate). The agonist concentration is expressed as a multiple of the (unknown) agonist microscopic dissociation constant (K_A in mechanism 10). A and B show the parallel rightward shifts in the agonist concentration-open probability curves (normalised to the maximum open probability) produced by increasing concentrations of calcium (0, 0.25,1.25 and 2.5 mM) when calcium is applied alone (A) or in the presence of a saturating concentration of ACh (32 mM, e.g. 20 times the ACh dissociation constant, B). Note that the effect of calcium is the same in A and B. C and D show the parallel rightward shifts in the agonist concentration-open probability curves (normalised to the maximum open probability) produced by increasing concentrations of ACh (0, 1.6, 3.2 and 8 mM) when ACh is applied alone (A) or in the presence of a saturating concentration of calcium (5 mM, e.g. 20 times the calcium dissociation constant, B). Note that the effect of ACh is the same in C and D.

References

1. del Castillo J, Katz B (1957) Interaction at end-plate receptors between different choline derivatives. Proc Roy Soc Lond B 146: 369-381.
2. Colquhoun D (1998) Binding, gating, affinity and efficacy: The interpretation of structure-activity relationships for agonists and of the effects of mutating receptors. Br J Pharmacol 125: 923-947.
3. Hill AV (1909) The mode of action of nicotine and curari, determined by the form of the contraction curve and the method of temperature coefficients. J Physiol 39: 361-373.
4. Maconochie DJ, Knight DE (1992) A study of the bovine adrenal chromaffin nicotinic receptor using patch clamp and concentration-jump techniques. J Physiol 454: 129-153.
5. Burzomato V, Beato M, Groot-Kormelink PJ, Colquhoun D, Sivilotti LG (2004) Single-channel behavior of heteromeric α1β glycine receptors: an attempt to detect a conformational change before the channel opens. J Neurosci 24: 10924-10940.
6. Mukhtasimova N, Lee WY, Wang HL, Sine SM (2009) Detection and trapping of intermediate states priming nicotinic receptor channel opening. Nature 459: 451-454.
7. Jadey S, Auerbach A (2012) An integrated catch-and-hold mechanism activates nicotinic acetylcholine receptors. J Gen Physiol 140: 17-28.
8. Schild HO (1949) pA_x and competitive drug antagonism. Br J Pharmacol 4: 277-280.
9. Colquhoun D (2007) Why the Schild method is better than Schild realised. Trends Pharmacol Sci 28: 608-614.

Discussion

While the functional behavior of pLGICs has been subject of extensive investigations, it is still a difficult task to deduce molecular mechanisms that relate the function of the receptors to the available structures, mostly because the necessary structural and functional data were not obtained from the same proteins. While the structure of ELIC provided the first insight at high resolution into the family of pLGICs, little was known about its function and physiology. Without the knowledge of ligands which activate ELIC, its use to study the mechanisms underlying the function of the family was limited.

In this thesis I have described the first investigations on structure-function relationships in ELIC by using an approach that combines X-ray crystallography and electrophysiology. Initially, ELIC agonists were identified by screening a library of small molecules. The knowledge of activating ligands has subsequently allowed me to study agonist binding and gating in ELIC. The biophysical properties of the open pore were characterized by determining the ion selectivity and single channel conductance. During the investigations, it was found that divalent cations have an inhibiting effect on ELIC, a property which is also known from eukaryotic receptors. In subsequent studies I was able to determine the binding site, which is responsible for the effect, and to reveal a mechanism for the inhibition of ELIC by divalent cations.

Activation of ELIC

Agonist Binding

The first attempts to identify agonists of ELIC during my PhD studies involved an *in silico* docking approach to find molecules which may bind to the canonical agonist binding site. These studies were carried out in collaboration with Dr. Peter Kolb and are not described in this thesis. Although the selected molecules were subsequently tested by electrophysiology, none of them was capable to activate ELIC. In retrospect, this is not surprising as the docking was performed with the structure of ELIC in the inactive state, whereas the activation likely alters to shape of the binding pocket. As the ELIC structure probably shows a resting state, the docking has provided a set of molecules which are predicted to bind with high affinity to this state. The identified binders thus may act as inhibitors of this allosteric receptor, because in contrast to inhibitors, agonists are known to bind the resting state with low affinity, but the active state with high affinity. It will be worthwhile to investigate whether any of the compounds identified by the docking would act as potent competitive inhibitor.

In parallel to the computational docking, a library of compounds was assembled based on simple structural considerations. These molecules were selected according to the chemical environment and the size of the putative agonist binding pocket, which was assumed to be at the same location as the canonical binding site of the

family. Additional information came from earlier crystallographic studies on ELIC, showing the binding of monovalent cations in the ligand binding site (*10*), which indicated that agonists are probably also positively charged.

The screening of this library on ELIC expressing *X.laevis* oocytes resulted in the identification of eleven molecules capable to activate ELIC. All identified agonists are linear primary amines of variable length, containing different functional groups. They activate ELIC with apparent affinities in the range from 260µM of cysteamine to 2.5mM of GABA. The potencies of the identified agonists are low compared to eukaryotic receptors, where they range from 0.2-170µM for the AChRs (*84*, *85*), 0.2-1.5µM for the $5HT_3$Rs (*86*), 0.3-30µM for GABARs (*87*) and 20-50µM for GlyRs (*88*, *89*). In eukaryotic receptors, the potencies of agonists are also strongly depending on the subunit composition of the ion channel. As the apparent affinity is a measure of both affinity and efficacy of the agonist, the high variation among the receptors may reflect the adaptation of the protein to its tissue specific function (*90*). If a similar adaptation can also be implied for ELIC, the native agonist has to be available in high concentrations. The low apparent affinity could additionally help to tightly regulate the activity of the channel, to avoid any background activity and related cytotoxic effects.

With the availability of activating ligands I hoped to be able to stabilize the open conformation of ELIC and to determine its structure by X-ray crystallography. However, the structures of ELIC in complex with agonists did not show any noticeable changes compared to the known structure. As the structure of ELIC in complex with the agonist bromopropylamine was only obtained at 4Å resolution, it did not allow the detailed characterization of the binding mode of the ligand and its interaction with the residues of the agonist binding pocket. The location of the ligand was consequently modeled based on the position of the bromine of the bound agonist, which was located in the anomalous difference map. The location of the ligand binding site of ELIC at the interface between the subunits is equivalent to the agonist binding sites of the eukaryotic receptors. As the site shows the strongest conservation to the GlyRs and GABARs, it is not surprising that the identified ligands are also similar to known agonists of these receptors and it is particularly remarkable to find the neurotransmitter GABA is among them. In contrast, substituted amines like AChR agonists and bulky primary amines like $5HT_3$R agonists are ineffective in activating ELIC.

The postulated binding mode of the agonist is in good agreement with the known structures of AChBPs and GluCl in complex with their agonists and also supports the theory of a common activation mechanism. Interestingly, the highest degree of conservation in the ligand binding pocket is found in the residues of the principal subunit that interact with the amino moiety of the ligand. Mutations of these amino acids result in inactive receptors, thus underlining their significant role in agonist binding. In contrast, most of the residues on the complementary side, which are not involved in the interaction with the amino group of the agonist, are only marginally conserved. Still, these residues play an important role in ligand binding, as the mutation R91A increased the apparent affinity for cysteamine and mutations of other

residues shifted the EC_{50} to higher agonist concentrations. Since the mutations in the complementary subunit have a less severe effect on activation compared to the mutations at the principal subunit, the latter may contribute most to agonist binding by stabilizing the positively charged amino moiety of the ligand. The less conserved amino acids on the complementary side might be involved in the discrimination of different but chemically related agonists. As the determinants of agonist specificity are located on several loops of the agonist binding site, receptor activation relies on the interplay of all amino acids at this crucial interface between the subunits to activate the receptor.

Gating

The identification of agonists also allowed an initial analysis of the kinetic properties of ELIC. Patch clamp measurements with fast solution exchange revealed a maximal macroscopic activation time constant at saturating agonist concentration of 10ms and a deactivation time constant of 50ms. The values show that the transitions between different states are slower in ELIC than in most eukaryotic receptors, where the activation time constants are in the range of 1ms to 4ms for most receptors (*91–94*). The fastest member of the family, the muscle AChR, even activates in the sub-millisecond time scale. Also the deactivation is slightly faster in eukaryotic receptors with time constants ranging from 10-30ms. The kinetic properties of eukaryotic receptors are probably adapted to their function in the nervous system to allow fast signaling at synapses. For functional investigations, the slower kinetics of ELIC may be an advantage, as it allows the investigation of kinetic processes that are too fast for concentration jump experiments in many eukaryotic receptors. It may thus be possible to detect subtle differences in activation caused by drugs or mutations.

As most eukaryotic receptors, ELIC enters a desensitized state after prolonged exposure to agonist. The discovery of desensitization in ELIC was surprising because the previous work on GLIC, another a prokaryotic member of the family, did not show any desensitization over an extended time range. As ELIC and GLIC are closer related to each other than to the eukaryotic members, ELIC was expected to show properties similar to GLIC. Whereas both channels were expected to exhibit a simpler functional behavior than eukaryotic counterparts, ELIC was found to share all the major functional features of eukaryotic receptors. The initial analysis of single channel experiments showed that the open probability during a cluster of channel openings is very high, which suggests that the agonists cysteamine and propylamine are very efficacious. Two conclusions can be drawn from this fact: First, the true microscopic affinity of the agonists to the resting state has to be rather low because the high efficacy increases the apparent affinity of the agonist. If the efficacy of ELIC activated with cysteamine is estimated to be 50, the resulting microscopic affinity of cysteamine to the resting state of ELIC would be as low as 15 to 20mM. Second, despite the low affinity of the agonists, the high open probability shows that cysteamine and propylamine are full and not partial agonists of ELIC. The identification of potent agonists confirmed that ELIC exhibits all major properties of eukaryotic receptors, which suggests that the conserved activation mechanism of the

family of pLGICs is also present in ELIC and that the protein is thus a valuable model system for the family.

Properties of the open Pore

The possibility to activate ELIC facilitated the investigation of its permeation properties. The quantification of the ion selectivity, based on the measurement of reversal potentials under asymmetric conditions, requires the control over both the intra- and extracellular solutions. This was achieved by using two different electrophysiological techniques, patch clamp and the recording of reconstituted ELIC in artificial bilayers.

One of the striking features in the electrophysiological recordings of ELIC is the detection of single channel events upon agonist application. The single channel conductance of ELIC was determined to a value of about 80pS at physiological ion concentrations, which distinguishes the protein as fast conducting ion channel. The conductance of ELIC is higher than that of most known eukaryotic pLGICs. It is ten times higher than the 8pS conductance of GLIC (*5*) and it is in the same range as the 85pS of the *T.califonica* AChR, the highest conducting member of the family (*14*). The large conductance facilitates the recording considerably and it makes ELIC a very good candidate for detailed single channel kinetic approaches.

Single channel data was also used to determine the ion selectivity of ELIC, which can be measured with high accuracy, since the measurements are not influenced by endogenous channels and transporters in the cell membrane, or impurities carried along the purification and reconstitution procedure. Since the measured reversal potential at asymmetric conditions is at the Nernst-potential of the respective cation, ELIC was determined to be cation selective. In contrast to the strict discrimination for cations over anions, the channel did not show any selectivity among the different monovalent cations potassium, sodium and caesium. Divalent calcium ions are conducted though the pore as well, but their presence reduces the conductance of the channel. This effect is known from other cation selective pLGICs and was studied in detail for AChRs, $5HT_3$Rs and GLIC (*45*, *62*, *95*). Divalent cations are thought to interact stronger with the residues of the pore than monovalent cations and their conductance thus saturates at comparably low ion concentrations, whereas the conductance of monovalent cations increases linear without saturation. Due to their higher affinity, divalent cations dwell longer in the pore than monovalents and thereby reduce the total ion flux through the channel.

The ion selectivity properties place ELIC in the cation selective branch of the family, with a large conductance for monovalent and divalent cations. All the facets of ion selectivity are strongly conserved within the cation selective pLGICs (*96*), consistent with the proposed similarity of the pore geometry and the conservation of the chemical properties of the pore lining residues, both constituting the main determinants of ion selectivity in pLGICs.

Structure determination of different states

High resolution crystal structures of pLGICs in different functional states are required to understand the conformational changes involved in receptor function. Until today, all available structures of pLGICs have been determined in a single distinct state, a non-conductive state of ELIC and the conductive state of GLIC and GluCl. All attempts to crystallize the non-conductive state of GLIC and GluCl were so far unsuccessful. With known ELIC agonists, broad crystallization efforts were carried out to crystallize the ELIC-agonist complex. The goal was to determine its structure in another, either conducting or desensitized conformation. The crystals from several conditions were analyzed and their structures were determined, but none of them revealed any conformational differences compared to the initial structure. This may have several reasons: In most cases, a protein crystallizes in the conformation of the thermodynamically lowest energy state. This is the open conformation of GLIC and GluCl and a non-conducting conformation of ELIC. In the case of GluCl, the open state was stabilized with the agonist glutamate and the allosteric modulator ivermectin (*13*). GLIC is locked in the open conformation due to the low pH of the crystallization condition, since protons activate the channel. The open state might also be stabilized by protonation of a site in the transmembrane domain of GLIC which if protonated, stabilizes the open pore conformation by a modulatory effect similar to ivermectin in GluCl (*97*). In contrast to GLIC and GluCl, ELIC could not be crystallized in the active conformation. Electrophysiological measurements revealed that ELIC only transiently adopts an active conformation before entering a desensitized state. Therefore, the open state is thermodynamically not stable.

The determined structures of ELIC in the apo form and the agonist complex did not reveal any appreciable conformational changes at the medium resolution data of the agonist complex. Liganded and unliganded structures show a non conductive state with an obstructed pore, even though the agonist was bound in its binding pocket. It is thus unclear if the structures show the resting state, which is stable in the absence of agonist, or the desensitized state, the most stable state with agonist bound. The underlying cause for this behavior could be that not all conformations of ELIC are accessible in the detergent solubilized state or that the crystal contacts stabilize the observed non-conducting conformation. All crystals, which diffracted to high resolution, were grown in conditions containing ammonium sulfate or barium acetate. Interestingly, it was impossible to detect the agonist in the ligand binding site in crystallization conditions containing ammonium ions and ligands were only visible in the electron density if the ammonium ions were replaced by sodium and lithium. This led to the speculation that ammonium may compete with the agonist for the binding pocket and thereby acts as a low affinity inhibitor which stabilizes the closed state. As Barium is also known to inhibit ELIC, it seems to be important to reach a certain degree of inhibition to stabilize the non-conducting state of ELIC and to produce well diffracting crystals.

Modulation of ELIC

The modulation of pLGICs is a physiologically and pharmaceutically important effect on this family of receptors as many drugs or natural toxins work either by enhancing or inhibiting their function. Even though activating ligands for ELIC have only been available for a short time, two different modes of the inhibition of ELIC were discovered. The first is the competitive inhibition of ELIC by acetylcholine. The second is the allosteric inhibition of ELIC by divalent cations. These modulators show striking parallels to the known and well characterized modulators of eukaryotic receptors. In the context of ELIC, the functional investigation can be extended with structural studies, thus offering the possibility to explain the effects of these modulators truly on a molecular level.

Inhibition by Acetylcholine

ACh was shown to act as a competitive inhibitor of ELIC (*98*). It binds to the agonist binding site of ELIC with an affinity of 1.5mM which is clearly a higher affinity to the resting state than the identified agonists. This underlines again the allosteric behavior of ELIC, where agonists have a low affinity to the resting state but a high affinity to the active state, whereas ACh has a high affinity to the resting state and no measureable affinity to the active state, since the active conformation cannot be adopted if ACh is bound. The distinct effects of cysteamine and acetylcholine demonstrate that agonists and antagonists selectively stabilize different conformations of the receptor.

Based on the various structures of AChBPs in complex with different agonists and antagonists it was found that all agonists are small molecules capable of activating the receptor. All antagonists were found to be big and bulky molecules ranging from alkaloids to small proteins. The proposed mechanism suggests that binding of these large molecules spreads the agonist binding site and inhibits the receptor activation by preventing C-loop capping (*99*). The competitive inhibition of ELIC by ACh seems to contradict the current view of competitive inhibition in pLGICs. ACh is not larger than the identified agonists for ELIC and the clear outward movement of the C-loop in the AChBP-antagonist complex is not visible in the ACh bound structure of ELIC. In contrary, even a contraction of the C-loop is observed. It is therefore not likely that ACh acts by a similar mechanism by preventing C-loop capping as both agonists and antagonists bind with a similar mode to the receptor. The binding pocket of ELIC including the conserved ring of aromatic amino acids responsible for the cation-π interaction can bind several different cations but seems to be able to differentiate between a positive charge of an amino- and a substituted amino group.

It was also shown that 2-dimethylaminoethylacetate, an ACh derivate with a tertiary instead of a quaternary amine, could activate ELIC with low potency. The observed activation is much slower compared with cysteamine. Even though it is not known yet if the compound acts as a full or a partial agonist, it hints towards a gradual behavior ranging from the quaternary ammonium compounds, which act as competitive antagonist, over the tertiary amines as partial agonist to the amines as full agonist.

Inhibition by divalent Cations

In this thesis, I showed that ELIC is inhibited by divalent cations on the extracellular side. Divalent cations, such as calcium, magnesium and zinc, are known to modulate the function of pLGIC in a positive or negative way. Our study investigated the inhibitory effects of calcium ions on ELIC in detail and showed that other alkaline earth metal and zinc ions act at the same site and by the same allosteric mechanism of inhibition. Even though the phenotypes of the inhibition by ACh and divalent cations are similar, the underlying mechanisms are fundamentally different.

Two effects of divalent cations on ELIC were observed. The first was a shift of the dose response curve to higher agonist concentrations in the presence of divalent cations. This effect did not saturate, even at high concentrations. Additionally, the maximal current decreased at higher concentrations of divalent cations. This reduction of the current could not be fully attributed to the lower conductance of ELIC in the presence of divalent cations. It shows in contrast to the shift of the dose response curve, that the inhibiting effect of divalent cations is not surmountable and thus cannot be caused by competitive inhibition.

Three barium binding sites were identified in ELIC by exploiting the anomalous scattering properties of barium by X-ray crystallography. The functional relevance of these sites was probed in a mutagenic approach, which showed that two of these sites do not contribute to the inhibition by divalent cations. One of the binding sites, called S_{out}, was found to be solely responsible for the allosteric inhibition of ELIC by divalents. It is located in the dimer interface between adjacent subunits. Barium was found to interact with acidic residues of the Cys-loop and the F-loop. All tested divalents bind to this site with affinities close to the environmental concentration of calcium, magnesium and zinc, thus suggesting that the effect may be relevant at physiological conditions. The location of this inhibitory site in the dimer interface of the receptor, 15Å from the agonist binding site, is intriguing as the structural rearrangements in this region are believed to lead to receptor activation upon agonist binding.

Divalent cations were found to allosterically inhibit ELIC by decreasing the efficacy of channel gating, not the affinity to the agonist. A four state kinetic model, which was proposed for eukaryotic receptors to explain the mechanism of partial agonists, can also explain all the observed effects of divalent cations on ELIC. The model consists of one agonist binding step and two gating steps, termed bind, flip and open. It was also used for the activation mechanism of ELIC, because only the model containing the flip-state allows the explanation of the different functional effects of divalent cations on ELIC activation.

The binding step is not inhibited by divalent cations, because the inhibition would be completely surmountable in this case, which was not the case in our recordings. To probe an effect on the flipping step, agonist concentration jump experiments were performed at conditions where the flip transition is the rate limiting step in receptor activation. The maximal activation rate was equal, both in the absence and the

presence of calcium at concentrations which have a measurable effect on the dose response curve. This means that the flip transition is not inhibited by divalent cations, at least at low concentrations. Therefore, it has to be the opening step which is affected by divalent cations (Figure 16).

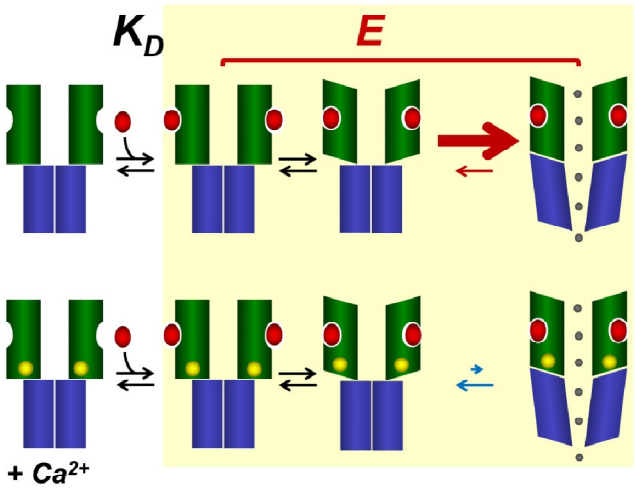

Figure 16 Activation mechanism of ELIC in absence and presence of divalent cations. Upon agonist application, ELIC adopts different functional states homologous to the eukaryotic receptors termed the resting state, the agonist bound resting state, the flip-state and finally the open state. In the activation process, the flipping is the rate limiting step. In the presence of divalent cations bound to the allosteric binding site, the activation of ELIC is inhibited by reducing the rate of channel opening.

There is still the possibility that the flip transition is also affected at higher calcium concentrations, but this hypothesis cannot be tested because the required agonist concentrations, to perform the concentration jump experiments, would become too high.

Mechanism of inhibition

A possible mechanism of inhibition can be deduced by comparing the structures of pLGIC in the open state, as seen in GLIC or GluCl, and ELIC in a non-conducting conformation. One of the most striking differences next to C-loop capping can be found in the F-loop. In GLIC and GluCl, the F-loop is tightly packed in the interior of the subunit interface, interacting with residues of both the principal and the complementary subunit. The F-loop in ELIC is larger compared to GLIC and GluCl and moved 5 to 10Å outwards, away from the core of the protein. Additionally, in all the structures of ELIC, the F-loop is not well resolved. This suggests that the F-loop of ELIC is intrinsically not well ordered and mobile, at least in the non-conductive state captured in the crystallization experiments. The divalent cations in their binding site S_{out} could prevent the movement of the F-loop of ELIC to adopt a GLIC or GluCl like open conformation and thereby impair channel gating.

The inhibition of ELIC by divalent cations also offers insights into the activation mechanism. In the absence of divalent cations, the mutants of the site S_{out} show a

reduced apparent affinity to the agonists compared to the native receptor, indicating an impaired function of the receptor and the importance of this region for receptor activation. As already seen, divalents do not interfere with the microscopic affinity of the agonists and, as our results suggest, the flip conversion of ELIC is also not affected. Thus, the conformational change of the F-loop is not part of the flipping of the receptor but it might be truly involved in the opening step.

From a structural point of view, it is unclear if the ELIC structures show the resting or a desensitized state. The functional characterization of the allosteric inhibition of ELIC shows that divalents act by stabilizing the resting state. In the performed experiments, the stabilization of the desensitized state would result in a shift of the dose response curve to lower agonist concentrations because the activation would not be affected but the maximal response would be reached faster due to the enhanced desensitization. Therefore, the results are compatible with the assumption that the structures of ELIC show a resting, not a desensitized state.

Comparison to eukaryotic receptors

The comparison of the allosteric inhibition of ELIC to the modulation of the eukaryotic receptors by divalent cations reveals striking similarities. The modulation in eukaryotic receptors can either be positive or negative but the identified residues that interact with divalent cations are located close to the S_{out} site of ELIC. The receptors that exhibit an inhibiting effect by divalent cations are $5HT_3$ and GABA receptors. The dose response curves of $5HT_3$ receptors shift to higher agonist concentrations in the presence of calcium, an effect very similar to ELIC, but the binding site is believed to be located at the extracellular mouth of the pore (*82*). GABA receptors are inhibited by zinc. It is unknown if zinc leads to a shift of the dose response because the effect was described by inhibition curves at a fixed agonist concentration (*79*). The identified residues interacting with zinc overlap with the S_{out} found in ELIC (Figure 17). Even though the primary sequence of the loops, which contain the interacting residues, are not conserved, it underlines the importance of this region in the modulation of pLGICs and hints towards a conserved mechanism where divalent cations can stabilize either the resting or the active state by binding to a region related to S_{out}.

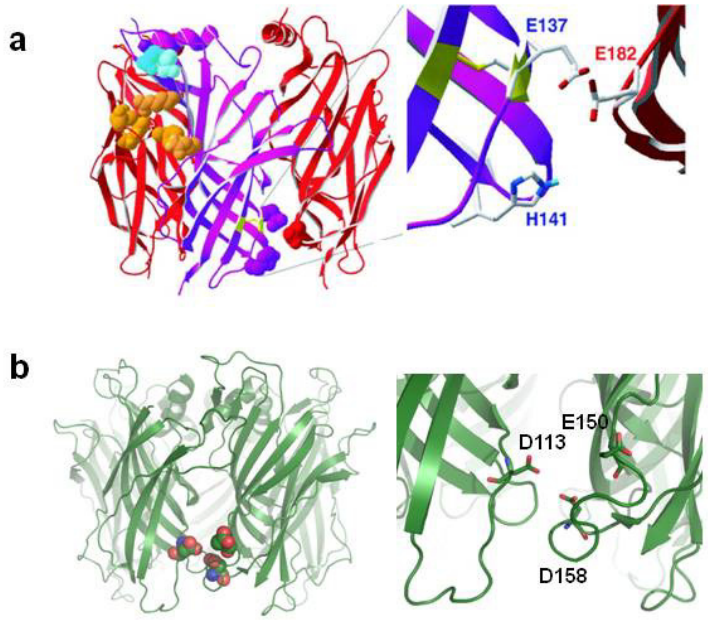

Figure 17 Comparison of the identified residues interacting with zinc in the GABA receptor (a) and different divalent cations in ELIC (b). The positions of the residues in the GABA receptor are modeled using a homology model based on the AChBP. In the GABA receptor, the identified histidine and glutamates coordinate zinc whereas the binding of divalent cations in ELIC only involves acidic amino acids. Despite the differences in the binding sites, both of them are located at similar positions in the subunit interface and could act by similar mechanisms.

The stabilization of distinct functional states is a hallmark of the modulation of allosteric proteins. Next to the binding site of divalent cations, there are different binding sites for other allosteric modulators known in pLGICs, such as benzodiazepines or ivermectin. The binding site for benzodiazepines in heteropentameric GABARs is located in the extracellular domain, a site which is homologous to the agonist binding site but not involved in agonist binding. In contrast, Ivermectin binds to a site in the transmembrane domain. Both of them are positive modulators and act by stabilizing the open state. The binding of benzodiazepines shifts the population of receptors towards the flip state, thus increasing the apparent affinity of the agonist and facilitating receptor activation (*66*, *73*). The binding of ivemectin slightly changes the relative position of the transmembrane helixes to each other. It thereby stabilizes the pore in the open conformation. The stabilized open conformation of the pore acts via the allosteric network of the receptor also on the ligand binding domain, thus locking the whole receptor in the active state. This leads, analogous to the benzodiazepines, to an increase of the apparent affinity of the agonists and to facilitated receptor activation (*13*).

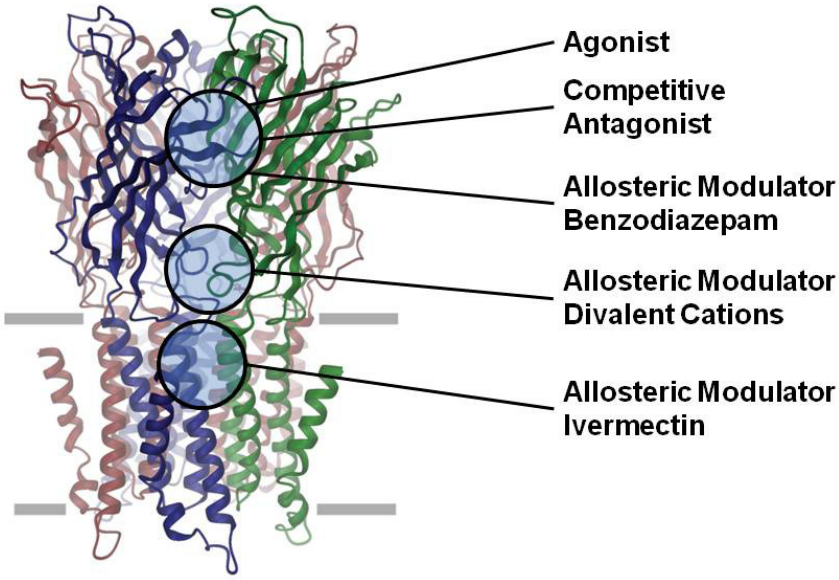

Figure 18 A ribbon representation of ELIC indicating the location of the binding sites of different molecules which act on pLGICs. Agonists and competitive antagonists act orthosteric in the agonist binding site, whereas benzodiazepines bind to a homologous site in the GABAR. Divalent cations bind to the newly identified binding site, located about 15Å from the agonist binding site. The ivermectin binding site is located in the transmembrane region of the invertebrate GluCl. All these molecules, independent of their effect, bind in the interface between the subunits, where they potently influence the conformational equilibrium of these allosteric receptors.

Even though the functional effects are different, agonists, antagonists or modulators act by stabilizing a certain state in the activation mechanism. Interestingly, the different binding sites are located in the dimer interfaces between the subunits of the receptor (Figure 18). In allosteric proteins, such as pLGICs, the communication between the subunits is crucial for their function. Thus, it is not surprising that the modulators successfully act at this important interface to influence the function of these proteins.

Physiological role of ELIC

The physiological role of most ion channels in prokaryotes as well as the function of ELIC in its host *Erwinia chrysanthemi* is still unknown. The only exceptions are mechanosensitive channels which act as emergency valves to release osmolytes in case of osmotic stress. Other ion channels could be involved in a yet unknown response to environmental stress or in a novel signal transduction pathway. A role in chemotaxis is not likely because most of them are also found in the membranes of immotile bacteria. The energy production in bacteria relies on the electrochemical gradients of protons and sodium which are closely linked to the membrane potential. Similar to animal cells, the resting potential of prokaryotes is mainly determined by their potassium gradient. The intracellular potassium concentration is 300 to 700mM resulting in a very negative resting potential of -120 to -200mV, indicating its importance for the electrochemical driving force of protons and sodium (*100*). Bacteria are small cells and the capacity of their membrane is therefore very small as well and the movement of only a few ions can already change the membrane

potential substantially. Ion channels in bacteria must therefore be tightly shut and should open only transiently.

The electrochemical requirements of prokaryotes offer two potential functions for ELIC. The protein could be involved in electrical signaling similar to neurotransmitter receptors in animals. It was shown in E.coli that the membrane potential of bacteria is variable and even highly dynamic. Next to providing the major driving force for energy production, membrane transport and flagellar motility, it could therefore also be involved in signaling processes (*101*). This signal transmission pathway is only known from the nervous systems of animals and was never observed in prokaryotes. The second possibility could be a role in restoring the negative membrane potential by potassium efflux, if the cell was depolarized before by proton or sodium influx.

One of the identified agonists of ELIC, GABA, is not only a neurotransmitter in animals but also produced and exported by bacteria upon acid stress. In the genome of *E.chrysanthemi*, the ELIC gene is located in an operon with two other genes. One of them is coding for a putative glutamate decarboxylase, the other for a transporter of the MFS family. This makes GABA a likely candidate for the natural agonist of ELIC, which is produced and transported to the periplasm by the host cell.

Alternatively, the agonist could also be an external signal. Plants produce GABA as well and secret it if the plant was wounded. Plant wounds are natural habitats of the plant pathogen *E.chrysanthemi* and offer a high concentration of nutrients. Both acid stress and the cotransport of nutrients with sodium lead to an increased influx of positive charges and thereby decrease the membrane potential. The activation of ELIC could then quickly restore the membrane potential, much faster than ion pumps which are used to establish the electrochemical gradient.

Conclusions

In this thesis I have described the work leading to the identification of agonists for ELIC. This has allowed me to carry out a study about the mechanisms of activation and allosteric inhibition of this receptor using both functional and structural methods. The functional characterization revealed a high degree of conservation compared to eukaryotic pLGICs. The agonist binding properties of ELIC are highly similar to GlyRs and GABARs whereas the ion selectivity places ELIC in the branch of the cation selective pLGICs, together with AChRs and $5HT_3$Rs. Next to activation, the mechanism of the allosteric modulation of ELIC by divalent cations could be resolved. This modulation, which is known from eukaryotic receptors, is assumed to play an important role in the regulation of the synaptic activity in the nervous system. The discovery of the inhibitory effect of divalent cations on ELIC is also important for future studies on ELIC, as care has to be taken on the concentration of divalent cations used in the experiments, to make the results from different research groups comparable.

Due to the structural and functional resemblance between ELIC and eukaryotic receptors, it is very likely that the main mechanisms of receptor activation are conserved. Any observation made in ELIC, and the mechanisms deduced from its behavior will thus likely extend to the whole family of pLGICs.

Since we know the high resolution structures of three pLGICs, ELIC is not the only pLGIC which allows detailed studies on structure-function on the same protein. However, the use of ELIC as a model system offers certain advantages over the other receptors with available structures. Compared to GLIC, ELIC is a true ligand-gated ion channel with small molecules as agonists, whereas GLIC senses its own protonation state to trigger activation. From an experimental view, ELIC does not require pH-jumps which can lead to artifacts in the measurements and undesired side effects in the cells used for expression. GluCl is a eukaryotic receptor with the highest similarity to the human receptors of pharmaceutical interest. However, the construct of GluCl, which was used for crystallization, is a homopentamer of the α-subunit which does probably not exist in the host organism *C.elegans*, as the native receptor is a heteropentamer formed by α and β subunits. Due to the artificial subunit composition, GluCl cannot be activated solely by its agonist glutamate, but additionally requires ivermectin for activation, which limits the impact of functional experiments. Moreover, since ELIC has the highest single channel conduction of all the receptors of known high-resolution structure, it is most suitable for kinetic investigations on a single channel level. The functional properties of ELIC, together with the possibility to produce high resolution structures, thus make it an attractive model system to elucidate the molecular mechanisms underlying the function of pLGICs.

Outlook

All the high resolution crystal structures of pLGICs were determined in a single functional state. However, the structure determination of different states of the same receptor, which is crucial to understand receptor function, has not been achieved.

One of the main future goals will thus be the crystallization of ELIC in a conducting conformation, even though this state is only transient in the native receptor. To overcome this problem, a mutagenic approach could be used to stabilize the receptor in the open conformation and to prevent desensitization. Additionally, the introduction of cysteines at specific positions could be used to establish intra- or intermolecular crosslinks to trap the open conformation. Another attempt could involve allosteric modulators. Similar to ivermectin in the case of GluCl, a positive allosteric modulator could stabilize ELIC in the open conformation. Unfortunately, such potent modulators of ELIC have not yet been identified.

The open conformation of ELIC would certainly increase the understanding of the function of pLGICs, but since any structure only provides a static picture, the activation mechanism and the sequence of the conformational rearrangements necessary to reach the conducting state would still have to be explored. Thus next to the structure determination of different functional states, functional experiments focusing on ligand recognition, the interface between the extracellular and transmembrane domain and the pore are needed. Due to the high single channel conductance, a detailed kinetic mechanism could be deduced from single channel measurements and the effect of mutations in certain regions of the receptor could directly be linked to the affected step in the activation mechanism. Other methods such as voltage clamp fluorimetry could be used to study the conformational changes of the extracellular domain simultaneously with the current elicited by the ion channel in the open state. The present studies offer only an initial view on the complex mechanisms that will have to be explored in detail in future studies.

Appendix A

Abbreviations

LGIC	Ligand-Gated Ion Channel
pLGIC	pentameric Ligand-Gated Ion Channel
ACh	acetylcholine
5HT	5-hydroxytryptamine, or serotonin
Gly	glycine
GABA	γ-amino butyric acid
ELIC	*Erwinia chrysanthemi* Ligand-Gated Ion Channel
GLIC	*Gloebacter violaceus* Ligand-Gated Ion Channel
SCAM	substituted cysteine accessibility method

Appendix B

Curriculum vitae

Iwan Zimmermann

Date of Birth:	October 4th 1982
Nationality:	Swiss
Place of Birth:	Glarus
Contact Address:	Schuppisstrasse 11
	8057 Zurich
	Switzerland
	i.zimmermann@bioc.uzh.ch

Education

Since 2008:	**PhD Student in Biochemisty** Institute of Biochemistry, University of Zurich Supervisor: Raimund Dutzler *Structural & Functional Characterization of Pentameric Ligand-Gated Ion Channels*
2008:	**Master of Science in Biochemistry** Institute of Biochemistry, University of Zurich Supervisor: Raimund Dutzler *Structural Characterization of the C-terminal Domain of a Prokaryotic Cation Chloride Cotransporter*
2006:	**Bachelor of Science in Biochemistry** University of Zurich
2002-2006	**Undergraduate Studies in Biochemistry** University of Zurich
1995 - 2001:	**High School Education** Kantonsschule Glarus, Kt. Glarus, Switzerland *Focus on Biology & Chemistry*

Languages:

German:	First Language
English:	Fluent
French:	Conversant

Publications

Zimmermann I, Marabelli A, Bertozzi C, Sivilotti L and Dutzler R. Inhibition of the Prokaryotic Ligand-Gated Ion Channel ELIC by Divalent Cations, *PLoS Biol (10)11*

Zimmermann I, Dutzler R. Ligand Activation of the Prokaryotic Pentameric Ligand-Gated Ion Channel ELIC, *PLoS Biol 9(6)*

Hilf R, Bertozzi C, Zimmermann I, Reiter A, Trauner D, Dutzler R. Structural basis of open channel block in a prokaryotic pentameric ligand-gated ion channel, *Nat Struct Mol Biol, 17, 11, 2010*

Warmuth S, Zimmermann I, Dutzler R. X-ray Structure of the C-Terminal Domain of a Prokaryotic Cation-Chloride Cotransporter, *Structure, Volume 17, Issue 4, 2009*

Zobi F, Hohl M, Zimmermann I, Alberto R. Binding of 9-Methylguanine to $[cis\text{-}Ru(2,2'\text{-}bpy)_2]^{2+}$: First X-ray Structure of a cis-Bis Purine Complex of Ruthenium *Inorg. Chem., 43 (9), 2004*

Posters

Zimmermann I, Marabelli A, Bertozzi C, Sivilotti L and Dutzler R. Inhibition of the Prokaryotic Ligand-Gated Ion Channel ELIC by Divalent Cations, 10th Symposium of the NCCR Structural Biology, 29th & 30th August 2012

Zimmermann I, Marabelli A, Bertozzi C, Sivilotti L and Dutzler R. Inhibition of the Prokaryotic Ligand-Gated Ion Channel ELIC by Divalent Cations, Gordon Research Conference on Ligand Recognition and Molecular Gating, 15th – 20th January 2012

Zimmermann I, Dutzler R. Ligand Activation of the Prokaryotic Pentameric Ligand-Gated Ion Channel ELIC, 9th Symposium of the NCCR Structural Biology, 1st & 2nd September 2011

Zimmermann I, Dutzler R. Ligand Activation of the Prokaryotic Pentameric Ligand-Gated Ion Channel ELIC, Gordon Research Conference on Membrane Transport, 19th – 24th June 2011

Hilf R, Bertozzi C, **Zimmermann I**, Reiter A, Trauner D, Dutzler R. Structural basis of open channel block in a prokaryotic pentameric ligand-gated ion channel, 9th Symposium of the NCCR Structural Biology, 2nd & 3rd September 2010

Talks at Conferences

Zimmermann I. Inhibition of the Prokaryotic Ligand-Gated Ion Channel ELIC by Divalent Cations, Gordon Research Conference on Ligand Recognition and Molecular Gating, 15th – 20th January 2012

Zimmermann I. Structural basis for ion permeation and block in prokaryotic pentameric ligand-gated ion channels, 7th Symposium of the European Protein Society, 14th – 18th June 2009

Literature

1. Millar, N. S., and Gotti, C. (2009) Diversity of vertebrate nicotinic acetylcholine receptors., *Neuropharmacology 56*, 237–46.

2. Moulton, G., Attwood, T. K., Parry-Smith, D. J., and Packer, J. C. L. (2003) Phylogenomic analysis and evolution of the potassium channel gene family., *Receptors & channels 9*, 363–77.

3. Ortells, M. O., and Lunt, G. G. (1995) Evolutionary history of the ligand-gated ion-channel superfamily of receptors., *Trends in neurosciences 18*, 121–7.

4. Tasneem, A., Iyer, L. M., Jakobsson, E., and Aravind, L. (2005) Identification of the prokaryotic ligand-gated ion channels and their implications for the mechanisms and origins of animal Cys-loop ion channels., *Genome biology 6*, R4.

5. Bocquet, N., Prado De Carvalho, L., Cartaud, J., Neyton, J., Le Poupon, C., Taly, A., Grutter, T., Changeux, J.-P., and Corringer, P.-J. (2006) A prokaryotic proton-Gated ion channel from the nicotinic acetylcholine receptor family, *Nature 445*, 116–119.

6. Banks, G., Kemenes, I., Schofield, M., O'Shea, M., and Korneev, S. a. (2009) Acetylcholine binding protein of mollusks is unlikely to act as a regulator of cholinergic neurotransmission at neurite-neurite synaptic sites in vivo., *FASEB journal : official publication of the Federation of American Societies for Experimental Biology 23*, 3030–6.

7. Brejc, K., Dijk, W. J. van, Klaasen, R. V., Schuurmans, M., van der Oost, J., Smit, A. B., and Sixma, T. K. (2001) Crystal structure of an ACh-binding protein reveals the ligand-binding domain of nicotinic receptors, *Nature 411*, 269–276.

8. Miyazawa, A., Fujiyoshi, Y., and Unwin, N. (2003) Structure and gating mechanism of the acetylcholine receptor pore, *Nature 423*, 949–955.

9. Unwin, N. (2005) Refined structure of the nicotinic acetylcholine receptor at 4A resolution., *Journal of molecular biology 346*, 967–89.

10. Hilf, R. J. C., and Dutzler, R. (2008) X-ray structure of a prokaryotic pentameric ligand-gated ion channel, *Nature 452*, 375–379.

11. Hilf, R. J. C., and Dutzler, R. (2009) Structure of a potentially open state of a proton-activated pentameric ligand-gated ion channel, *Nature 457*, 115–118.

12. Bocquet, N., Nury, H., Baaden, M., Le Poupon, C., Changeux, J.-P., Delarue, M., and Corringer, P.-J. (2009) X-ray structure of a pentameric ligand-gated ion channel in an apparently open conformation., *Nature 457*, 111–4.

13. Hibbs, R. E., and Gouaux, E. (2011) Principles of activation and permeation in an anion-selective Cys-loop receptor., *Nature 474*, 54–60.

14. Imoto, K., Busch, C., Sakmann, B., Mishina, M., Konno, T., Nakai, J., Bujo, H., Mori, Y., Fukuda, K., and Numa, S. (1988) Rings of negatively charged amino acids determine the acetylcholine receptor channel conductance., *Nature 335*, 645–8.

15. Xu, M., and Akabas, M. H. (1993) Amino acids lining the channel of the gamma-aminobutyric acid type A receptor identified by cysteine substitution., *The Journal of biological chemistry 268*, 21505–8.

16. Akabas, M. H., Kaufmann, C., Archdeacon, P., and Karlin, a. (1994) Identification of acetylcholine receptor channel-lining residues in the entire M2 segment of the alpha subunit., *Neuron 13*, 919–27.

17. Reeves, D. C., Goren, E. N., Akabas, M. H., and Lummis, S. C. (2001) Structural and electrostatic properties of the 5-HT3 receptor pore revealed by substituted cysteine accessibility mutagenesis., *The Journal of biological chemistry 276*, 42035–42.

18. Beckstein, O., and Sansom, M. S. P. (2006) A hydrophobic gate in an ion channel: the closed state of the nicotinic acetylcholine receptor., *Physical biology 3*, 147–59.

19. White, B. H., and Cohen, J. B. (1992) Agonist-induced changes in the structure of the acetylcholine receptor M2 regions revealed by photoincorporation of an uncharged nicotinic noncompetitive antagonist., *The Journal of biological chemistry 267*, 15770–83.

20. Wilson, G., and Karlin, A. (2001) Acetylcholine receptor channel structure in the resting, open, and desensitized states probed with the substituted-cysteine-accessibility method., *Proceedings of the National Academy of Sciences of the United States of America 98*, 1241–8.

21. DEL CASTILLO, J., and KATZ, B. (1957) Interaction at end-plate receptors between different choline derivatives., *Proceedings of the Royal Society of London. Series B, Containing papers of a Biological character. Royal Society (Great Britain) 146*, 369–81.

22. MONOD, J., WYMAN, J., and CHANGEUX, J. P. (1965) ON THE NATURE OF ALLOSTERIC TRANSITIONS: A PLAUSIBLE MODEL., *Journal of molecular biology 12*, 88–118.

23. Jackson, M. B. (1986) Kinetics of unliganded acetylcholine receptor channel gating., *Biophysical journal 49*, 663–72.

24. Bhattacharya, A., Dang, H., Zhu, Q.-M., Schnegelsberg, B., Rozengurt, N., Cain, G., Prantil, R., Vorp, D. a, Guy, N., Julius, D., Ford, A. P. D. W., Lester, H. a, and Cockayne, D. a. (2004) Uropathic observations in mice expressing a constitutively active point mutation in the 5-HT3A receptor subunit., *The Journal of neuroscience : the official journal of the Society for Neuroscience 24*, 5537–48.

25. Colquhoun, D. (1998) Binding, gating, affinity and efficacy: the interpretation of structure-activity relationships for agonists and of the effects of mutating receptors., *British journal of pharmacology 125*, 924–47.

26. Silman, I., and Karlin, A. (1969) Acetylcholine receptor: covalent attachment of depolarizing groups at the active site., *Science (New York, N.Y.) 164*, 1420–1.

27. Corringer, P. J., Le Novère, N., and Changeux, J. P. (2000) Nicotinic receptors at the amino acid level., *Annual review of pharmacology and toxicology 40*, 431–58.

28. Celie, P. H. N., van Rossum-Fikkert, S. E., van Dijk, W. J., Brejc, K., Smit, A. B., and Sixma, T. K. (2004) Nicotine and carbamylcholine binding to nicotinic acetylcholine receptors as studied in AChBP crystal structures., *Neuron 41*, 907–14.

29. Zhong, W., Gallivan, J. P., Zhang, Y., Li, L., Lester, H. a, and Dougherty, D. a. (1998) From ab initio quantum mechanics to molecular neurobiology: a cation-pi binding site in the nicotinic receptor., *Proceedings of the National Academy of Sciences of the United States of America 95*, 12088–93.

30. Beene, D. L., Brandt, G. S., Zhong, W., Zacharias, N. M., Lester, H. A., and Dougherty, D. A. (2002) Cation-π Interactions in Ligand Recognition by Serotonergic (5-HT3A) and Nicotinic Acetylcholine Receptors: The Anomalous Binding Properties of Nicotine, *Biochemistry 41*, 10262–10269.

31. Padgett, C. L., Hanek, A. P., Lester, H. a, Dougherty, D. a, and Lummis, S. C. R. (2007) Unnatural amino acid mutagenesis of the GABA(A) receptor binding site residues reveals a novel cation-pi interaction between GABA and beta 2Tyr97., *The Journal of neuroscience : the official journal of the Society for Neuroscience 27*, 886–92.

32. Pless, S. A., Millen, K. S., Hanek, A. P., Lynch, J. W., Lester, H. A., Lummis, S. C. R., and Dougherty, D. A. (2008) A cation-pi interaction in the binding site of the glycine receptor is mediated by a phenylalanine residue., *The Journal of neuroscience : the official journal of the Society for Neuroscience 28*, 10937–42.

33. Miller, P. S., and Smart, T. G. (2010) Binding, activation and modulation of Cys-loop receptors., *Trends in pharmacological sciences 31*, 161–74.

34. Hansen, S. B., Sulzenbacher, G., Huxford, T., Marchot, P., Taylor, P., and Bourne, Y. (2005) Structures of Aplysia AChBP complexes with nicotinic agonists and antagonists reveal distinctive binding interfaces and conformations., *The EMBO journal 24*, 3635–46.

35. Shi, J., Koeppe, J. R., Komives, E. a, and Taylor, P. (2006) Ligand-induced conformational changes in the acetylcholine-binding protein analyzed by hydrogen-deuterium exchange mass spectrometry., *The Journal of biological chemistry 281*, 12170–7.

36. Bouzat, C., Gumilar, F., Spitzmaul, G., Wang, H., Rayes, D., Hansen, S. B., Taylor, P., and Sine, S. M. (2004) Coupling of agonist binding to channel gating in an ACh-binding protein linked to an ion channel., *Nature 430*, 896–900.

37. Hilf, R. J., and Dutzler, R. (2009) A prokaryotic perspective on pentameric ligand-gated ion channel structure., *Current opinion in structural biology 19*, 418–24.

38. Lee, W. Y., and Sine, S. M. (2005) Principal pathway coupling agonist binding to channel gating in nicotinic receptors, *Nature 438*, 243–247.

39. Lee, W. Y., Free, C. R., and Sine, S. M. (2008) Nicotinic receptor interloop proline anchors beta1-beta2 and Cys loops in coupling agonist binding to channel gating., *The Journal of general physiology 132*, 265–78.

40. Lee, W. Y., Free, C. R., and Sine, S. M. (2009) Binding to gating transduction in nicotinic receptors: Cys-loop energetically couples to pre-M1 and M2-M3 regions., *The Journal of neuroscience : the official journal of the Society for Neuroscience 29*, 3189–99.

41. Ochoa, E. L., Chattopadhyay, A., and McNamee, M. G. (1989) Desensitization of the nicotinic acetylcholine receptor: molecular mechanisms and effect of modulators., *Cellular and molecular neurobiology 9*, 141–78.

42. KATZ, B., and THESLEFF, S. (1957) A study of the desensitization produced by acetylcholine at the motor end-plate., *The Journal of physiology 138*, 63–80.

43. Corringer, P. J., Bertrand, S., Bohler, S., Edelstein, S. J., Changeux, J. P., and Bertrand, D. (1998) Critical elements determining diversity in agonist binding and desensitization of neuronal nicotinic acetylcholine receptors., *The Journal of neuroscience : the official journal of the Society for Neuroscience 18*, 648–57.

44. Feltz, A., and Trautmann, A. (1982) Desensitization at the frog neuromuscular junction: a biphasic process., *The Journal of physiology 322*, 257–72.

45. Li, S. C., Hoyles, M., Kuyucak, S., and Chung, S. H. (1998) Brownian dynamics study of ion transport in the vestibule of membrane channels., *Biophysical journal 74*, 37–47.

46. Doyle, D. a., Morais Cabral, J., Pfuetzner, R. A., Kuo, A., Gulbis, J. M., Cohen, S. L., Chait, B. T., and MacKinnon, R. (1998) The structure of the potassium channel: molecular basis of K+ conduction and selectivity., *Science (New York, N.Y.) 280*, 69–77.

47. Xu, M., and Akabas, M. H. (1996) Identification of channel-lining residues in the M2 membrane-spanning segment of the GABA(A) receptor alpha1 subunit., *The Journal of general physiology 107*, 195–205.

48. Bocquet, N., Nury, H., Baaden, M., Le Poupon, C., Changeux, J.-P., Delarue, M., and Corringer, P.-J. (2008) X-ray structure of a pentameric ligand-gated ion channel in an apparently open conformation, *Nature* 2–5.

49. Imoto, K., Busch, C., Sakmann, B., Mishina, M., Konno, T., Nakai, J., Bujo, H., Mori, Y., Fukada, K., and Numa, S. (1988) Rings of negatively charged amino acids determine the acetylcholine receptor channel conductance, *Nature 335*, 645–648.

50. Galzi, J. L., Devillers-Thiéry, A., Hussy, N., Bertrand, S., Changeux, J. P., and Bertrand, D. (1992) Mutations in the channel domain of a neuronal nicotinic receptor convert ion selectivity from cationic to anionic., *Nature 359*, 500–5.

51. Gunthorpe, M. J., and Lummis, S. C. (2001) Conversion of the ion selectivity of the 5-HT(3a) receptor from cationic to anionic reveals a conserved feature of the ligand-gated ion channel superfamily., *The Journal of biological chemistry 276*, 10977–83.

52. Keramidas, A., Moorhouse, A. J., Pierce, K. D., Schofield, P. R., and Barry, P. H. (2002) Cation-selective mutations in the M2 domain of the inhibitory glycine receptor channel reveal determinants of ion-charge selectivity., *The Journal of general physiology 119*, 393–410.

53. Wotring, V. E., Miller, T. S., and Weiss, D. S. (2003) Mutations at the GABA receptor selectivity filter: a possible role for effective charges., *The Journal of physiology 548*, 527–40.

54. Imoto, K., Konno, T., Nakai, J., Wang, F., Mishina, M., and Numa, S. (1991) A ring of uncharged polar amino acids as a component of channel constriction in the nicotinic acetylcholine receptor., *FEBS letters 289*, 193–200.

55. Kelley, S. P., Dunlop, J. I., Kirkness, E. F., Lambert, J. J., and Peters, J. A. (2003) A cytoplasmic region determines single-channel conductance in 5-HT3 receptors., *Nature 424*, 321–4.

56. Hansen, S. B., Wang, H.-L., Taylor, P., and Sine, S. M. (2008) An ion selectivity filter in the extracellular domain of Cys-loop receptors reveals determinants for ion conductance., *The Journal of biological chemistry 283*, 36066–70.

57. Bean, B. P., Cohen, C. J., and Tsien, R. W. (1983) Lidocaine block of cardiac sodium channels., *The Journal of general physiology 81*, 613–42.

58. Adler, M., Oliveira, a C., Albuquerque, E. X., Mansour, N. a, and Eldefrawi, a T. (1979) Reaction of tetraethylammonium with the open and closed conformations of the acetylcholine receptor ionic channel complex., *The Journal of general physiology 74*, 129–52.

59. Kaldany, R. R., and Karlin, A. (1983) Reaction of quinacrine mustard with the acetylcholine receptor from Torpedo californica., *The Journal of biological chemistry 258*, 6232–42.

60. Pascual, J. M., and Karlin, A. (1998) Delimiting the binding site for quaternary ammonium lidocaine derivatives in the acetylcholine receptor channel., *The Journal of general physiology 112*, 611–21.

61. Bocquet, N., Prado de Carvalho, L., Cartaud, J., Neyton, J., Le Poupon, C., Taly, A., Grutter, T., Changeux, J.-P., and Corringer, P.-J. (2007) A prokaryotic proton-gated ion channel from the nicotinic acetylcholine receptor family., *Nature 445*, 116–9.

62. Hilf, R. J. C., Bertozzi, C., Zimmermann, I., Reiter, A., Trauner, D., and Dutzler, R. (2010) Structural basis of open channel block in a prokaryotic pentameric ligand-gated ion channel., *Nature structural & molecular biology 17*, 1330–6.

63. ARUNLAKSHANA, O., and SCHILD, H. O. (1959) Some quantitative uses of drug antagonists., *British journal of pharmacology and chemotherapy 14*, 48–58.

64. Kenakin, T. P. (2009) A Pharmacology Primer 3rd ed. Elsevier Academic Press.

65. Lape, R., Colquhoun, D., and Sivilotti, L. G. (2008) On the nature of partial agonism in the nicotinic receptor superfamily, *Nature 454*.

66. Lavoie, a M., and Twyman, R. E. (1996) Direct evidence for diazepam modulation of GABAA receptor microscopic affinity., *Neuropharmacology 35*, 1383–92.

67. Urban, B. W., Bleckwenn, M., and Barann, M. (2006) Interactions of anesthetics with their targets: non-specific, specific or both?, *Pharmacology & therapeutics 111*, 729–70.

68. Sessoms-Sikes, J. S., Hamilton, M. E., Liu, L., Lovinger, D. M., and Machu, T. K. (2003) A mutation in transmembrane domain II of the 5-hydroxytryptamine(3A) receptor stabilizes channel opening and alters alcohol modulatory actions., *The Journal of pharmacology and experimental therapeutics 306*, 595–604.

69. Arias, H. R., Bhumireddy, P., and Bouzat, C. (2006) Molecular mechanisms and binding site locations for noncompetitive antagonists of nicotinic acetylcholine receptors., *The international journal of biochemistry & cell biology 38*, 1254–76.

70. Nury, H., Van Renterghem, C., Weng, Y., Tran, A., Baaden, M., Dufresne, V., Changeux, J.-P., Sonner, J. M., Delarue, M., and Corringer, P.-J. (2011) X-ray structures of general anaesthetics bound to a pentameric ligand-gated ion channel., *Nature 469*, 428–31.

71. Li, P., Slimko, E. M., and Lester, H. a. (2002) Selective elimination of glutamate activation and introduction of fluorescent proteins into a Caenorhabditis elegans chloride channel., *FEBS letters 528*, 77–82.

72. Adelsberger, H., Lepier, a, and Dudel, J. (2000) Activation of rat recombinant alpha(1)beta(2)gamma(2S) GABA(A) receptor by the insecticide ivermectin., *European journal of pharmacology 394*, 163–70.

73. Shan, Q., Haddrill, J. L., and Lynch, J. W. (2001) Ivermectin, an unconventional agonist of the glycine receptor chloride channel., *The Journal of biological chemistry 276*, 12556–64.

74. Brown, a M., Hope, a G., Lambert, J. J., and Peters, J. a. (1998) Ion permeation and conduction in a human recombinant 5-HT3 receptor subunit (h5-HT3A)., *The Journal of physiology 507 (Pt 3*, 653–65.

75. Galzi, J. L., Bertrand, S., Corringer, P. J., Changeux, J. P., and Bertrand, D. (1996) Identification of calcium binding sites that regulate potentiation of a neuronal nicotinic acetylcholine receptor., *The EMBO journal 15*, 5824–32.

76. Vernino, S., Amador, M., Luetje, C. W., Patrick, J., and Dani, J. a. (1992) Calcium modulation and high calcium permeability of neuronal nicotinic acetylcholine receptors., *Neuron 8*, 127–34.

77. Hsiao, B., Mihalak, K. B., Repicky, S. E., Everhart, D., Mederos, A. H., Malhotra, A., and Luetje, C. W. (2006) Determinants of zinc potentiation on the alpha4 subunit of neuronal nicotinic receptors., *Molecular pharmacology 69*, 27–36.

78. Nevin, S. T., Cromer, B. a, Haddrill, J. L., Morton, C. J., Parker, M. W., and Lynch, J. W. (2003) Insights into the structural basis for zinc inhibition of the glycine receptor., *The Journal of biological chemistry 278*, 28985–92.

79. Hosie, A. M., Dunne, E. L., Harvey, R. J., and Smart, T. G. (2003) Zinc-mediated inhibition of GABA(A) receptors: discrete binding sites underlie subtype specificity., *Nature neuroscience 6*, 362–9.

80. Mclaughlin, J. T., Fu, J., Sproul, A. D., and Rosenberg, R. L. (2006) Role of the Outer Beta-Sheet in Divalent Cation Modulation of Alpha-7 Nicotinic Receptors, *Molecular Pharmacology 70*, 16–22.

81. Niemeyer, M. I., and Lummis, S. C. (2001) The role of the agonist binding site in Ca(2+) inhibition of the recombinant 5-HT(3A) receptor., *European journal of pharmacology 428*, 153–61.

82. Thompson, A. J., and Lummis, S. C. R. (2009) Calcium modulation of 5-HT3 receptor binding and function., *Neuropharmacology 56*, 285–91.

83. Hu, X.-Q., and Lovinger, D. M. (2005) Role of aspartate 298 in mouse 5-HT3A receptor gating and modulation by extracellular Ca2+., *The Journal of physiology 568*, 381–96.

84. Briggs, C. a, and McKenna, D. G. (1998) Activation and inhibition of the human alpha7 nicotinic acetylcholine receptor by agonists., *Neuropharmacology 37*, 1095–102.

85. McGehee, D. S., and Role, L. W. (1995) Physiological diversity of nicotinic acetylcholine receptors expressed by vertebrate neurons., *Annual review of physiology 57*, 521–46.

86. Jackson, M. B., and Yakel, J. L. (1995) The 5-HT3 receptor channel., *Annual review of physiology 57*, 447–68.

87. Mortensen, M., Patel, B., and Smart, T. G. (2011) GABA Potency at GABA(A) Receptors Found in Synaptic and Extrasynaptic Zones., *Frontiers in cellular neuroscience 6*, 1.

88. Bormann, J., Rundström, N., Betz, H., and Langosch, D. (1994) Residues within transmembrane segment M2 determine chloride conductance of glycine receptor homo- and hetero-oligomers., *The EMBO journal 13*, 1493.

89. Rajendra, S., Lynch, J. W., and Schofield, P. R. (1997) The glycine receptor., *Pharmacology & therapeutics 73*, 121–46.

90. Chang, Y., Huang, Y., and Whiteaker, P. (2010) Mechanism of Allosteric Modulation of the Cys-loop Receptors, *Pharmaceuticals 3*, 2592–2609.

91. Corradi, J., Gumilar, F., and Bouzat, C. (2009) Single-channel kinetic analysis for activation and desensitization of homomeric 5-HT(3)A receptors., *Biophysical journal 97*, 1335–45.

92. Maconochie, D. J., Zempel, J. M., and Steinbach, J. H. (1994) How quickly can GABAA receptors open?, *Neuron 12*, 61–71.

93. Lavoie, a M., Tingey, J. J., Harrison, N. L., Pritchett, D. B., and Twyman, R. E. (1997) Activation and deactivation rates of recombinant GABA(A) receptor channels are dependent on alpha-subunit isoform., *Biophysical journal 73*, 2518–26.

94. Legendre, P. (1998) A reluctant gating mode of glycine receptor channels determines the time course of inhibitory miniature synaptic events in zebrafish hindbrain neurons., *The Journal of neuroscience : the official journal of the Society for Neuroscience 18*, 2856–70.

95. Dani, J. a, and Eisenman, G. (1987) Monovalent and divalent cation permeation in acetylcholine receptor channels. Ion transport related to structure., *The Journal of general physiology 89*, 959–83.

96. Jensen, M. L., Schousboe, A., and Ahring, P. K. (2005) Charge selectivity of the Cys-loop family of ligand-gated ion channels., *Journal of neurochemistry 92*, 217–25.

97. Wang, H.-L., Cheng, X., and Sine, S. M. (2012) Intramembrane proton binding site linked to activation of bacterial pentameric ion channel., *The Journal of biological chemistry 287*, 6482–9.

98. Pan, J., Chen, Q., Willenbring, D., Yoshida, K., Tillman, T., Kashlan, O. B., Cohen, A., Kong, X.-P., Xu, Y., and Tang, P. (2012) Structure of the pentameric ligand-gated ion channel ELIC cocrystallized with its competitive antagonist acetylcholine., *Nature communications 3*, 714.

99. Du, J., Dong, H., and Zhou, H.-X. (2012) Size matters in activation/inhibition of ligand-gated ion channels., *Trends in pharmacological sciences 33*, 482–93.

100. Brown, A. D. (1964) Aspects of Bacterial Response To the Ionic Environment., *Bacteriological reviews 28*, 296–329.

101. Kralj, J. M., Hochbaum, D. R., Douglass, A. D., and Cohen, A. E. (2011) Electrical spiking in Escherichia coli probed with a fluorescent voltage-indicating protein., *Science (New York, N.Y.) 333*, 345–8.